MICROWAVE EMISSION AND SCATTERING FROM VEGETATED TERRAIN

by

TERRELL GENE SIBLEY

August 1973

supported by
National Aeronautics and Space Administration
Grant NGL 44-001-001

TEXAS A&M UNIVERSITY
REMOTE SENSING CENTER
COLLEGE STATION, TEXAS

TECHNICAL REPORT RSC-44

MICROWAVE EMISSION AND SCATTERING FROM VEGETATED TERRAIN

by

TERRELL GENE SIBLEY

August 1973

supported by

National Aeronautics and Space Adminstration

Grant NGL 44-001-001

ABSTRACT

In this report, models are developed for the apparent temperature and backscatter coefficient of vegetated terrain to illustrate the effects of vegetation on the sensitivity of these parameters to variations of soil moisture. Three types of terrain are simulated for both the passive and the active case: a uniform canopy over a smooth surface, plant rows on a smooth surface, and plant rows on a rough surface. In each case the canopy is defined by its overall dimensions and by its electric permittivity, which is determined from the Weiner model for dielectric mixture. Emission and scattering from both the soil and the canopy are considered, but atmospheric effects are neglected.

The expression for the apparent temperature of vegetated terrain includes terms for the apparent temperature of the bare soil and of the canopy. The bare soil term is modified by an exponential term to account for attenuation of radiation from the soil by the canopy. The term which represents radiation by the canopy assumes that the canopy is homogeneous layer. The expression for the apparent temperature of row crops is the average of the apparent temperatures of covered or shadowed soil and visible bare soil. A rough surface is represented by a surface rough-

ness factor and a coefficient of effective area of specular refraction.

The expression for the backscatter coefficient of vegetated terrain is similar to the expression for apparent temperature. The term for backscatter from smooth, bare soil is determined by the physical optics method. The term for backscatter from the canopy is a modified form of a model for scattering from long, thin dielectric cylinders.

Caluclated data indicate that the sensitivity of the apparent temperature and backscatter coefficient to variations of soil moisture, decreases as the amount of vegetation increases. It is shown that the same effect results from increasing signal frequency or angle of incidence.

Several sets of equivalent vegetation states, defined as different combinations of parameters which yield equivalent data, are tabulated. It is shown that in many cases the height-density product of a uniform canopy may be used to identify equivalent states.

ACKNOWLEDGEMENTS

The author wishes to express sincere gratitude to Dr. John W. Rouse, Jr., who offered much helpful advice during the course of the study.

Appreciation is expressed to Dr. Thomas Schmugge of the Earth Observations Branch, NASA/Goddard Space Flight Center, for his assistance in obtaining radiometer data from Chickasha, Oklahoma, and Weslaco, Texas. Also, the assistance of Mr. Bruce Blanchard of the Southern Plains Watershed Research Center, who provided ground support data from Chickasha, is gratefully acknowledged.

Funding for this project was provided by the National Aeronautics and Space Administration under Grant NGL 44-001-001.

TABLE OF CONTENTS

Chapter Page

Chapter | Page

LIST OF TABLES

LIST OF FIGURES

Figure | Page

CHAPTER I

INTRODUCTION

The Potential for Microwave Sensors in Agricultural Remote Sensing

Remote sensing techniques have become established tools for agricultural planning and management. However, only in recent years has the potential value of microwave sensors in agricultural applications been examined. Radar and microwave radiometers have the potential for performing certain tasks presently performed by photographic sensors, and other tasks which cannot be accomplished through photography. For example, since the development of synthetic aperture radar systems, it has been possible to produce radar imagery with resolution of several meters from high altitudes. Such imagery may provide as much information about certain types of terrain as photographic imagery. Furthermore, the ability to obtain radar imagery does not depend on the time of day and is almost independent of weather conditions.

Microwave sensors are valuable not so much for the characteristics of the instruments, but for the region of

the electromagnetic spectrum in which they operate. The microwave band extends from 0.3 GHz to 300 GHz. However, most research in agricultural remote sensing has been confined to frequencies less than 36 GHz (centimeter wavelengths) because of economic and technical advantages [1]. Radiation at the lower frequencies can penetrate clouds and fog without serious degradation of the signal. Using cross-polarization techniques, radar echoes from the ground can be detected even during rain. Furthermore, at the lower frequencies the depth of penetration through vegetation and soil may be several centimeters. A discussion of microwave penetration of soil is given in Appendix A.

The use of microwave frequencies for remote sensing does have certain inherent disadvantages. Data are often difficult to interpret because several variables affect the measurements: frequency, polarization, angle, permittivity and roughness of the surface, etc. Data from vegetated terrain depend in general upon the characteristics of both the plants and the soil. Sometimes the total effect of the unknown surface parameters is unpredictable, in which case no information about the surface can be derived from the data. However, if a single parameter has an overriding effect on the data, then variations of this parameter can be detected.

Experimental proof of the variation of the

permittivity of soil with moisture content has stimulated research in the area of measuring soil moisture with microwave remote sensors. Some radiometer data from bare ground indicate that the moisture content of the soil can be determined with fair accuracy from the apparent temperature of the soil. However, similar data from vegetated fields show very little correlation with apparent temperature.

Objective

There is no question that the permittivity of soil is a function of moisture content. Therefore, the moisture content affects the emission and scattering of microwave energy from the ground to the same degree to which the permittivity affects these processes. Obviously, as the height or density of vegetation increases, the permittivity of the soil becomes less significant. The question is, can the moisture content of a soil surface which is more than slightly vegetated be measured with microwave sensors?

The objective of this thesis is to determine the effect of vegetation on the ability to measure moisture content by microwave remote sensing techniques. Both active and passive sensors are considered. Apparent temperatures and scattering coefficients are computed as functions of soil moisture for several simulated vegetated terrains.

Scope of Report

The models developed for calculation of the apparent temperature and scattering coefficient are intended to be only first approximations of vegetated terrain. To account for attenuation by and radiation from the vegetation, the canopy is assumed to be a homogeneous medium. Scattering from the canopy is accounted for by using a model for scattering from a particular class of vegetation.

Since the investigation is concerned only with the effects of vegetation and soil moisture on emission and scattering, the effects of atmospheric propagation have been ignored. A discussion of atmospheric effects is given in Appendix B.

Chapter II briefly reviews some theories and experiments which provide the background for this investigation.

In Chapter III models are developed for the apparent temperature of some simple vegetated surfaces. To include the effects of vegetation, the permittivity of the plant canopy is derived from a model for the permittivity of a dielectric mixture. Expressions are derived for the apparent temperature of a smooth, uniformly vegetated surface and for row crops on smooth and rough surfaces.

Chapter IV treats scattering from the surfaces modeled in Chapter III. Scattering from an arbitrarily rough surface is described by defining an effective area of

specular reflection.

Chapter V presents microwave data obtained from vegetated terrain, and compares them with the results of Chapters III and IV.

CHAPTER II

THEORETICAL AND EXPERIMENTAL BACKGROUND

The scattering and emission of electromagnetic waves from natural surfaces are complicated processes which are very difficult to describe because the characteristics of a natural surface are not easily quantified. Vegetation is even more difficult to describe than soil because its configuration is constantly changing.

Despite the difficulties encountered, progress has been made in describing the parameters which effect scattering and emission from natural terrain and in developing practical applications of the theory. In particular, much effort has been devoted to developing techniques of remotely monitoring soil moisture content. This chapter gives a brief review of some of the theories and experiments which have contributed to an understanding of the problem.

Peake's Model for Apparent Temperature

The model for apparent surface temperature developed by Peake [2] expresses the emissivity of a surface in terms of its scattering coefficients. By employing an empirically derived expression for the differential scattering coefficient, the problem of determining the emissivity of a

surface for all angles is reduced to determining a measurable constant at any particular angle. Peake's theoretical predictions are in fair agreement with experimental measurements of the apparent temperature of asphalt and grass. A brief description of Peake's development is given below.

For an element of surface area S upon which radiation of intensity I_o is incident from a direction (θ_o, ϕ_o), the differential scattering coefficient is defined by

$$\gamma(\theta_o \phi_o ; \theta_s \phi_s) = \frac{4\pi R^2 I_s}{I_o S \cos\theta_o} \qquad \text{(II-1)}$$

where I_s is the intensity of radiation at a distance R from the surface in the direction (θ_s, ϕ_s).

Considering that either of two orthogonal polarization states may be specified for both the incident and scattered radiation, there are actually four scattering coefficients. Each of these may be represented in general by $\gamma_{ij}(o,s)$. The subscript i indicates the polarization of the incident radiation, and j the polarization of the scattered radiation. The letters o and s represent the directions (θ_o, ϕ_o) and (θ_s, ϕ_s). As a consequence of the reciprocity theorem, the scattering coefficients satisfy the relation,

$$\gamma_{ij}(o,s)\cos\theta_o = \gamma_{ji}(s,o)\cos\theta_s \qquad \text{(II-2)}$$

where each of i and j may represent either polarization.

The albedo and the absorption coefficient of the surface are both determined by the differential scattering coefficients. The albedo is defined as the fraction of power (of a specific polarization) incident on a surface from a direction (θ_o, ϕ_o) which is scattered into the upper hemisphere. Considering that the scattered radiation may be of either polarization, the albedo is

$$A_i(o) = \frac{1}{4\pi}\int[\gamma_{ii}(o,s) + \gamma_{ij}(o,s)]\,d\Omega_s \qquad \text{(II-3)}$$

The absorption coefficient $a_i(o)$ is the fraction of power incident from direction (θ_o, ϕ_o) with polarization i, which is absorbed by the surface. Considering only natural surfaces which are so thick that no transmission occurs, the absorption coefficient is simply

$$a_i(o) = 1 - A_i(o) \qquad \text{(II-4)}$$

The emissivity of a surface can be related to the absorption coefficient by deriving a generalized statement of Kirchhoff's law. The emissivity is defined as

$$e_i(o) = \frac{\text{Power emitted with polarization i by unit area of surface into element of solid angle } d\Omega_o \text{ in the direction } \theta_o\phi_o}{\text{Power emitted with same polarization by unit area of blackbody at same temperature into same element of solid angle}}$$

Considering a surface in thermodynamic equilibrium with the upper hemisphere, it is assumed that as much energy of a given polarization leaves the surface in a given direction as falls upon it from that direction. This assumption leads to

$$1 = e_i(o) + \frac{1}{4\pi}\int \frac{\cos\theta_s}{\cos\theta_o}\left[\gamma_{ii}(s,o) + \gamma_{ij}(s,o)\right]d\Omega_s \qquad \text{(II-5)}$$

Applying the reciprocity relation of (II-2), (II-5) becomes

$$1 = e_i(o) + \frac{1}{4\pi}\int \left[\gamma_{ii}(o,s) + \gamma_{ij}(o,s)\right]d\Omega_s \qquad \text{(II-6)}$$

The last term of the expression is now recognized as the albedo of the surface. Comparing (II-6) with (II-4), it is clear that the emission coefficient, for either polarization, is equal to the absorption coefficient.

The surface emissivity determines only one of three

components of the apparent temperature. The total apparent temperature for a particular polarization may be expressed generally as

$$T_a = T_g + T_s + T_p \qquad (II-7)$$

where T_g = contribution of the thermal radiation emitted by the surface

T_s = contribution of scattered diffuse radiation of the atmosphere

T_p = contribution of scattered radiation from point or quasi-point sources

A complete model of the measured apparent temperature should account for the effects of the atmosphere between the ground and the sensor. However, Peake's model assumes that the radiated power is measured near enough to the ground so that effects of the intervening atmosphere are negligible.

From the definition of the emission coefficient, the first contribution is simply the product of the emission coefficient and the actual ground temperature.

$$T_g(o) = e(o)T_g \qquad \text{(II-8)}$$

The second contribution, that of the scattered diffuse radiation of the atmosphere, depends upon the scattering coefficients of the surface and the apparent temperature of the radiation incident on the surface from above. Assuming that $T_i(s)$ and $T_j(s)$ are the apparent temperatures of the radiation with polarization states i and j incident from the direction (θ_s, ϕ_s), the contribution to the apparent surface temperature is

$$T_{si}(o) = \frac{1}{4\pi}\int\left[T_i(s)\gamma_{ii}(s,o) + T_j(s)\gamma_{ji}(s,o)\right]\frac{\cos\theta_s}{\cos\theta_o}\,d\Omega_s \qquad \text{(II-9)}$$

From the reciprocity relations it follows that

$$T_{si}(o) = \frac{1}{4\pi}\int\left[T_i(s)\gamma_{ii}(o,s) + T_j(s)\gamma_{ij}(o,s)\right]d\Omega_s \qquad \text{(II-10)}$$

The third contribution is due primarily to the sun. Peake showed that for K_a band the value of T_{pi} is much less than one degree Kelvin. Therefore, the last term of (II-7) can generally be neglected.

Writing the emission coefficient in terms of the

scattering coefficients, and assuming that $T_i(s) = T_j(s)$, the apparent surface temperature may be expressed as

$$T_{ai}(o) = T_g\left\{1 - \frac{1}{4\pi}\int\left[\gamma_{ii}(o,s)+\gamma_{ij}(o,s)\right]d\Omega_s\right\} + \frac{1}{4\pi}\int T_i(s)\left[\gamma_{ii}(o,s)+\gamma_{ij}(o,s)\right]d\Omega_s \quad \text{(II-11)}$$

Evaluation of (II-11) requires that the scattering coefficients be expressed analytically. Peake found the following expression to be applicable and consistent with measurements.

$$\gamma_{vv}(o,s) + \gamma_{vh}(o,s) = \gamma_o\left[\frac{\cos\theta_o + \cos\theta_s}{2\cos\theta_o}\right] \quad \text{(II-12)}$$

where γ_o is a constant, v denotes vertical polarization, and h denotes horizontal polarization. The value of γ_o is on the order of 0.1.

The advantages of Peake's model are that it is applicable to any surface satisfying the assumption of thermal equilibrium, and it is relatively simple to evaluate. No distinction is made between bare and vegetated surfaces. Each is considered simply a natural surface with a characteristic γ_o.

The assumption of thermal equilibrium is generally violated by vegetated surfaces. Kumar [3] has reported that the temperature of plants may be as much as 20°C above ambient. Furthermore, plants may warm or cool within minutes, or even seconds. Nevertheless, Peake's model has

been used to predict with fair accuracy the apparent temperature of certain vegetated surfaces [2].

Peake's Model for Long, Thin Dielectric Cylinders

To better predict the scattering from certain types of vegetation, Peake developed a model for scattering from long, thin dielectric cylinders [4]. The cylinders are assumed to be randomly spaced and oriented, with greater probability of vertical orientation. Since the model accounts for attenuation and multiple scattering within the plant canopy, it seems to predict the scattering coefficient of many vegetated surfaces rather well. However, application of the model is limited by several assumptions or restrictions, as described below.

All of the cylinders are assumed to be semi-infinite in length, extending downward from the plane $z = 0$. Consequently, scattering from the ground need not be considered.

All cylinders are assumed to be identical in shape, size, and electrical properties. The cylinders are round with diameter much smaller than a wavelength.

The incident field entering the volume which contains the cylinders is assumed to be attenuated exponentially as it propagates vertically into the medium. This attenuation is due to both absorption and scattering. The attenuation

constant is denoted α.

The cylinders are randomly spaced and oriented. It is assumed that all azimuth angles are equally likely. The probability that a cylinder is directed at an angle θ_i from the vertical is $p(\theta_i)d\Omega$, where $d\Omega$ is a unit solid angle. A probability density

$$p(\theta_i) = \frac{3}{2\pi} \cos^2\theta_i \qquad \text{(II-13)}$$

is assumed. The average number of cylinders per unit area is denoted N. The spacing between cylinders is considered large enough with respect to a wavelength that the phase difference between scattered fields is random. Consequently, the total average scattering cross section is the sum of the individual cross sections.

With the above assumptions, Peake derived four expressions for the bistatic cross section per unit area of vegetated ground. Since these expressions are rather long, only the simplest is repeated here as an example:

$$\sigma^{\circ}_{hh}(\theta_i, \theta_s \phi_s) = B_p\left[(3 - 2\sin^2\phi_s) + t(8 - 10\sin^2\phi_s) + t^2(24 - 23\sin^2\phi_s)\right] \qquad \text{(II-14)}$$

where

$$B_p = \frac{(AN)(Ak^2)\left[(\epsilon_r' - 1) + (\epsilon_r'')^2\right]}{\left\{ 28\pi\left[\frac{3}{5}\left(\frac{a}{k}\right)^2 + 3(\cos\theta_i + \cos\theta_s)^2 + \right.\right.} \quad \text{(II-15)}$$
$$\left.\left. \sin^2\theta_i + \sin^2\theta_s - 2\sin\theta_i \sin\theta_s \cos\phi_s \right\}\right.$$

In these equations, A is the cross sectional area of a cylinder, N is the average number of cylinders per unit area, and $\epsilon_r' + j\epsilon_r''$ is the relative permittivity of each cylinder.

Peake has estimated the permittivity of vegetation as

$$\epsilon_r' + j\epsilon_r'' = 2.5(1-f) + f\epsilon_{rw} \qquad \text{(II-16)}$$

where f is the fraction of water by weight in the plant, and ϵ_{rw} is the relative permittivity of water. For microwave frequencies the latter parameter can be approximated by

$$\epsilon_{rw} = 5 + \frac{75}{1 - j(1.85/\lambda)} \qquad \text{(II-17)}$$

The factor t appearing in (II-14) is the transmission coefficient for the surface of a cylinder at normal incidence. It is taken to be

$$t = \frac{2}{1 + \epsilon_r'} \qquad \text{(II-18)}$$

The value of the attenuation constant appearing in (II-15) depends upon the polarization of the incident radiation. This parameter is not easily evaluated in practice. However, Peake has estimated the value of α for horizontal and vertical polarization as follows:

$$\alpha_h = k\left[\frac{3}{16} AN\epsilon_r'' \sec\theta_i\right](1+3t^2)$$

$$\alpha_v = k\left[\frac{3}{16} AN\epsilon_r'' \sec\theta_i\right]\left[(1+3t^2) + \sin^2\theta_i(1-t^2)\right] \qquad \text{(II-19)}$$

As with all scattering models, there are certain advantages and disadvantages of applying Peake's model. One of the advantages of the model is that it accounts for most of the factors known to effect the scattering cross section of vegetation: wavelength, incidence and scattering angles, water content, etc. However, the fact that the model accounts for all of these presents a disadvantage in that some of these parameters are difficult to evaluate accurately.

A serious limitation on the application of this model is the assumption that the power scattered from the ground is entirely negligible. The model is applicable only to cases for which the height and density of vegetation are greater than certain minimum values. Peake's model cannot be applied directly to the present investigation, in which the variation of scattering cross section due to variations

of soil moisture content is of interest.

Measurement of Permittivity of Soil

Since the variation of permittivity with moisture content is responsible for changes of the scattering cross section and radiometric temperature of soil, the behavior of the permittivity with varying moisture is of interest. Several investigators have measured the relative permittivity of soil at different microwave frequencies. The procedures used and results obtained by two of these are discussed below.

Measurements by Lundien

Measurements were made by Lundien [5] to determine the effects of frequency, density, moisture content, and soil type on the dielectric constant of soil. Relative dielectric constants of more than 400 samples of twelve types of soil were determined. The moisture content of the samples varied from 0% to 51.5%. Measurements were made at frequencies of 1.074, 1.125, 1.311, 1.412, and 1.499 GHz.

The technique used by Lundien employs an L-band interferometer system as illustrated in Figure II-1. Prior to making a measurement, a reference standard is placed between the antennas, and the attenuator and phase shifter of the known leg are adjusted to give a null. The reference

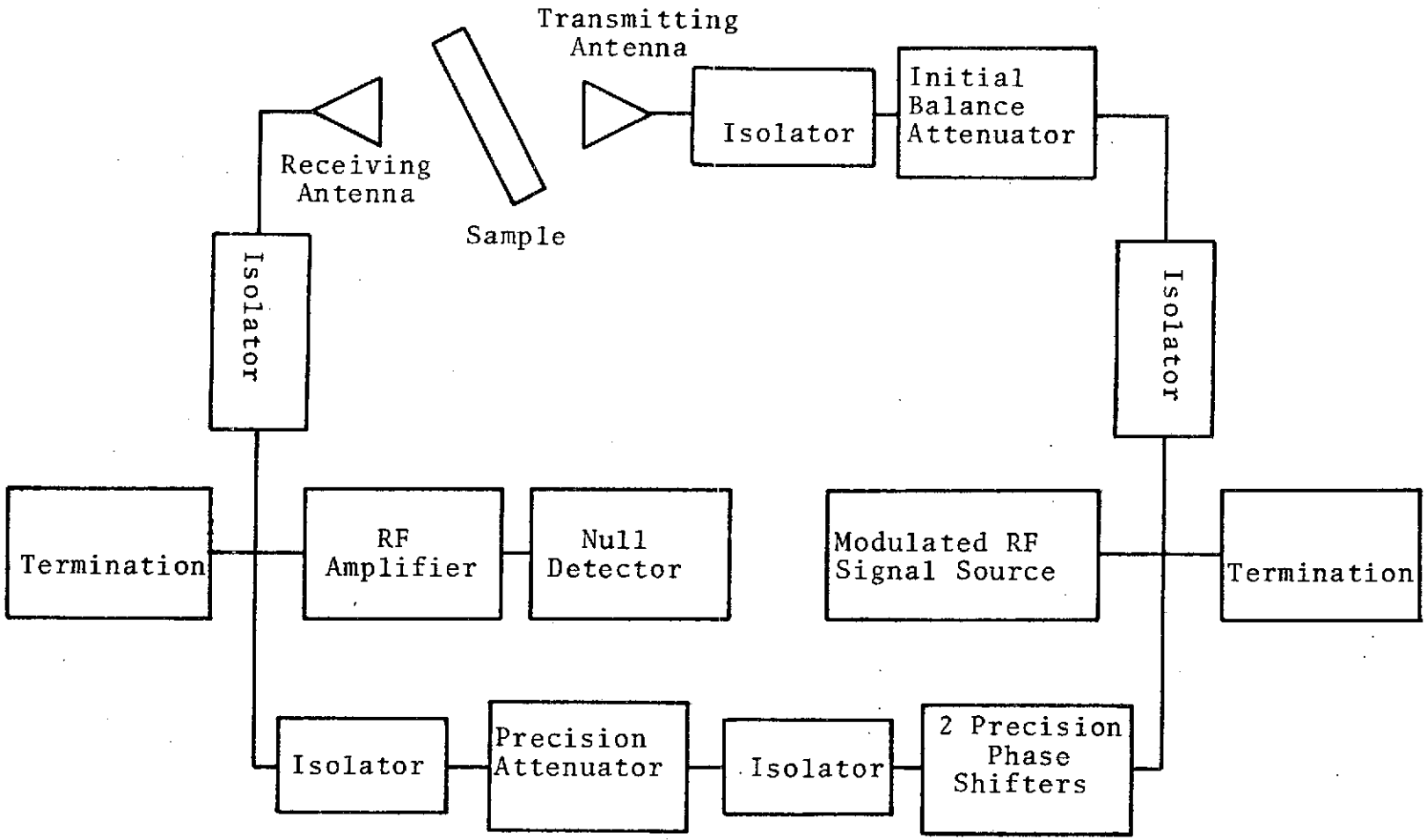

Figure II-1. Block diagram of L-band interferometer [5].

standard is then replaced by a sample of known thickness, and the circuit is again adjusted to give a null. The permittivity of the sample can be determined from the difference in attenuation and phase of the sample and the reference standard.

Inaccuracies due to multiple reflections and edge effects can be reduced or eliminated by placing the sample at an oblique angle with respect to the propagation path. Lundien used 45°, but the selection of angle is somewhat arbitrary.

Lundien determined the relative dielectric constant and the loss tangent of each sample from tables computed from the following relation:

$$|T| \exp(jT') = \frac{(1-r^2)\exp(-j\phi)}{1-r^2\exp(-j2\phi)} \qquad \text{(II-20)}$$

where T = complex voltage transmission coefficient

T' = transmission phase

r = reflection coefficient

For perpendicular polarization,

$$r = \frac{\cos\theta - \sqrt{\epsilon_r - \sin^2\theta}}{\cos\theta + \sqrt{\epsilon_r - \sin^2\theta}} \qquad \text{(II-21a)}$$

and for parallel polarization,

$$r = \frac{\epsilon_r \cos\theta - \sqrt{\epsilon_r - \sin^2\theta}}{\epsilon_r \cos\theta + \sqrt{\epsilon_r - \sin^2\theta}} \qquad \text{(II-21b)}$$

The imaginary part of the relative permittivity can be obtained as the product of the relative dielectric constant and the loss tangent.

Lundien found the behavior of the dielectric constant to be very similar for all soils tested. The relative dielectric constant increases with increasing water content from a minimum of approximately 3. Over an intermediate range of moisture levels, the relative dielectric constant of sand is generally about 15% greater than that of clay. Of course there are numerous cases which fall within the extremes.

Lundien's measurements show no relation of the dielectric constant to the compaction of the samples. Various samples were prepared with three different compactive forces: 5.74, 11.83, and 18.47 N/cm^2. The lack of variation of the data due to differing compaction seems to indicate that the dielectric constant is more dependent on the volumetric water content (grams per cubic centimeter) than on the percent moisture by weight.

Considering the data obtained for all samples, Lundien formulated an average relation between water content and relative dielectric constant as follows:

$$VWC = \frac{\epsilon_r'}{80} - \frac{0.26}{\epsilon_r' - 1} + 0.11 \qquad \text{(II-22)}$$

where VWC = volumetric water content, g/cm^3

ϵ_r' = relative dielectric constant

The range of frequencies over which Lundien measured the dielectric constant was too small to provide conclusive information about the effects of frequency on the dielectric constant. However, comparison of Lundien's results with data from a previous study [6] indicates that the dielectric constant of sand and silt is approximately constant over the range of frequencies from 0.3 GHz to 1.5 GHz. The permittivity of various soils has been measured at higher frequencies by other investigators, as discussed below.

Measurements by Wiebe

The relative permittivity of nine types of Texas soil was measured by Wiebe [7]. Several samples of each soil were prepared with different moisture contents and compaction. The results were very similar to those obtained by Lundien.

Wiebe investigated two techniques for measuring the relative permittivity. Figure II-2 illustrates the arrangement of equipment for the "free space" technique in which the sample to be measured is placed between two antennas. For the other technique, the antennas are removed and a section of waveguide inserted. A portion of the

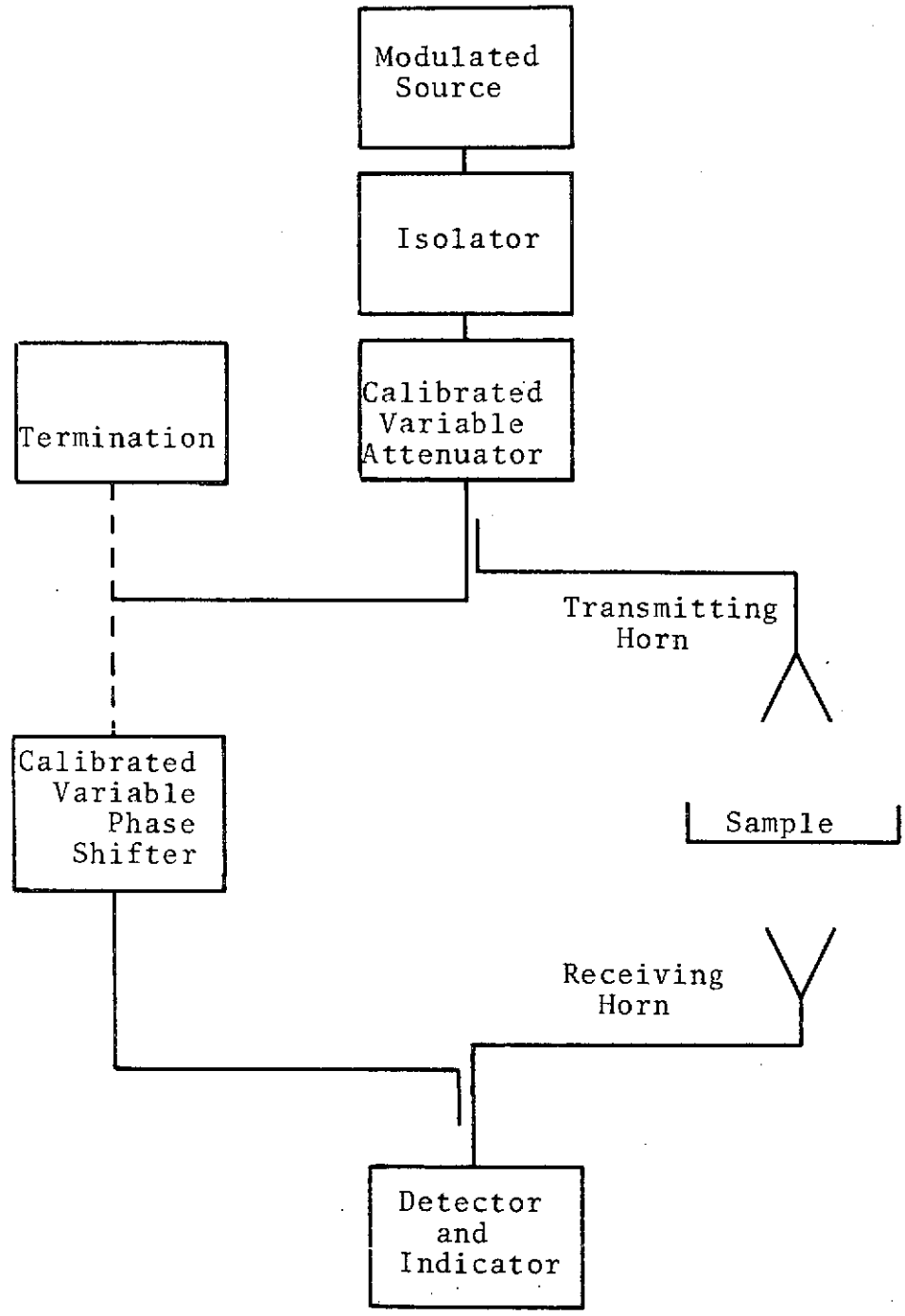

Figure II-2. Wiebe's arrangement for measuring relative permittivity of soil [7].

waveguide is removable and is used to contain the sample.

The procedure is essentially the same for both techniques. With no sample in place, the phase and attenuation are adjusted to give a convenient reference level on the indicator. When the sample is inserted, the attenuator and phase shifter are readjusted to give the same reading on the indicator. The difference in attenuation and phase from the initial settings are the attenuation and phase shift due to the sample. By varying the length of the sample, the attenuation and phase shift can be plotted as functions of sample length. The slopes of these curves give the attenuation constant α and the phase constant β. The relative permittivity of the sample is determined from one of the following sets of equations. For the free space technique,

$$\epsilon_r' = \frac{\beta^2 - \alpha^2}{\beta_o^2} \qquad \text{(II-23a)}$$

$$\epsilon_r'' = \frac{2\alpha\beta}{\beta_o^2} \qquad \text{(II-23b)}$$

where β_o is the phase constant of free space, and for the waveguide method,

$$\epsilon_r' = \frac{\beta^2 - \alpha^2 + K_c^2}{\beta_o^2} \qquad \text{(II-24a)}$$

$$\epsilon_r'' = \frac{2\alpha\beta}{\beta_o^2} \qquad \text{(II-24b)}$$

where K_c is the wave number evaluated at the cut-off wavelength of the guide.

Wiebe made measurements with both techniques at 9.0 GHz to evaluate the quality of the measurements. Satisfied that both methods gave good results, Wiebe chose to make further measurements with the waveguide method at a frequency of 10.625 GHz.

Wiebe's measurements are generally consistent with those of Lundien. The behavior of the permittivity as a function of moisture content is essentially the same for all soils tested. In addition, the permittivity of sand is found to be 15% to 20% greater than that of clay over an intermediate range of moisture.

By measuring the samples immediately after wetting and after 24 hours of curing, Wiebe was able to show the change of permittivity due to adsorption of water. The permittivity is highest immediately after wetting, when most of the water is still in a free state. The effective permittivity of bound water is less than that of free water. Therefore, as more water molecules adhere to the soil, the average permittivity of the water decreases, thereby decreasing the permittivity of the soil-water mixture.

Some of Wiebe's data show more dependence on

compaction than Lundien's data. The apparent difference may be due to the fact that Wiebe used percent moisture content (by weight) as a measure of water content of a sample rather than volumetric water content, as used by Lundien.

Ground-Based Measurement of the Apparent Temperature of Smooth Sand

Having knowledge of the permittivity of sand, Richerson [8] performed an experiment to test the accuracy of Peake's model for apparent temperature. A specialized form of Peake's model was used to predict the apparent temperature of a smooth bed of sand for various moisture contents. Data were obtained with a 31.4 GHz radiometer mounted on a small tower adjacent to the test surface.

Richerson modified Peake's model by inserting the relation

$$\gamma_{ii}(o,s) = 4\pi|R_i|^2(\csc\theta_o)\,\delta(\theta_s-\theta_o)\,\delta\left(\theta_s-\theta_o-\frac{\pi}{2}\right)$$

for the differential scattering coefficient of a smooth surface, into (II-3). It follows that the albedo of the smooth surface is

$$A_i(\theta_o,\Phi_o) = |R_i(\theta_o)|^2 \qquad \text{(II-25)}$$

where $R_i(\theta_o)$ is the Fresnel reflection coefficient. In addition, Richerson added a third term to (II-11) to

account for radiation of the atmosphere between the surface and the radiometer.

The measured apparent temperatures were not in good agreement with predictions. The moisture content of surfaces for which results were reported varied from 7.56% to 13.2%. Over this range of moisture there was no significant change of apparent temperature.

Several reasons for the discrepency between theoretical and measured apparent temperatures can be cited. By considering the effects of a non-ideal antenna pattern, Richerson was able to predict smaller variations of apparent temperature due to moisture. Furthermore, Richerson pointed out that the short wavelength (9.55 mm) sensor is very sensitive to surface characteristics. Not only did roughness effect the measurements, but drying of the soil at the surface caused significant changes in the apparent temperature.

Experiments similar to Richerson's have been performed by other investigators with active systems. The results of the experiment described below show more clearly the effect of surface roughness at various frequencies.

Ground-Based Measurement of the Reflectivity of Moist Soil

Stiles, et al. [9], measured the power reflectivity of

some test surfaces with various moisture contents to determine whether moisture content could be monitored by radar. Measurements were made with a swept-frequency system with a frequency range of 4.0 to 26.5 GHz. The results show a definite relation between moisture content and reflectivity. However, measurements of rough surfaces indicate an "apparent moisture" less than the actual moisture content.

Data obtained from smooth sand at 6.0 GHz show a definite increase of reflectivity with increasing moisture content. The relation is apparently linear. A similar relation is evident at 26 GHz, but the reflection coefficient does not increase as rapidly (as a function of moisture) as at the lower frequency.

The reflectivity of a rough surface is lower than that of a smooth surface for all frequencies. However, the difference between reflectivity of smooth and rough surfaces is much greater at higher frequencies. The roughest surface tested by Stiles had a reflection coefficient of 0.28 at 8 GHz and 0.04 at 26 GHz, while the reflection coefficient of the smooth surface was almost constant at 0.36 over the same frequency range. These data emphasize the fact that there is no absolute scale for roughness. Any rough surface may be considered smooth for sufficiently long wavelengths.

The results of the experiment prove the possibility of

monitoring the moisture content of smooth surfaces with radar. However, the difficulty of remotely measuring the moisture content of an arbitrarily rough surface is also apparent.

Airborne Measurements of Apparent Temperature

To better determine the feasibility of measuring soil moisture content with passive microwave sensors, personnel of NASA/Goddard Space Flight Center have conducted flights over selected agricultural test sites to gather microwave radiometer data. Ground support data for each flight included the moisture content of several soil samples from each field along the flight line. The data from two such flights have been analyzed at Texas A&M University to determine the correlation of apparent temperature with moisture content.

Apparent Temperatures of Bare Fields

Data obtained from Weslaco, Texas, were analyzed by Jean [10]. The data included apparent temperatures measured at 1.42, 2.69, 4.99, and 10.69 GHz. The fields at Weslaco were rough but not vegetated. The moisture content varied from 6.7% to 35%.

To quantify the correlation of apparent temperature with moisture content, Jean computed a rank difference

coefficient of correlation for each set of data. This coefficient is defined by

$$\rho = 1 - \frac{6 \sum_{i=1}^{n} (u_i - v_i)^2}{n(n^2 - 1)}$$

where u_i = rank of the element x_i in data set {X}

v_i = rank of the element y_i in data set {Y}

n = number of pairs of data $\{x_i, y_i\}$

Considering the values of the correlation coefficient for each data set, the 2.69 GHz data showed the best correlation and the 1.42 GHz data the next best. However, none of these showed a strong correlation.

To illustrate graphically the correlation of apparent temperature with moisture, Jean plotted the average apparent temperature of each field as a function of the average moisture content. Figure II-3 is an example of the results. The data are from the horizontal channel of the 1.42 GHz sensor. The straight line was fit by a least squares technique. The slope of the lines is -1.2°K per percent moisture.

The data presented by Jean clearly indicate the potential for remote measurement of soil moisture in bare fields. However, similar results have not yet been obtained for vegetated fields.

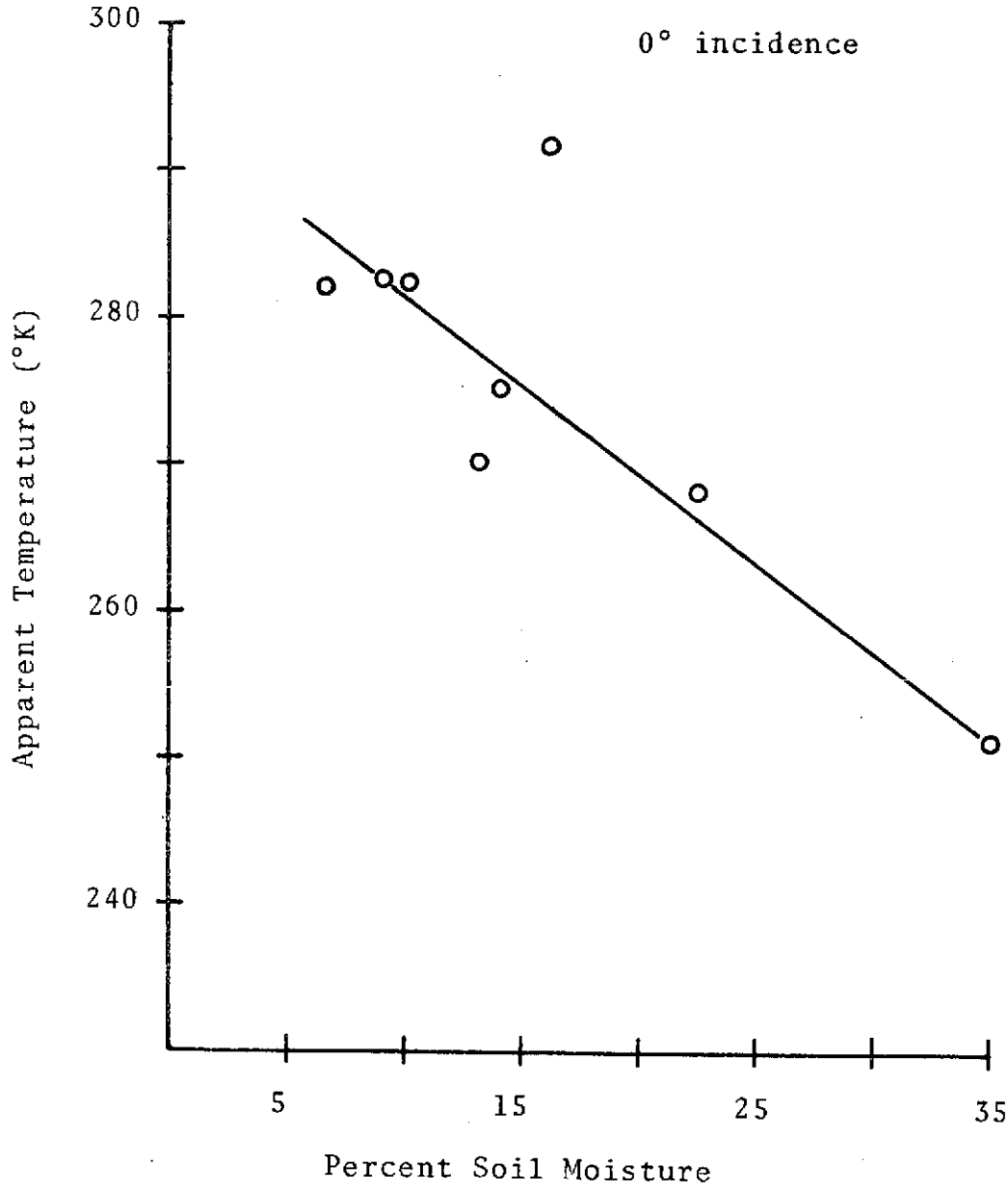

Figure II-3. Average apparent temperature at 1.42 GHz for fields at Weslaco, Texas [10].

Apparent Temperatures of Vegetated Fields

An analysis similar to Jean's has been performed by Kroll [11] on data obtained from Chickasha, Oklahoma. The data include apparent temperatures measured at 1.42, 4.99, 10.69, and 37 GHz.

The surface conditions of the test fields at Chickasha were quite different from those at Weslaco. The fields at Chickasha were relatively flat. Furthermore, most were covered with young wheat varying in height up to about 25 cm.

Figure II-4 is a plot of apparent temperature versus moisture content for the 1.42 GHz data. There is no clear relation between moisture and apparent temperature. This may be due partly to the limited range of moisture available. However, it may be that the effects of the vegetation suppress the effects of varying moisture in the soil.

The theories and experimental results presented in this chapter are not adequate to describe emission and scattering from soil beneath a plant canopy. The difficulty of predicting quantitatively the apparent temperature of even a smooth surface of known permittivity has been shown . However, other experimental data indicate that the apparent temperature of bare soil is indeed a function of moisture content. An attempt to predict the apparent temperature of some simple vegetated surfaces is discussed in

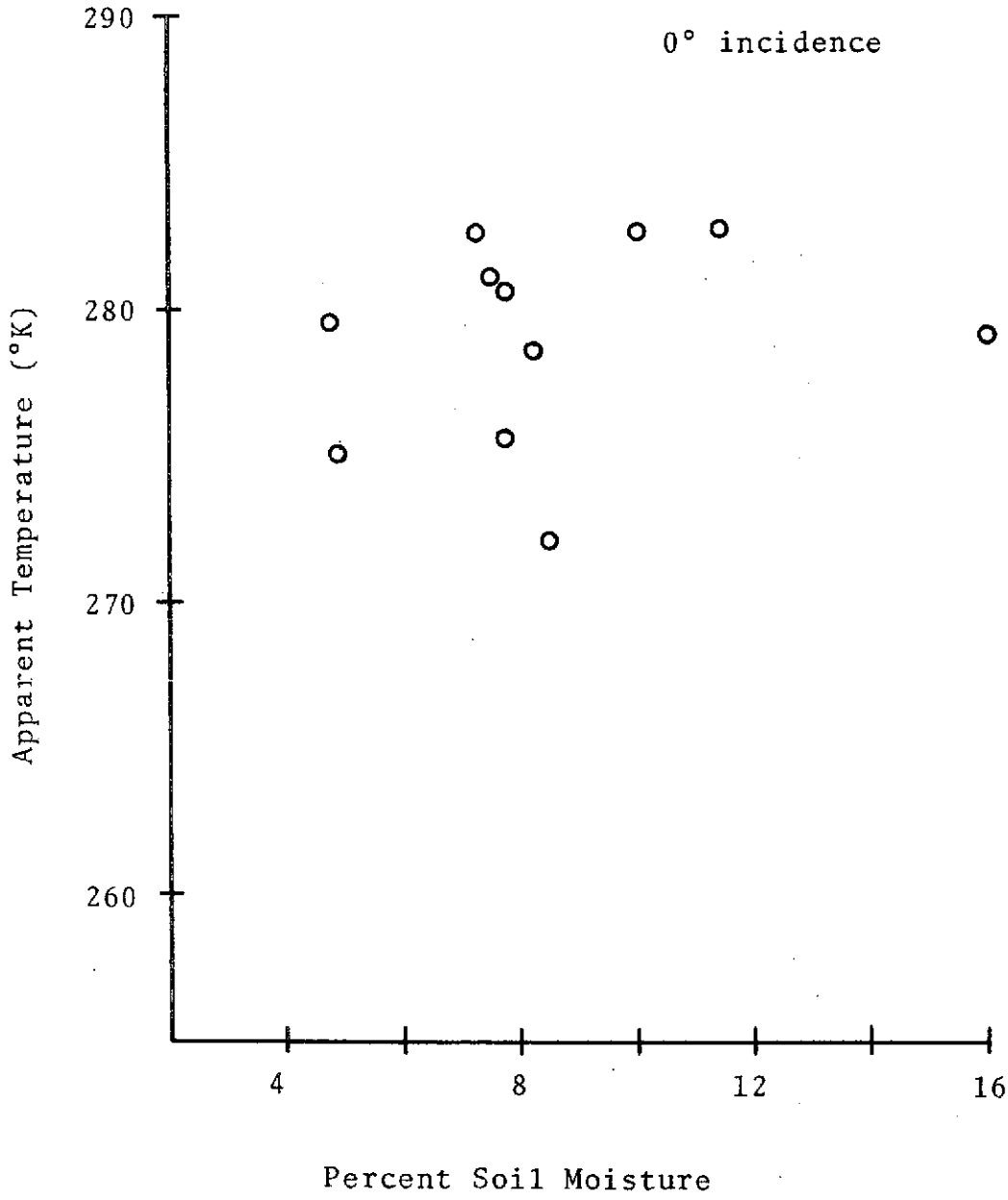

Figure II-4. Average apparent temperature at 1.42 GHz for fields at Chickasha, Oklahoma.

the following chapter.

CHAPTER III

APPARENT TEMPERATURE OF VEGETATED TERRAIN

The apparent temperature of any object is a measure of the thermal radiation emanating from the body in a particular direction with a particular polarization. For microwave frequencies the apparent temperature is related to the radiant power through the Rayleigh-Jeans approximation of Planck's Blackbody Radiation Law [2],

$$I_o = \frac{kT\Delta f}{\lambda^2} \quad \frac{\text{watts}}{m^2(\text{steradian})} \tag{III-1}$$

where k = Boltzmann's constant

T = temperature in degrees Kelvin

Δf = a narrow band of frequencies

λ = a wavelength of center frequency

Only for a blackbody, that is, an ideal absorber, does (III-1) give the relation between the thermal radiation and the actual temperature of the body. For any real object the temperature T of (III-1) is the apparent temperature, but is not the actual temperature of the body.

The apparent temperature of vegetated terrain results from contributions of radiation from several sources. The most significant contribution is the thermal emission from the ground. In general this contribution includes

radiation from both the soil and the vegetation. A second contribution is from part of the diffuse radiation of the atmosphere which is scattered by the ground toward the sensor. Scattering may be due to both soil and plants. Another contribution may be due to the scattering of radiation from quasi-point sources into the antenna beam. This contribution is usually negligible [2]. The final contribution to the apparent temperature of the ground is from the radiation of the atmosphere between the ground and the sensor.

The purpose of this chapter is to determine the variation of the apparent temperature of vegetated terrain as a function of soil moisture content. Calculation of the apparent temperature is facilitated by considering only thermal emission of the soil and vegetation. Atmospheric effects are discussed in Appendix B.

Elements of the Transmission Problem

The determination of the apparent temperature is primarily a problem in propagation through dielectric layers. Part of the thermal radiation which originates within the soil is transmitted across the surface of the soil into the canopy. The transmitted radiation then propagates through the canopy and into the atmosphere.

The most useful descriptors of the dielectric media

are their permittivities. These are discussed below.

Permittivity of the Soil

As noted in Chapter II, the permittivities of various types of soil have been measured at several microwave frequencies [5], [7]. For most soils a curve of relative permittivity as a function of moisture content is very similar to Figure III-1. Although the permittivity is a function of frequency, data presented by Wiebe [7] indicate that the change in permittivity over the frequency range from 1.42 GHz to 31.4 GHz is no more than might be caused by a variation in soil type. Therefore, the curves of Figure III-1 may be assumed to represent the relative permittivity of some particular soil at any particular frequency in that range.

Permittivity of Vegetation

It is not surprising that the permittivity of vegetation is also a function of water content, since plants are composed largely of water. From observation of X-band data, Peake and Oliver [12] have formulated the following approximation for the permittivity of vegetation:

$$\epsilon_v = \left(\frac{F}{2}\right) \mathcal{R}e(\epsilon_w) + j\left(\frac{F}{3}\right) \mathcal{I}m(\epsilon_w) \qquad \text{(III-2)}$$

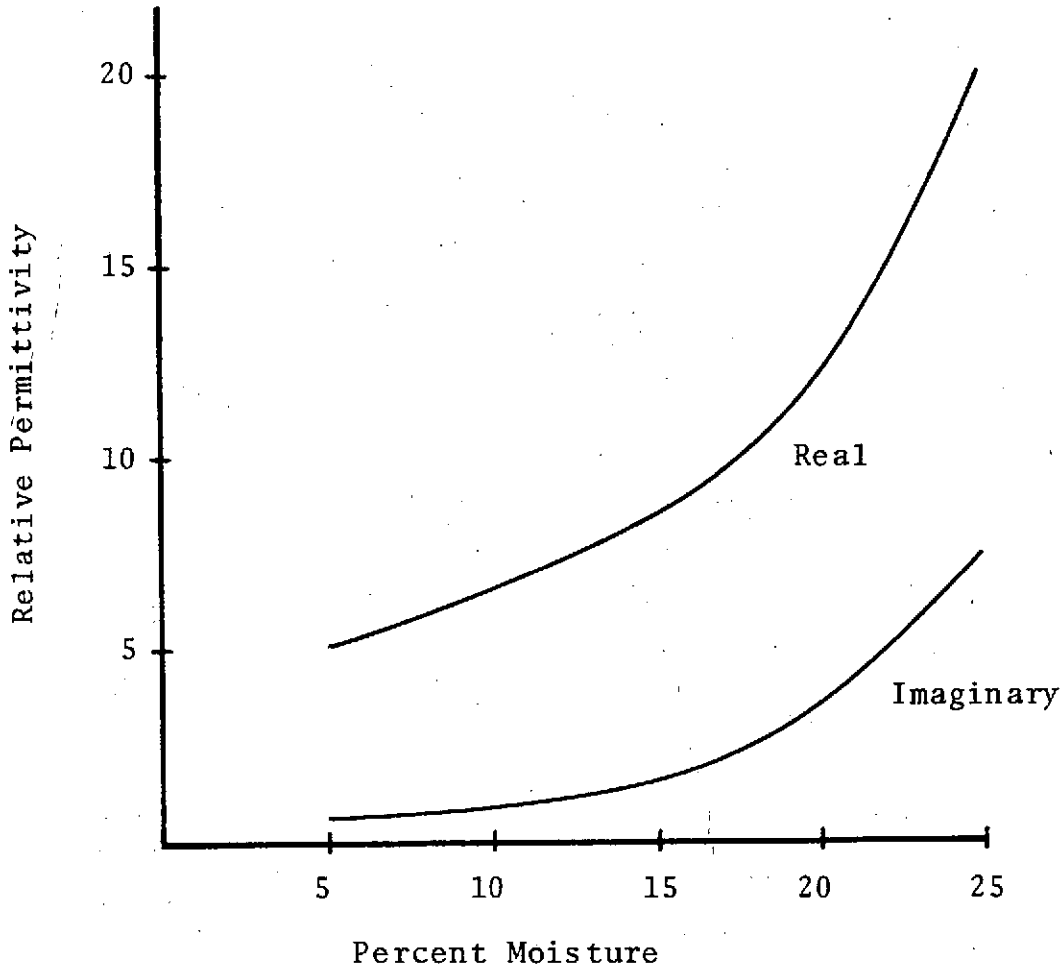

Figure III-1. Relative complex permittivity of a typical soil at microwave frequencies.

where F = fraction of water by weight in the plant

ε_w = permittivity of water

This approximation is valid only for frequencies above 1 GHz, in which case the ionic conductivity of dissolved salts is negligible [12].

Water has been found by experiment to exhibit Debye type relaxation [13]. Debye relaxation is defined by the exponential behavior of the displacement current in a dielectric to which an electric field is suddenly applied [14]. This behavior is expressed as

$$D(t>0) = \epsilon_\infty E + (\epsilon_s - \epsilon_\infty)\left(1 - e^{-\frac{t}{T}}\right)E \qquad \text{(III-3)}$$

where ε_∞ = instantaneous dielectric constant

ε_s = static dielectric constant

T = relaxation time

If an electric field having sinusoidal time variation is applied to such a dielectric, the complex permittivity is

$$\epsilon = \epsilon_\infty + \frac{\epsilon_s - \epsilon_\infty}{1 + j2\pi f T} \qquad \text{(III-4)}$$

For application to water at microwave frequencies it is convenient to convert $2\pi T$ to an equivalent frequency. Thus, (III-4) may be written

$$\epsilon = \epsilon_\infty + \frac{\epsilon_s - \epsilon_\infty}{1 + j\left(f/f_o\right)} \qquad \text{(III-5)}$$

The high frequency dielectric constant ε_∞ is constant, but the static dielectric constant ε_s and the relaxation frequency f_o are functions of temperature. There is some disagreement about the value of ε_∞, but 5.5 is acceptable [13]. The static dielectric constant is

$$\varepsilon_s = 87.7 - 0.4(T-273)$$

where T is the temperature in degrees Kelvin. For temperatures between 273°K and 303°K, f_o is approximated by

$$f_o = 9.0 + 0.405(T-273) \text{ GHz}$$

Using these parameters in (III-5) yields the value of ε_w for (III-2).

Permittivity of a Dielectric Mixture

The permittivity given by (III-2) is that of the plant material only. The canopy above the soil is a mixture of vegetation and air. Since the canopy is treated as a single medium in the analysis which follows, it is necessary to determine the permittivity of the plant-air mixture.

A model applicable to the present case is the Weiner model for a dielectric mixture as presented by Evans [15]. The relative permittivity of the mixture is related to the relative permittivities of the constituent media through the formula,

$$\frac{\epsilon_m - 1}{\epsilon_m + u} = p \cdot \frac{\epsilon_1 - 1}{\epsilon_1 + u} + (1-p)\frac{\epsilon_2 - 1}{\epsilon_2 + u} \qquad \text{(III-6)}$$

in which p is the fraction of the total volume occupied by medium 1.

The parameter u in (III-6) is called the Formzahl. This parameter describes the dispersion of one medium within the other. The value of u may be any non-negative number. The significance of several values of the Formzahl is illustrated in Figure III-2. It seems very difficult to select an appropriate value of u for a plant canopy. However, Figure III-3 illustrates that the selection of u is not critical in the range u = 10 to u = 25, since the relative dielectric constant varies by only about 15% around the mean value.

The derivation of an explicit expression for ϵ_m is facilitated by assuming that medium 2 is air with relative permittivity equal to unity. Thus, the last term of (III-6) vanishes, leaving

$$\frac{\epsilon_m - 1}{\epsilon_m + u} = p \frac{\epsilon_1 - 1}{\epsilon_1 + u}$$

which leads to

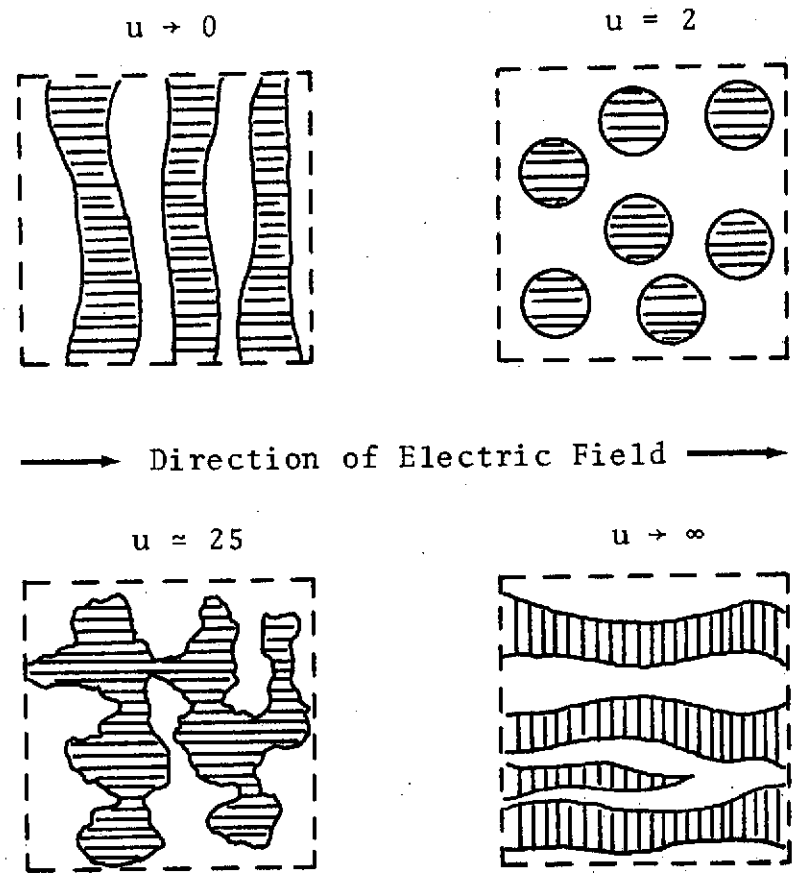

Figure III-2. Various types of mixture represented by the Formzahl. (After Evans [7])

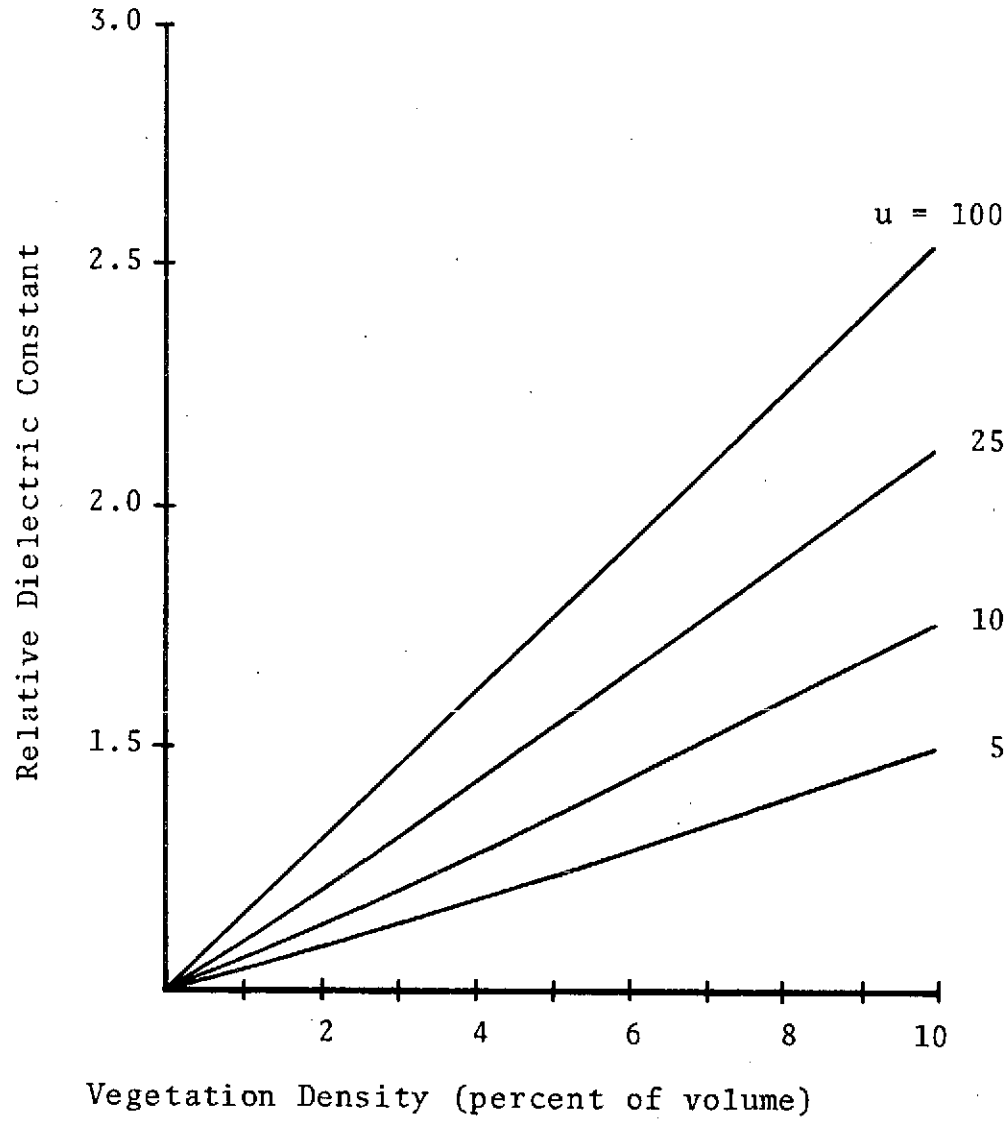

Figure III-3. Relative dielectric constant of a plant canopy for various values of the Formzahl.

$$\epsilon_m = \frac{\epsilon_1(1+pu) + u(1-p)}{\epsilon_1(1-p) + p + u} \qquad \text{(III-7)}$$

where ϵ_1 is the relative permittivity of the vegetation, and p is the fraction of the canopy volume which is occupied by vegetation.

Smooth, Uniformly Vegetated Surface

The simplest model for vegetated ground is a smooth surface covered by a continuous canopy of uniform height. The soil is assumed homogeneous with permittivity as illustrated in Figure III-1 (p. 37). The plant canopy is represented by a homogeneous dielectric layer with permittivity as given by (III-7). The atmosphere is assumed lossless and nonradiating.

Three processes determine the apparent temperature of the vegetated ground. First a portion of the thermal radiation incident on the surface from below is transmitted across the boundary toward the sensor. The transmitted field experiences attenuation as it propagates through the canopy. Finally, the thermal radiation from the canopy augments the radiation from the surface which propagates through the canopy.

Transmission Coefficient

The power radiated into the plant canopy is equal to the power incident on the surface from below times the transmission coefficient of the surface. The transmission coefficient is defined by

$$T_i = \frac{\text{Power transmitted with polarization i}}{\text{Power incident with polarization i}}$$

and can be expressed in terms of the permittivities of the two media. For this derivation the second medium is assumed to be air, since it is usually air which forms the boundary with the soil.

The relation between the incident and transmitted fields is shown in Figure III-4 for vertical and horizontal polarizations. The angles θ and ψ are related by Snell's law of refraction [16],

$$v_2 \sin\psi = v_1 \sin\theta \qquad \text{(III-8)}$$

where v_2 = velocity of propagation in air

v_1 = velocity of propagation in soil

The velocity of propagation in air may be assumed equal to the free space velocity of light. The velocity of propagation in soil is

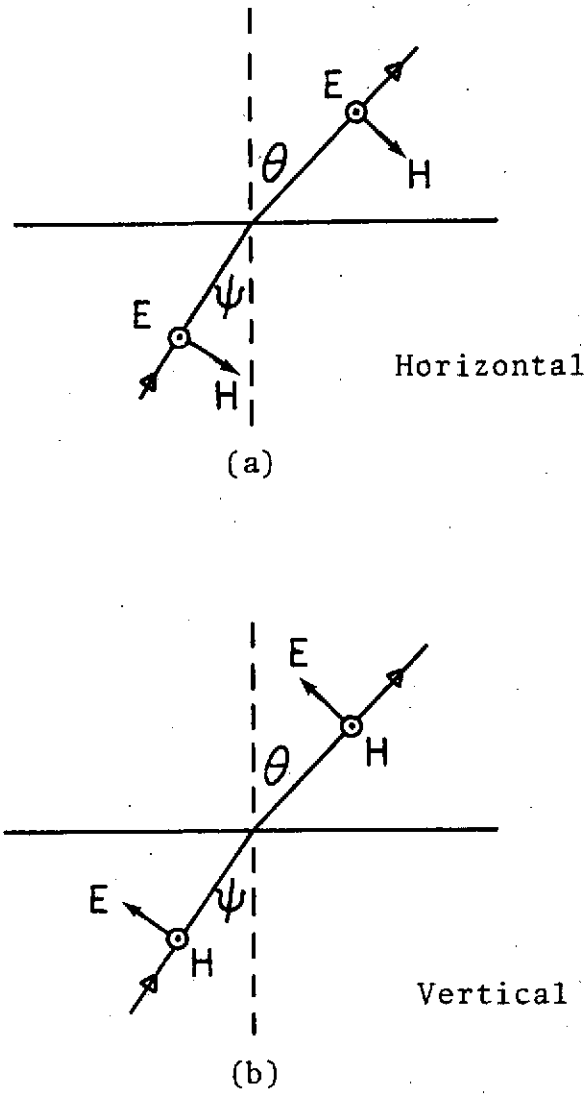

Figure III-4. Orientation of incident and transmitted fields.

$$V_1 = \left[\sqrt{\frac{\mu\epsilon'}{2}\left(\sqrt{1 + \left(\epsilon''/\epsilon'\right)} + 1\right)} \right]^{-1}$$

where ϵ' = real part of permittivity

ϵ'' = imaginary part of permittivity

The incident and transmitted power densities (watts/square meter) are determined by Poynting's theorem [17],

$$\bar{\mathcal{P}}_{Avg} = \frac{1}{2}\mathcal{R}e\left[\bar{E} \times \bar{H}^*\right]$$

For the case of horizontal polarization [Figure III-4(a), p. 45] the incident fields are

$$\bar{E}_1 = E_1 \hat{x}$$

$$\bar{H}_1 = \left(\frac{E_1}{\eta_1}\cos\psi\right)\hat{y} - \left(\frac{E_1}{\eta_1}\sin\psi\right)\hat{z}$$

where $\eta_1 = \sqrt{\mu/\epsilon}_1$ is the intrinsic impedance of the soil. Performing the cross multiplication leads to

$$\bar{\mathcal{P}}_{Avg} = \frac{1}{2}\mathcal{R}e\left[E_1\left(\frac{E_1}{\eta_1}\right)^*\left(\hat{y}\sin\psi + \hat{z}\cos\psi\right)\right]$$

or

$$\left|\bar{\mathcal{P}}_{Avg}\right| = \frac{1}{2}\left|E_1\right|^2 \mathcal{R}e\left(\frac{1}{\eta_1}\right) \qquad \text{(III-9)}$$

for the incident power density. The power incident upon a surface element dS is

$$P_{Avg} = \frac{1}{2}|E_1|^2 \mathcal{R}e\left(\frac{1}{\eta_1}\right) dS \cos\psi \qquad \text{(III-10)}$$

The transmitted fields are

$$\bar{E}_0 = \tau_H E_1 \hat{x}$$

$$\bar{H}_0 = \frac{\tau_H E_1}{\eta_0}\left(\hat{y}\cos\theta - \hat{z}\sin\theta\right)$$

where τ_H is the transmission coefficient for the horizontally polarized electric field.

$$\tau_H = \frac{2\sqrt{\epsilon_1}\cos\psi}{\sqrt{\epsilon_1}\cos\psi + \sqrt{\epsilon_0}\cos\theta} \qquad \text{(III-11)}$$

Applying Poynting's theorem yields

$$\bar{\mathcal{P}}_{Avg} = \frac{1}{2}\mathcal{R}e\left[\tau_H E_1\left(\frac{\tau_H E_1}{\eta_0}\right)^*\left(\hat{y}\sin\theta + \hat{z}\cos\theta\right)\right]$$

or

$$\left|\bar{\mathcal{P}}_{Avg}\right| = \frac{1}{2}|E_1|^2|\tau_H|^2\left(\frac{1}{\eta_0}\right) \qquad \text{(III-12)}$$

for the transmitted power density. The power transmitted from a surface element dS is

$$P_{Avg} = \frac{1}{2}|E_1|^2|\tau_H|^2\left(\frac{1}{\eta_0}\right) dS\cos\theta \qquad \text{(III-13)}$$

The desired transmission coefficient is simply the ratio of (III-13) to (III-10).

$$T_H = \frac{|\tilde{\tau}_H|^2}{\eta_0}\left[\mathcal{R}e\left(\frac{1}{\eta_1}\right)\right]^{-1}\frac{\cos\theta}{\cos\psi} \qquad \text{(III-14)}$$

A similar analysis for the case of vertical polarization [Figure III-4(b), p. 45] leads to

$$T_v = \frac{|\tilde{\tau}_v|^2}{\eta_0}\left[\mathcal{R}e\left(\frac{1}{\eta_1}\right)\right]^{-1}\frac{\cos\theta}{\cos\psi} \qquad \text{(III-15)}$$

where

$$\tilde{\tau}_v = \frac{2\sqrt{\epsilon_0}\cos\psi}{\sqrt{\epsilon_0}\cos\psi + \sqrt{\epsilon_1}\cos\theta} \qquad \text{(III-16)}$$

Attenuation by Canopy

Since the canopy is represented as a lossy dielectric, an attenuation constant can be determined for the canopy. The attenuation constant α is defined as the real part of the complex propagation constant of the electric field.

$$\gamma = \alpha + j\beta$$

Noticing that the propagation constant is also written [17]

$$\gamma = \sqrt{j\omega\mu(\sigma + j\omega\epsilon')}$$

a solution for the attenuation constant in terms of the permittivity can be obtained. The result is

$$\alpha = \sqrt{\frac{\mu\epsilon'}{2}\left(\sqrt{1+\left(\frac{\sigma}{\omega\epsilon'}\right)^2}-1\right)} \qquad \text{(III-17)}$$

Since the ratio σ/ω is equal to the imaginary part of the permittivity, (III-17) may be written in a more convenient form.

$$\alpha = \sqrt{\frac{\mu\epsilon'}{2}\left(\sqrt{1+\left(\frac{\epsilon''}{\epsilon'}\right)^2}-1\right)}$$

where ϵ' = real part of permittivity

ϵ'' = imaginary part of permittivity

From (III-9) it is clear that the average power propagated is proportional to the square of the magnitude of the electric field. The magnitude of a field having propagated a distance D through a medium with attenuation constant α is

$$E = E_o e^{-\alpha D}$$

where E_o is the initial field strength. Therefore, the power at the same point is

$$P = P_o e^{-2\alpha D}$$

The power radiated from the soil may be represented by its apparent temperature. The apparent temperature just

above the surface is equal to the product of the ground temperature, the emissivity of the soil, and the transmission coefficient. Measurements of the apparent temperature of smooth sand [7] indicate that the emissivity is greater than 0.95. However, for a qualitative analysis such as the present, any value of emissivity may be assumed. Considering the attenuation by the canopy, the contribution of the soil to the total apparent temperature is

$$\left(T_{ai}\right)_{Soil} = T_g \varepsilon_s T_i e^{-2\alpha H \sec\theta} \qquad \text{(III-18)}$$

where T_g = ground temperature

ε_s = emissivity of soil

T_i = transmission coefficient for polarization i

H = canopy height

Radiation from Canopy

The canopy not only decreases the apparent temperature of the soil, but also contributes to the total apparent temperature through thermal emission. Although most of the radiation is emitted by the leaves of the plants, it is assumed that all points within the canopy emit radiation equally.

The contribution of the canopy to the total apparent temperature may be derived from a general expression for

the apparent temperature of a dielectric layer of thickness H. The expression is [18]

$$T_a = \int_0^H T(h)\varepsilon_\delta(h) e^{-\left[\int_h^H a(z)\sec\theta\, dz\right]} \sec\theta\, dh \qquad \text{(III-19)}$$

where $T(h)$ = temperature of medium at height h

$\varepsilon_\delta(h)$ = differential emission coefficient

$a(z)$ = power attenuation constant at height z

Assuming that the temperature, attenuation constant, and emittance are constant within the canopy, (III-19) becomes

$$(T_a)_{Canopy} = T_c\, \varepsilon_\delta \sec\theta \int_0^H e^{-2a\sec\theta(H-h)} dh$$

where α is defined by (III-17). Performing the integration leads to

$$(T_a)_{Canopy} = T_c\left(\frac{\varepsilon_\delta}{2a}\right)\left(1 - e^{-2aH\sec\theta}\right) \qquad \text{(III-20)}$$

According to Kirchhoff's law [2], if the radiating layer is in thermal equilibrium with its environment, the differential emission coefficient (radiation per unit length) is equal to the absorption coefficient, expressed in (III-20) as 2α. As stated in Chapter II, the assumption of thermal equilibrium is often violated by a plant canopy. It may be stated quite generally, however, that the emission coefficient is equal to the product of 2α and an

energy transfer factor f. Thus, (III-20) may be written

$$\left(T_a\right)_{Canopy} = T_c f \left(1 - e^{-2\alpha H \sec\theta}\right) \qquad \text{(III-21)}$$

where f < 1 represents a gain of energy by the canopy, and f > 1 represents loss of energy by the canopy.

Theoretical Predictions

For reference, the apparent temperature of a smooth soil surface is illustrated in Figure III-5. The apparent temperatures for horizontal and vertical polarizations are plotted as functions of refraction angle for two values of soil moisture content. With vertical polarization the apparent temperature has a characteristic peak at the Brewster angle. It is clear that for angles less than the Brewster angle, an increase in moisture causes a decrease in the apparent temperature.

The total apparent temperature of the vegetated surface is obtained by combining (III-18) and (III-21).

$$T_{ai} = T_g \varepsilon_s T_i e^{-2\alpha H \sec\theta} + T_c f \left(1 - e^{-2\alpha H \sec\theta}\right) \qquad \text{(III-22)}$$

Apparent temperatures computed from (III-22) are plotted as functions of soil moisture content in Figure III-6. The vegetation was assumed to occupy 5% of the

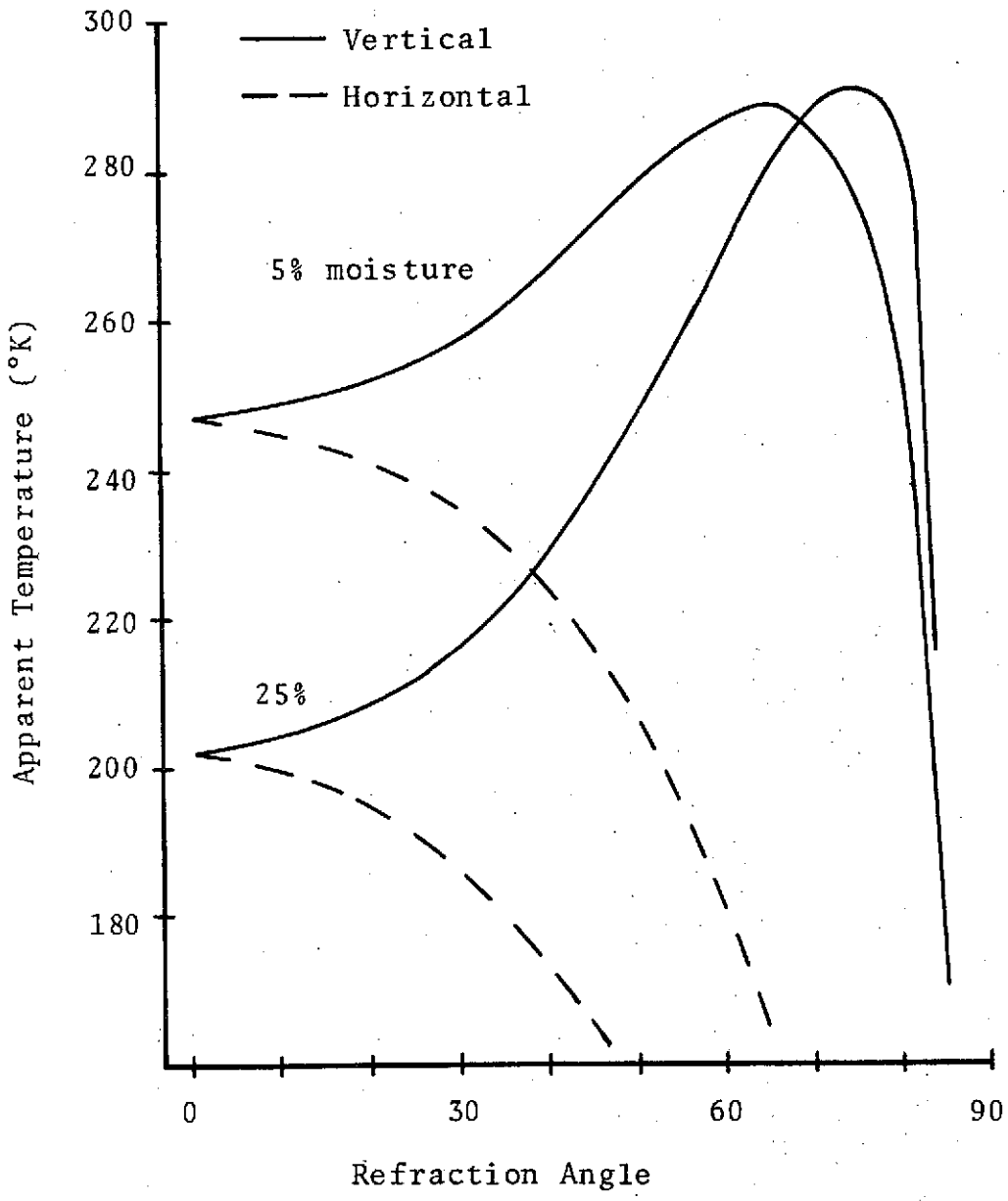

Figure III-5. Apparent temperature of smooth, bare ground.

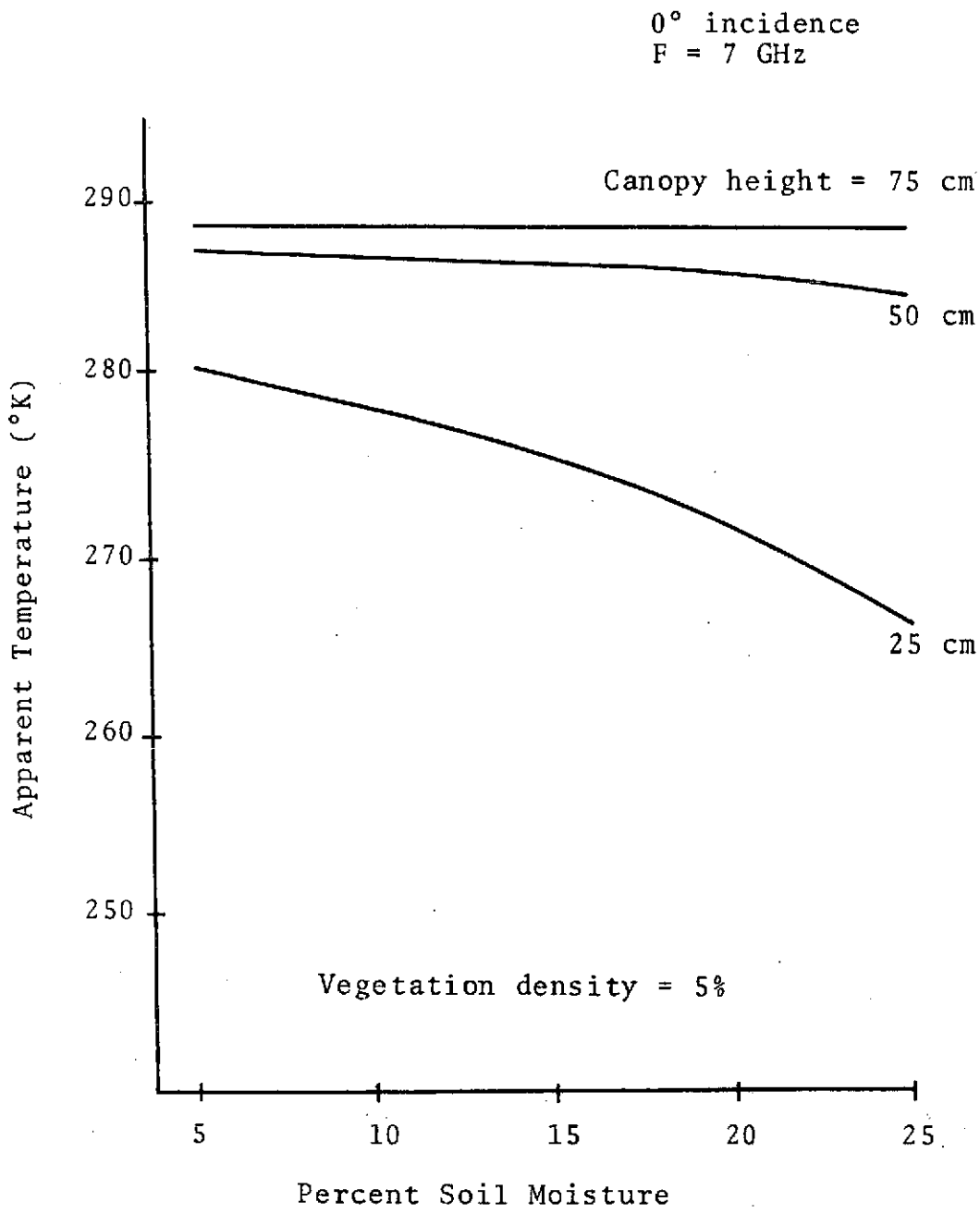

Figure III-6. Apparent temperature of uniformly vegetated surface as function of soil moisture for various canopy heights.

total volume of the canopy. The height of the canopy was varied from 25 cm to 100 cm. It is clear that increasing the height of the canopy decreases the sensitivity of the apparent temperature to variations in soil moisture.

Increasing the density of vegetation has the same effect as increasing height, as illustrated in Figure III-7. To compute the data of this figure, the canopy height was assumed to be 50 cm, and the percentage of canopy volume occupied by vegetation was varied from 1% to 10%. From observation of fields of grain sorghum and cotton, it has been determined that the density of these crops may be less than 1%. However, depending on the method of planting and amount of growth, the vegetation density may be 3% to 5%. It can be seen in Figure III-7 that as the density of vegetation increases, the apparent temperature increases and becomes less sensitive to variations of soil moisture.

The significance of the contribution of the canopy to the apparent temperature also depends on the frequency of radiation considered, as illustrated in Figure III-8. A canopy height of 50 cm is assumed. At 3 GHz the sensitivity of apparent temperature to soil moisture is approximately 1.5°C/percent moisture. At 5 GHz the sensitivity is about 0.5°C/percent moisture, and at 7 GHz the dependence on moisture is almost negligible.

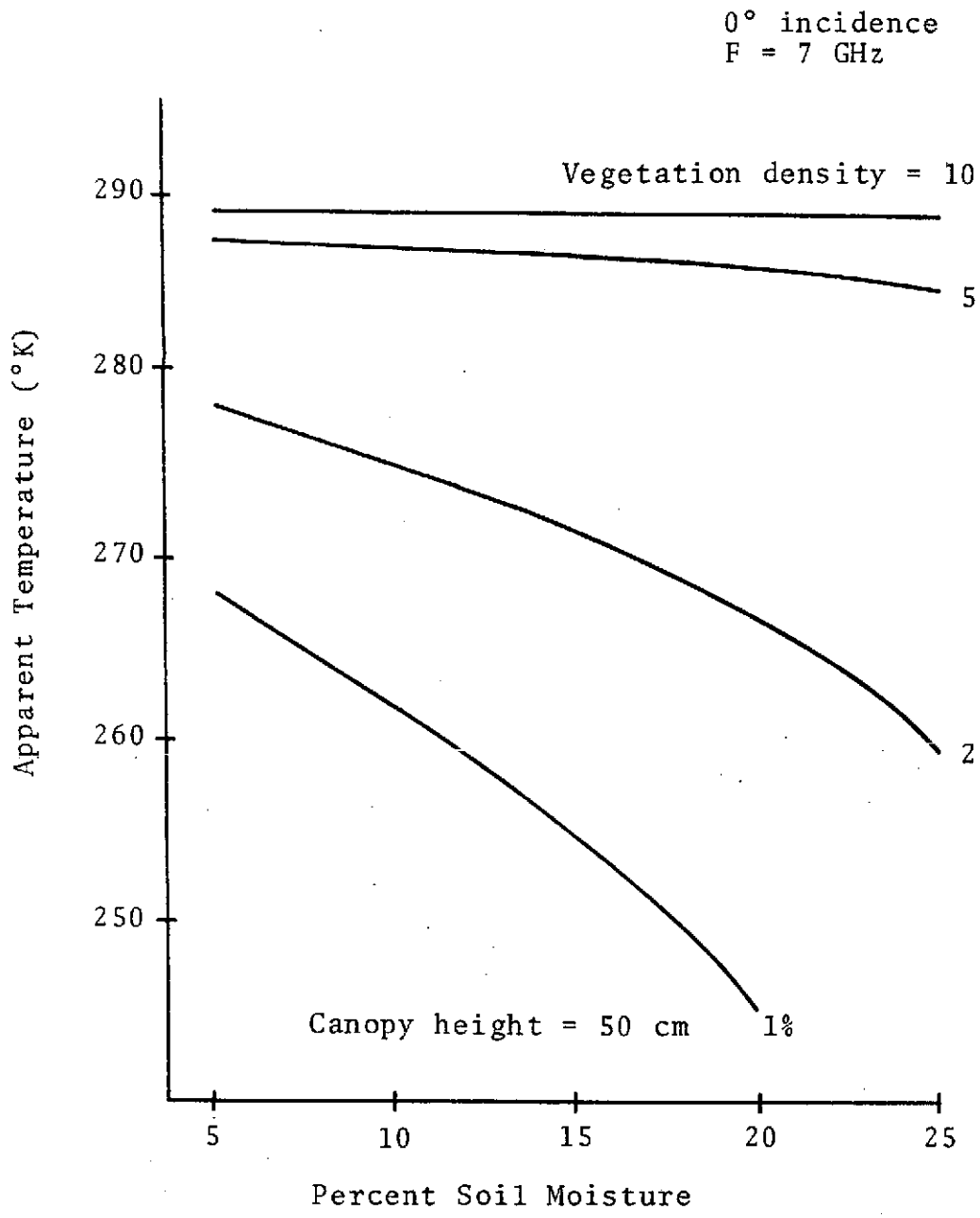

Figure III-7. Apparent temperature of uniformly vegetated surface as function of soil moisture for various densities of vegetation.

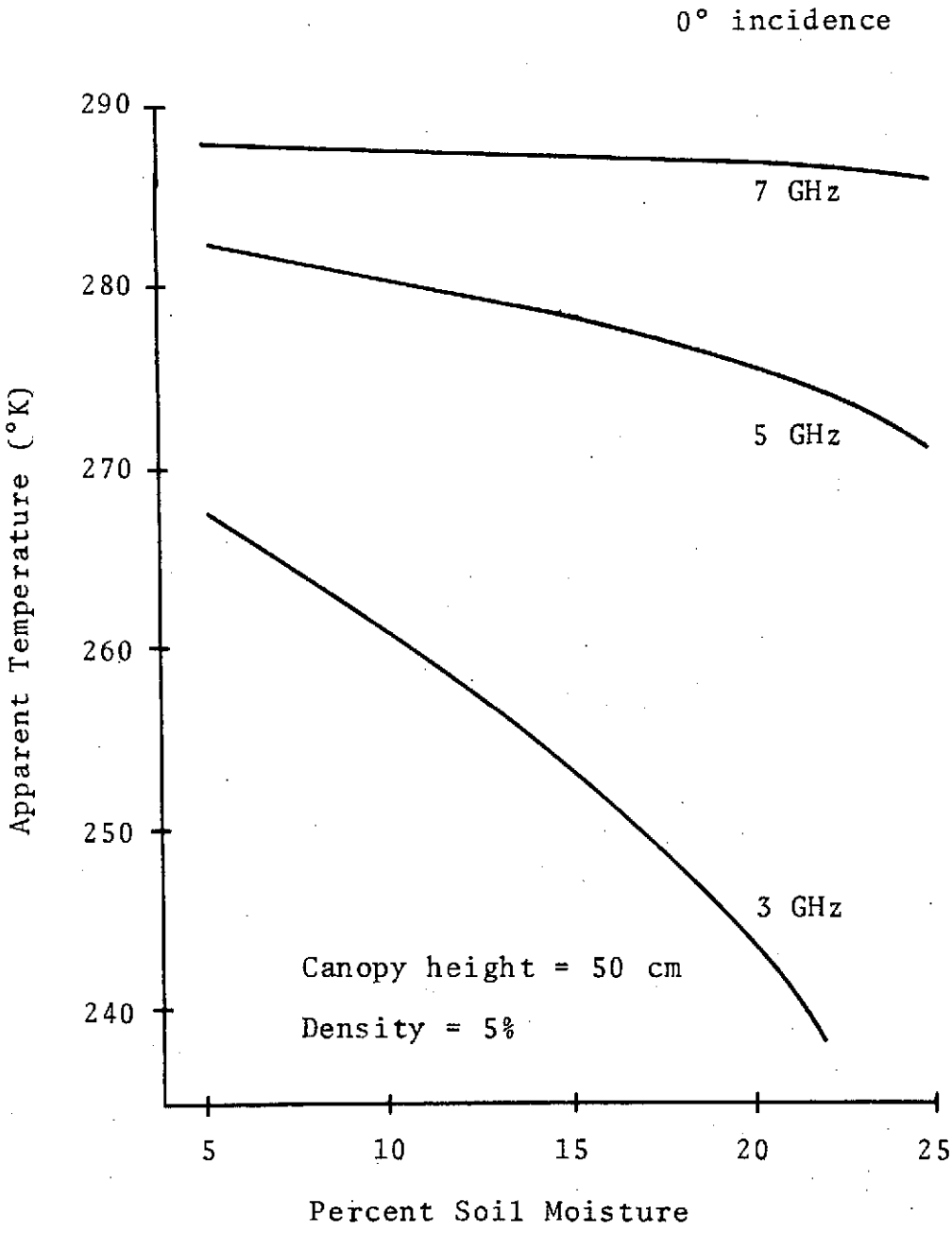

Figure III-8. Apparent temperature of uniformly vegetated surface for various frequencies.

Row Crops

An expression for the apparent temperature of row crops can be developed using the parameters derived for the case of uniform vegetation. More variables must be involved, since the apparent temperature of row crops depends not only on the height and density of vegetation, but also on the distance between rows and the angle from which the ground is observed.

The geometry of the problem is illustrated in Figure III-9. For simplicity the rows are assumed to be rectangular in cross section. The medium which comprises each row is a homogeneous dielectric with permittivity defined by (III-2) and (III-7). The surface of the soil is assumed to be an infinite plane. The direction from which the terrain is observed is defined by a refraction angle, θ, and an azimuth angle, ϕ, both of which assume only values less than or equal to $\pi/2$. The direction $\theta = 0$ is normal to the surface, and $\phi = 0$ is perpendicular to the rows.

Emission Perpendicular to Rows

Before the general form of the apparent temperature of row crops is derived, the special case of $\phi = 0$ is considered.

A cross-sectional view of a few rows is given in Figure III-10. The height and width of each row are denoted

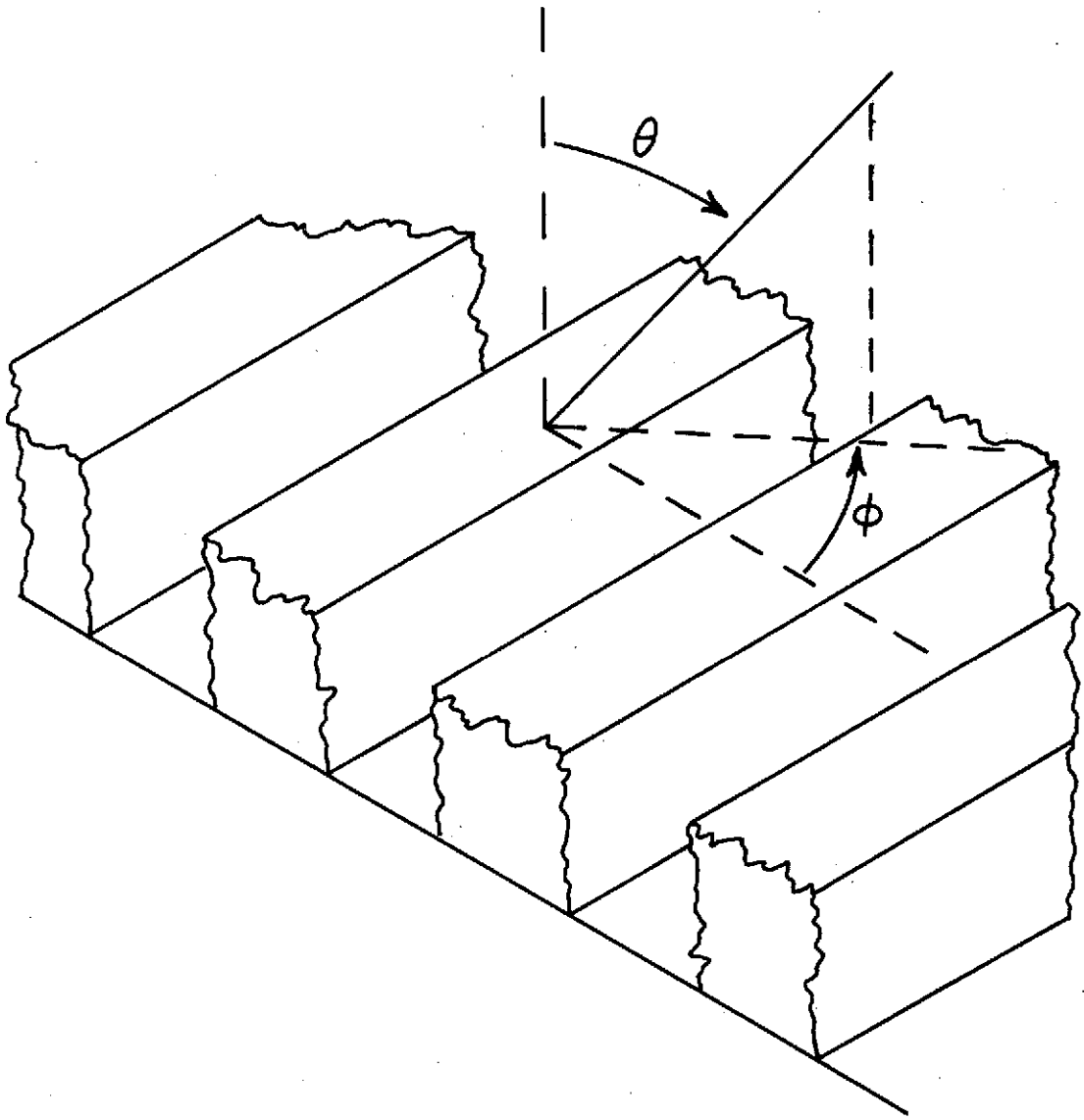

Figure III-9. Geometry for radiation from row crops.

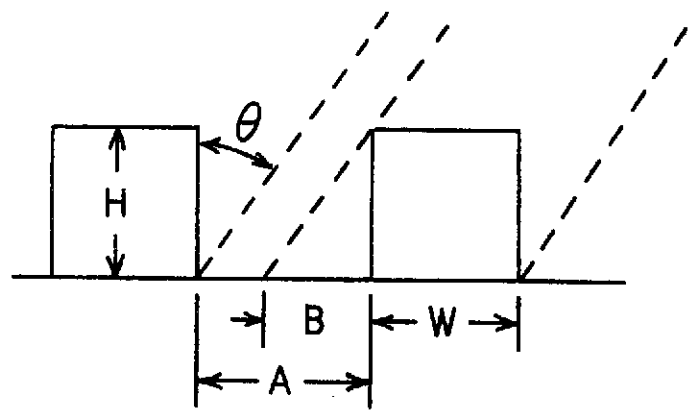

(a)

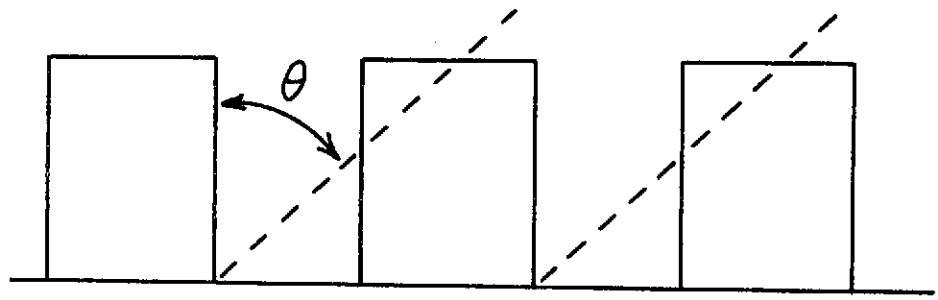

(b)

Figure III-10. Geometry for emission perpendicular to rows.

H and W, respectively. The width of the non-vegetated space between rows is denoted A. A dimension B = H tan θ is also defined.

The length (A + W) may be considered a unit length or a period. The power radiated into the direction (θ, ϕ) by any region of length (A + W) is equal to that radiated into the same direction by any other region of equal length. Therefore, the apparent temperature of a large area is equal to the average apparent temperature of the region specified in Figure III-10(a).

If B < A as in Figure III-10(a), only a portion of the radiated power experiences attenuation. The distance traversed through the canopy depends upon the point on the surface from which the radiation emerges. The average length of the path through the canopy is equal to the cross-sectional area of the canopy divided by the projection of (B + W) into a plane normal to the refraction direction.

$$d = \frac{HW}{(B+W)\cos\theta} \qquad \text{(III-23)}$$

where d is the average distance traversed through the canopy in the direction (θ, ϕ = 0).

The total apparent temperature is the average of the contributions from the bare soil and the vegetated area.

In general,

$$T_{ai} = \frac{(A - B)(T_{ai})_{Bare} + (B + W)(T_{ai})_{Veg}}{A + W} \qquad \text{(III-24)}$$

The contribution of the bare soil is simply

$$(T_{ai})_{Bare} = T_g \varepsilon_s T_i \qquad \text{(III-25)}$$

where T_g = temperature of ground

ε_s = soil emissivity

T_i = transmission coefficient for polarization i

The contribution of the region in which the soil is covered or shadowed by vegetation is given by (III-22), which is repeated here.

$$(T_{ai})_{Veg} = T_g \varepsilon_s T_i e^{-2\alpha d} + T_c f\left(1 - e^{-2\alpha d}\right) \qquad \text{(III-26)}$$

in which the attenuation distance Hsec θ has been replaced by d.

A somewhat different expression is obtained for the case in which B > A. In such a case, all of the soil is either covered or shadowed by vegetation. Consequently, the total apparent temperature is given by (III-26), and

the average attenuation distance is

$$d = \frac{HW}{(A+W)\cos\theta} \qquad \text{(III-27)}$$

Emission at Any Azimuth Angle

The formulas which express the apparent temperature of row crops for the special case of $\phi = 0$ can easily be modified for the general case, $0 \leq \phi \leq \pi/2$.

Figure III-11 illustrates the geometry for propagation through the canopy at an arbitrary angle. The dimension B is defined generally as

$$B = H(\tan\theta)(\cos\phi) \qquad \text{(III-28)}$$

The projection of the canopy cross section onto the plane of observation is HWsec ϕ. As before, the average attenuation path is expressed as this cross-sectional area divided by the projection of (B + W) onto a plane normal to the direction of observation.

$$d = \frac{HW\sec\phi}{(B+W)\sec\phi\cos\theta} \qquad \text{(III-29)}$$

$$= \frac{HW}{(B+W)\cos\theta}$$

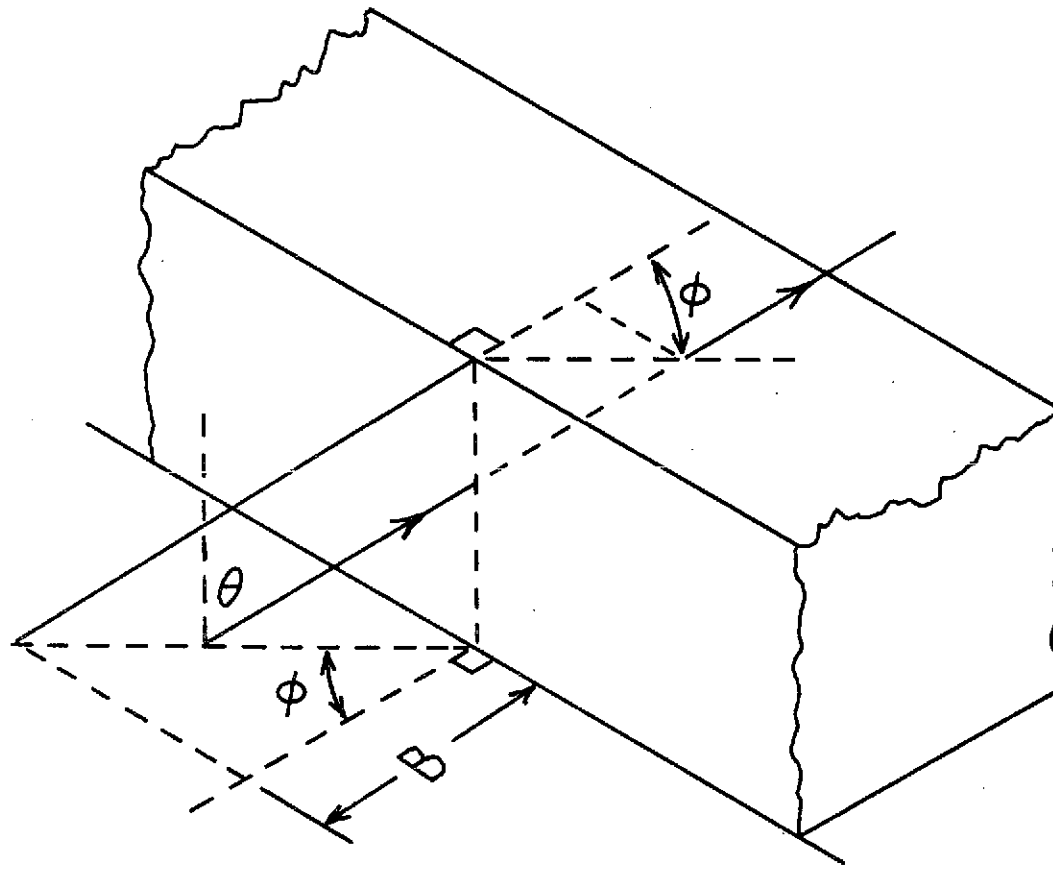

Figure III-11. Geometry for propagation through canopy at arbitrary azimuth angle.

which is identical to (III-23).

It follows that the other equations developed for the special case $\phi = 0$ also are true for the general case. Those expressions which apply when $A > B$ and those which apply when $A < B$ may be combined into a single expression by defining a special function as follows.

$$L(A,B) = B \text{ when } B < A$$

$$L(A,B) = A \text{ when } A \leq B$$

The apparent temperature of row crops may now be expressed as

$$T_{ai} = \frac{[A - L(A,B)](T_{ai})_{Bare} + [L(A,B) + W](T_{ai})_{veg}}{A + W} \qquad \text{(III-30)}$$

where the contribution of the bare soil is given by (III-25), the contribution of the vegetated soil is given by (III-26), and the average attenuation distance is

$$d = \frac{HW}{[L(A,B) + W]\cos\theta} \qquad \text{(III-31)}$$

Theoretical Predictions

The dimensions selected to describe the theoretical row crops approximate the dimensions of certain actual

crops. Fields of young cotton and grain sorghum have been observed to determine the height-width ratio of these plants. Since the standard row spacing of these crops is 40 inches, the dimension (A + W) has been set at one meter.

Apparent temperatures computed from (III-30) are plotted in Figures III-12(a) through (c) as functions of soil moisture. In general, the apparent temperature decreases as the moisture content increases. The data for both polarizations exhibit the same behavior, although the vertical polarization data are consistently higher than the horizontal data. However, as the amount of plant cover increases, the sensitivity to changes of soil moisture decreases, as well as the difference between horizontal and vertical polarization measurements.

Figures III-13(a) and (b) illustrate the dependence of the apparent temperature on the angle from which the terrain is observed. According to the model developed, vegetation causes a net increase in the apparent temperature of the ground. Therefore, the apparent temperature of row crops is greatest when measured from large refraction angles and small azimuth angles, in which cases the bare soil between rows is shadowed by the plants. The apparent temperature decreases as the azimuth angle is increased, reaching a minimum at $\phi = 90$.

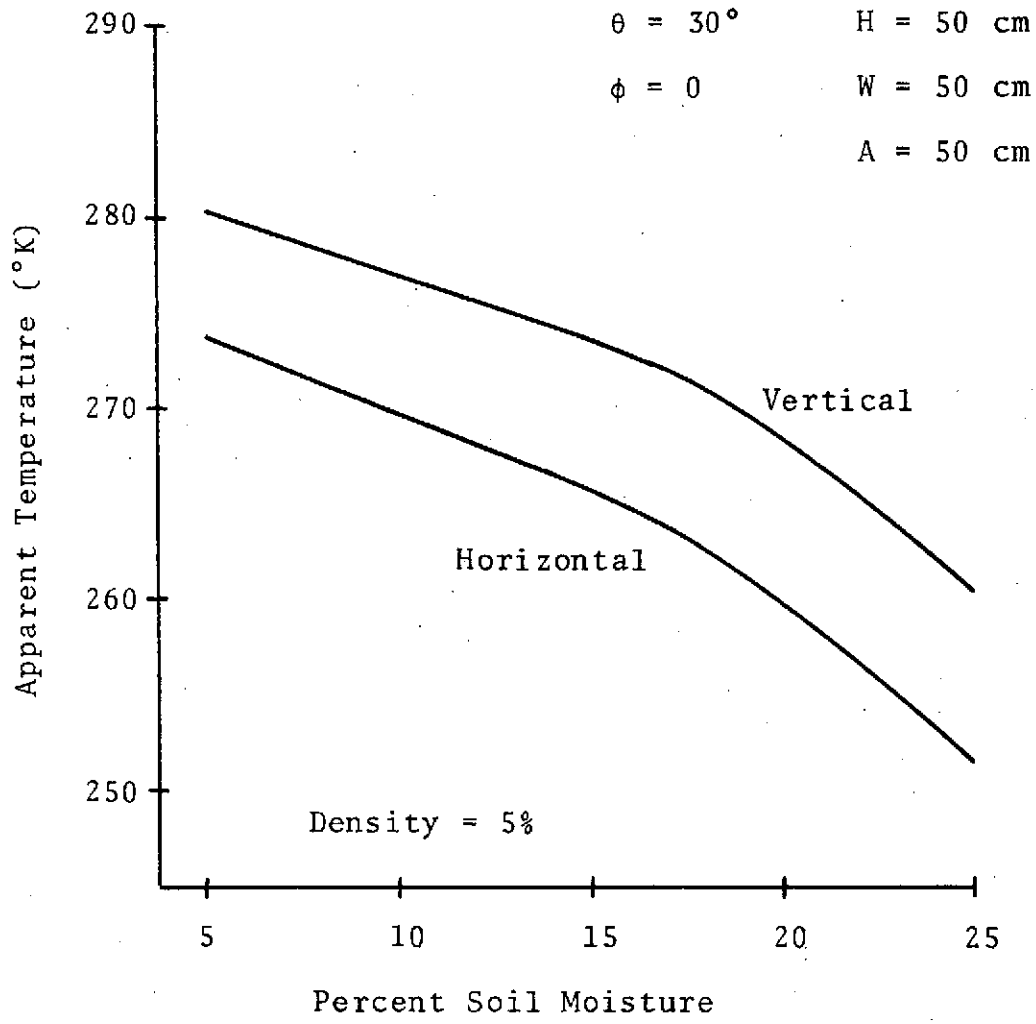

Figure III-12 (a). Apparent temperature of row crops as function of soil moisture.

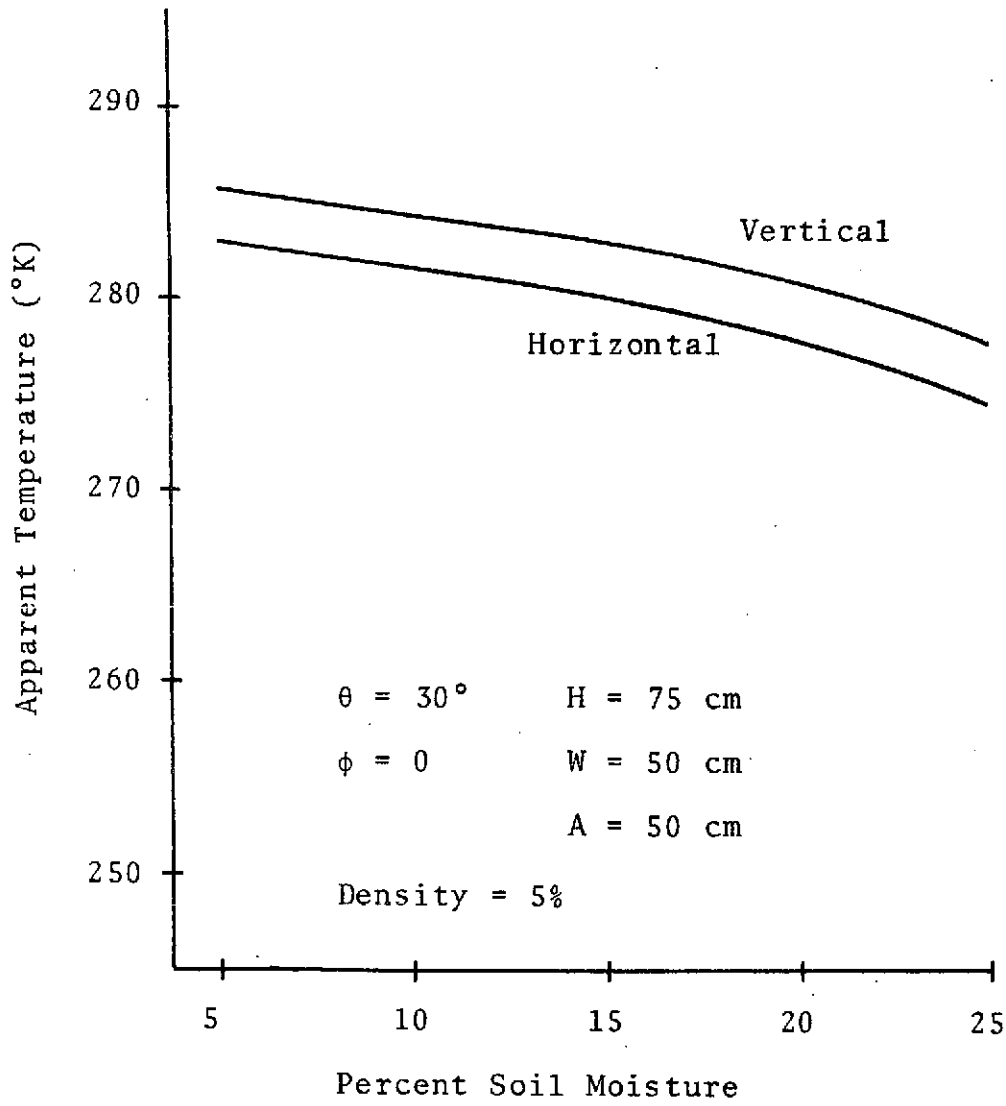

Figure III-12 (b). Apparent temperature of row crops as function of soil moisture.

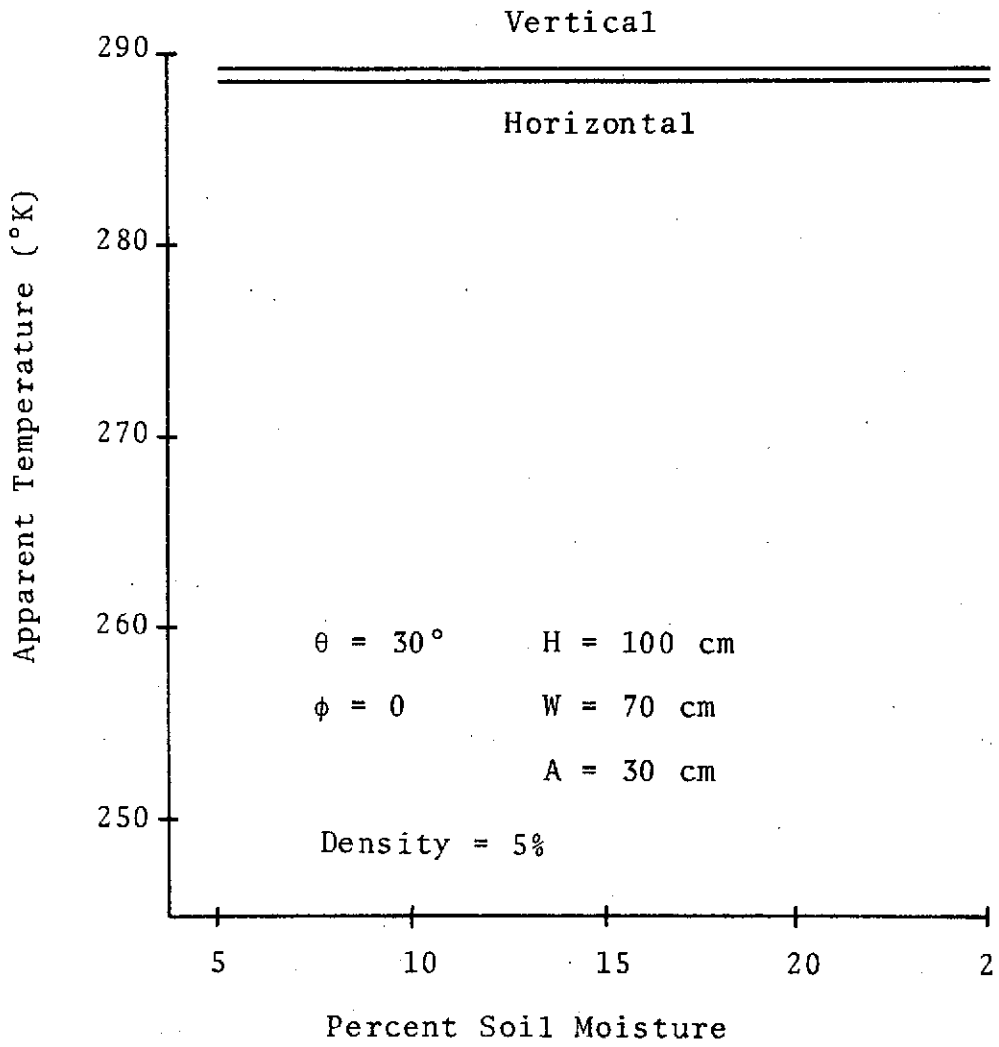

Figure III-12 (c). Apparent temperature of row crops as function of soil moisture.

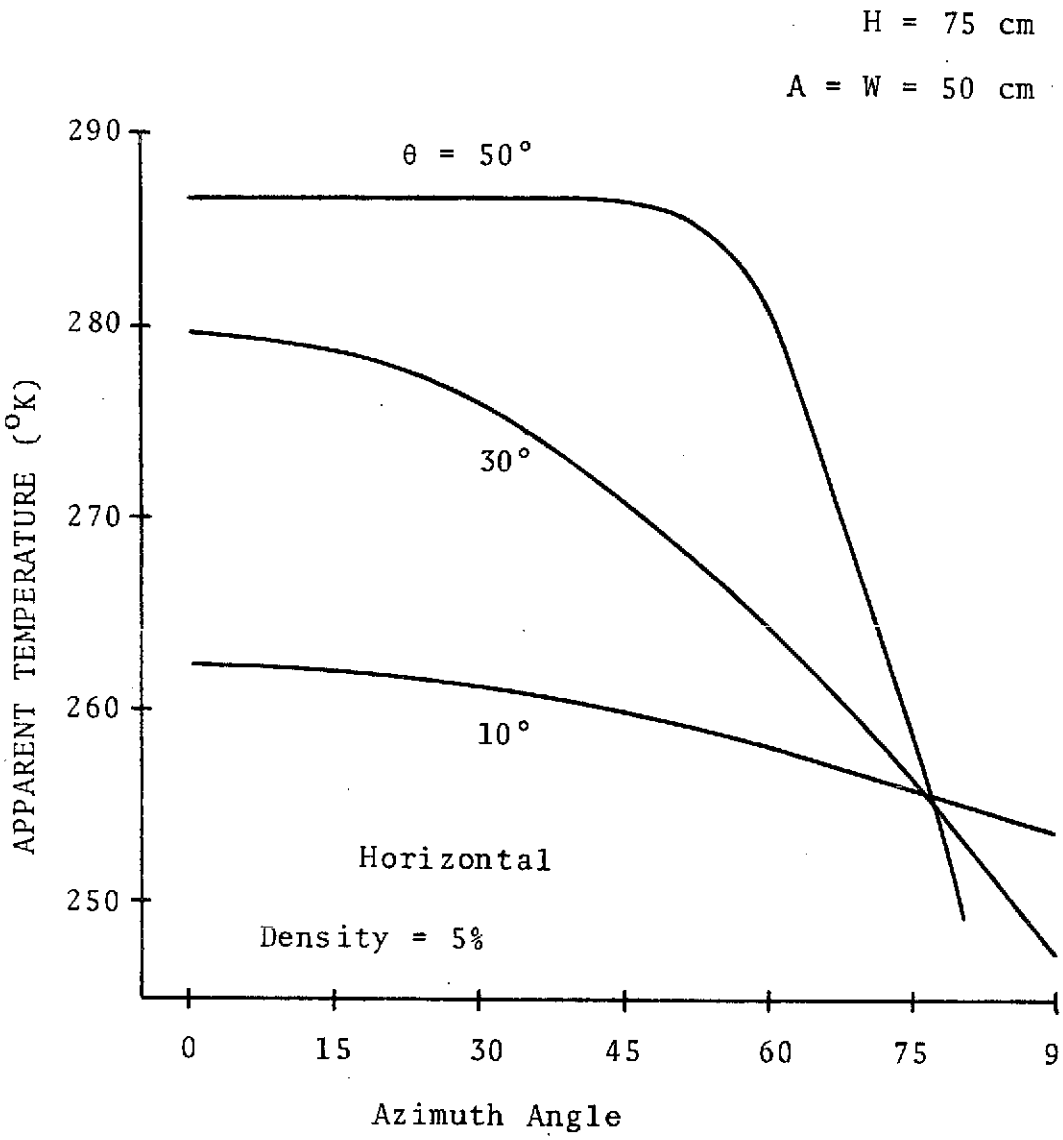

Figure III-13 (a). Apparent temperature of row crops as function of azimuth angle.

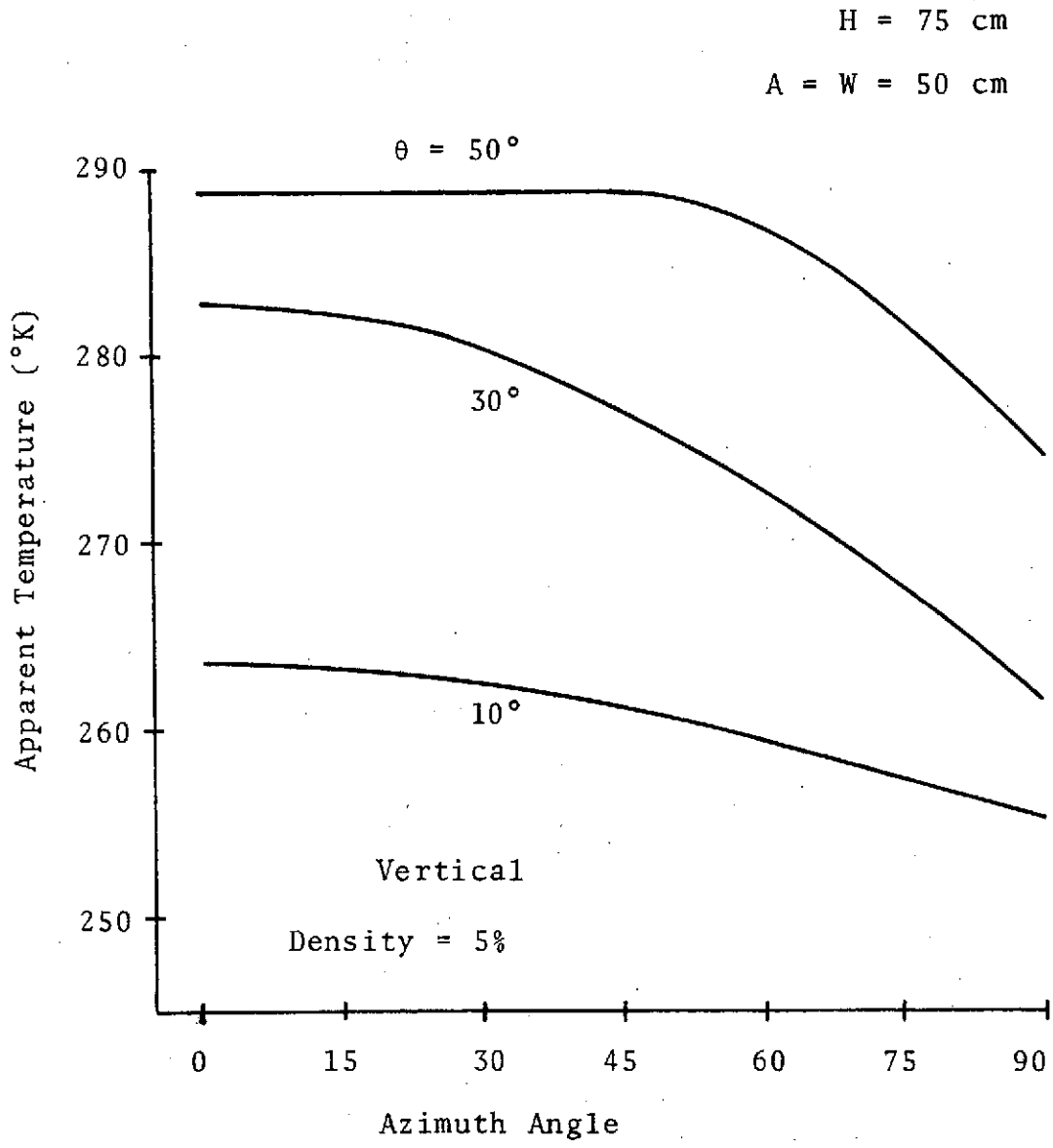

Figure III-13 (b). Apparent temperature of row crops as function of azimuth angle.

Emission from a Rough Surface

The models developed for the apparent temperature of vegetated terrain are ideal, since smooth surfaces have been assumed. No such surface is encountered in practice. However, for cases in which surface variations are small with respect to a wavelength of the radiation being measured, the smooth surface model may be a reasonable approximation. It is desirable to have a model applicable to a rough surface.

A model for emission of thermal radiation from a rough surface has been developed by Johnson [19]. Johnson's model expresses the radiation refracted into a direction (θ_s, ϕ_s) in terms of the radiation incident from (θ_i, ϕ_i) and a "coefficient of effective area". The results of Johnson's derivation are presented below and modified for application to the measurement of apparent temperature.

Transmissive Scattering Coefficients

The emission of radiation from a rough surface is referred to by Johnson as "transmissive scattering" since the process is similar to ordinary scattering. Electromagnetic energy incident on the surface from a direction (θ_i, ϕ_i) is refracted into various directions depending on the characteristics of the surface. The intensities of

the fields refracted into a particular direction (θ_s, ϕ_s) are given by the transmissive scattering coefficients, defined as follows:

$$\tau_{EHH}(i,s) = \frac{E_H(\theta_s,\phi_s)}{E_H(\theta_i,\phi_i)} \qquad \tau_{HHH}(i,s) = \frac{H_H(\theta_s,\phi_s)}{H_H(\theta_i,\phi_i)}$$

$$\tau_{EVV}(i,s) = \frac{E_V(\theta_s,\phi_s)}{E_V(\theta_i,\phi_i)} \qquad \tau_{HVV}(i,s) = \frac{H_V(\theta_s,\phi_s)}{H_V(\theta_i,\phi_i)}$$

$$\tau_{EVH}(i,s) = \frac{E_V(\theta_s,\phi_s)}{E_H(\theta_i,\phi_i)} \qquad \tau_{HVH}(i,s) = \frac{H_V(\theta_s,\phi_s)}{H_H(\theta_i,\phi_i)}$$

$$\tau_{EHV}(i,s) = \frac{E_H(\theta_s,\phi_s)}{E_V(\theta_i,\phi_i)} \qquad \tau_{HHV}(i,s) = \frac{H_H(\theta_s,\phi_s)}{H_V(\theta_i,\phi_i)}$$

The subscripts H and V denote horizontal and vertical polarization with respect to the mean coordinate system. For the transmission coefficients the first subscript indicates either electric or magnetic fields, the second indicates polarization of the scattered field, and the third indicates the polarization of the incident field.

The development which follows is based on the assumption that each element of surface area has an "effective area" oriented in such a way as to cause specular refraction from (θ_i, ϕ_i) into (θ_s, ϕ_s).

Localized Parameters

Each element of surface area is described by two normals, one internal and one external. Each of these normals is defined by a zenith angle and an azimuth angle with respect to the mean coordinate system. Internal and external coordinate systems may be selected so that both normals are defined by a single directional pair (θ_n, ϕ_n).

The direction of the effective normal is implied by the incident and scattering directions. The normal lies in the plane formed by the incident and scattering directions. Furthermore, the normal must be such that the local angle of incidence, θ_{in}, and the local angle of refraction, θ_{sn}, are related by Snell's law of refraction,

$$v_2 \sin\theta_{in} = v_1 \sin\theta_{sn}$$

where v_1 is the velocity of propagation in the lower medium, and v_2 is the velocity of propagation in the upper medium.

The local angles of incidence and refraction are related to other parameters by the Law of Cosines for sides of oblique spherical triangles,

$$\cos\theta_{in} = \cos\theta_i \cos\theta_n + \sin\theta_i \sin\theta_n \cos(\phi_n - \phi_i) \qquad \text{(III-32a)}$$

$$\cos\theta_{sn} = \cos\theta_s \cos\theta_n + \sin\theta_s \sin\theta_n \cos(\phi_n - \phi_s) \qquad \text{(III-32b)}$$

An incident field polarized either vertically or horizontally with respect to the mean coordinates appears to have both vertical and horizontal components with respect to the local coordinates. The locally polarized components can be obtained by rotating the incident polarization coordinates about the line of incidence. The angle of rotation is determined from the Law of Cosines for sides of oblique spherical triangles,

$$\cos a_i = \frac{\cos\theta_n - \cos\theta_{in}\cos\theta_i}{\sin\theta_{in}\sin\theta_i} \qquad \text{(III-33)}$$

The mean polarization of the scattered fields is obtainable by a similar rotation of local polarization coordinates about the line of refraction. The angle of rotation is determined by

$$\cos a_r = \frac{\cos\theta_n - \cos\theta_{sn}\cos\theta_s}{\sin\theta_{sn}\sin\theta_s} \qquad \text{(III-34)}$$

Effective Surface Area

Each element of surface area has a corresponding

projection on the mean coordinate plane. Except for a perfectly smooth surface, the actual surface area is greater than the projected mean area. The "surface roughness factor" is defined as the actual surface area per unit projected area,

$$\delta = \frac{dS}{dA} \; ; \; \delta \geq 1 \qquad \text{(III-35)}$$

The refraction of radiation from (θ_i, ϕ_i) into (θ_s, ϕ_s) implies an effective area oriented so as to cause specular refraction. A "coefficient of effective area" is defined to relate the effective area to the actual surface area.

$$dA_{eff} = \beta \, dS \; ; \; 0 \leq \beta \leq 1 \qquad \text{(III-36)}$$

where β is the coefficient of effective area.

The roughness of the surface may be described by the distribution of the normals. The zenith and azimuth angles are treated as random variables with joint probability density $f_{\theta\phi}(\theta_n, \phi_n)$. Assuming that the azimuth angle is uniformly distributed and independent of the zenith angle, the joint density may be expressed as

$$f_{\theta\phi}(\theta_n, \phi_n) = \frac{1}{2\pi} f_{\theta}(\theta_n) \qquad \text{(III-37)}$$

where $f_{\theta}(\theta_n)$ is the marginal density of the zenith angle

of the normal.

The coefficient of effective area and the surface roughness factor are related to the statistics of the surface normals. The probability that the normal is oriented in the proper direction, within an interval $d\theta$, $d\phi$ is $(1/2\pi)f_{\theta}(\theta_n)d\theta\ d\phi$. Since a solid angle bounded by $d\theta$, $d\phi$ is defined as

$$d\Omega = \sin\theta\ d\theta\ d\phi$$

the probability that the surface normal is oriented within $d\Omega$ is $(1/2\pi\sin\theta)f_{\theta}(\theta_n)d\Omega$. The coefficient of effective area is

$$\beta = \frac{f_{\theta}(\theta_n)}{2\pi \sin\theta_n} \qquad \text{(III-38)}$$

which is the fraction of the total surface oriented within a unit solid angle about a particular direction. The projection of this area on the mean plane is $\beta\cos\theta_n$. The mean projected area per unit surface area is obtained by integrating over the hemisphere.

$$\frac{dA}{dS} = \iint \frac{f_{\theta}(\theta_n)\cos\theta_n}{2\pi \sin\theta_n}\, d\Omega \qquad \text{(III-39)}$$

From (III-35) and (III-39) the surface roughness factor is

$$\delta = \frac{dS}{dA} = \frac{1}{\int_0^{\pi/2} f_\theta(\theta_n) \cos\theta_n \, d\theta_n} \qquad \text{(III-40)}$$

From (III-35) and (III-36) the effective area may be expressed generally as

$$dA_{eff} = \beta\delta \, dA$$

Substituting (III-38) and (III-40),

$$dA_{eff} = \frac{f_\theta(\theta_n) \, dA}{2\pi \sin\theta_n \int_0^{\pi/2} f_\theta(\theta_n) \cos\theta_n \, d\theta_n} \qquad \text{(III-41)}$$

which expresses the effective area causing specular refraction from (θ_i, ϕ_i) into (θ_s, ϕ_s), as a function of surface parameters.

Apparent Temperature of the Surface

As stated earlier in this chapter, the apparent temperature of any object is a measure of the radiant power emanating from the body. Johnson expresses the polarized spectral radiance of a rough surface in terms of the internal radiation, the transmission coefficients, and the surface characteristics. Correcting for an apparent transposition error, Johnson's expression is [19, Eq. IV-43]

$$N_v = \frac{\beta\delta\cos\theta_{in}}{\cos\theta_i}\left(\tau_{EVV}\,\tau_{HVV}\,I_V + \tau_{EVH}\,\tau_{HVH}\,I_H\right) \qquad \text{(III-42)}$$

$$N_H = \frac{\beta\delta\cos\theta_{in}}{\cos\theta_i}\left(\tau_{EHH}\,\tau_{HHH}\,I_H + \tau_{EHV}\,\tau_{HHV}\,I_V\right)$$

where N_V, N_H = polarized component of radiated power

I_V, I_H = polarized component of internal incident power

The electric field transmission coefficients are

$$\tau_{EHH} = \tau_{EH}\cos a_i \cos a_r + \tau_{EV}\sin a_i \sin a_r$$

$$\tau_{EVV} = \tau_{EV}\cos a_i \cos a_r + \tau_{EH}\sin a_i \sin a_r$$

$$\tau_{EVH} = \tau_{EV}\sin a_i \cos a_r - \tau_{EH}\cos a_i \sin a_r$$

$$\tau_{EHV} = \tau_{EV}\cos a_i \sin a_r - \tau_{EH}\sin a_i \cos a_r$$

where τ_{EV} and τ_{EH} are the Fresnel transmission coefficients for vertical and horizontal polarization. The magnetic field transmission coefficients are given by the same expressions, changing each subscript E to H.

The radiance expressed by (III-42) is the power refracted into the direction (θ_s, ϕ_s) due to power incident from a single direction (θ_i, ϕ_i). The various orientations of surface elements allow radiation from other incident directions to be refracted into (θ_s, ϕ_s). Assuming that the vertical and horizontal components of the incident radiation are equivalent, the apparent temperature of a rough surface without vegetation is

$$T_{aI} = T_g \varepsilon_s \iint \frac{\beta \delta \cos\theta_{in}}{\cos\theta_i} \left(\tau_{EIV} \tau_{HIV} + \tau_{EIH} \tau_{HIH} \right) d\Omega_i \qquad \text{(III-43)}$$

where the subscript I denotes either vertical or horizontal polarization.

The total apparent temperature of a vegetated rough surface is obtained from the equations derived earlier in the chapter by inserting (III-43) for the contribution of the soil.

CHAPTER IV

SCATTERING COEFFICIENT OF VEGETATED TERRAIN

Whenever electromagnetic energy is incident upon some object, a portion of that energy is reflected, or reradiated from the body. If the surface is very smooth the reflected energy due to an incident plane wave may be concentrated into a single direction. Such reflection is termed specular. The energy reflected from a rough surface is generally scattered into various directions. Such scattering is termed diffuse. In general, the reradiated energy from any object includes both specular and diffuse components.

The radar cross section of an object is defined as the area required to intercept an amount of power which, when scattered isotropically, produces the same power density at the receiver as the target [20]. The power density (watts/m^2) of the incident radiation is

$$\mathcal{P}_i = \frac{|E_i|^2}{\eta_o}$$

where η_o is the impedance of the atmosphere. The cross-sectional area of an ideal, lossless, isotropically scattering target is denoted σ. Therefore, the power scattered from the ideal target is

$$P_t = \sigma \mathcal{P}_i$$

and the power density at the radar receiver, a distance R from the target is

$$\mathcal{P}_r = \frac{\sigma |E_i|^2}{4\pi R^2 \eta_o} = \frac{|E_r|^2}{\eta_o}$$

where E_r is the electric field intensity at a distance R from the target. Thus, the radar cross section of an arbitrary target is defined to be

$$\sigma = 4\pi R^2 \left| \frac{E_r}{E_i} \right|^2 \qquad \text{(IV-1)}$$

regardless of the actual cross-sectional area.

An extended target which is too large to fall within the radar antenna beam is best described by the radar cross section per unit area, also known as the scattering coefficient. This parameter is usually denoted σ°. It may be defined as the radar cross section of the target divided by the area of illuminated surface.

In general, scattering from vegetated terrain includes scattering from both the soil and the plant canopy. However, one of the two components may have a predominant effect on the total scattering coefficient. In this chapter models are developed for the backscattering coefficients of certain types of vegetated terrain to determine the dependence of the backscatter coefficient on the moisture content of the soil.

Elements of the Scattering Problem

Energy incident upon the vegetated surface is generally scattered by both the canopy and the soil. Furthermore, that portion of the incident field which eventually reaches the soil, experiences additional attenuation due to absorption within the canopy. Similarly, the radiation scattered by the soil surface is attenuated as it propagates upward through the canopy.

The soil and the canopy are described by their permittivities as in Chapter III. The soil is assumed to have the relative permittivity illustrated in Figure III-1 (p. 37) as a function of moisture content. The permittivity of vegetation, computed from (III-2) is used to determine the equivalent permittivity of the canopy according to (III-7).

Smooth, Uniformly Vegetated Surface

The first type of terrain considered is a smooth surface covered by a uniform layer of vegetation. For the purpose of computing the attenuation due to the vegetation, the canopy is assumed to be a homogeneous dielectric layer. The backscatter coefficient of the soil is derived by the physical optics method. Scattering from the canopy is accounted for by a modified form of Peake's model for scattering from long, thin dielectric cylinders.

Backscatter Coefficient of Smooth Surface

The backscatter coefficient is determined by deriving an expression for the scattered electric field at the receiver due to a plane wave incident on the surface. The scattered field is given in general by the Stratton-Chu integral as modified by Silver [21].

The scattering geometry is illustrated in Figure IV-1. The unit vectors $\bar{n}_1$ and $\bar{n}_2$ define the incident and scattering directions, respectively. Following Fung [22] and Leader [23] a local orthonormal coordinate system $\bar{n}_1$, $\bar{t}$, $\bar{d}$ is constructed as follows:

$$\bar{t} = \frac{\bar{n}_1 \times \bar{n}}{\left[1 - (\bar{n}_1 \cdot \bar{n})^2\right]^{1/2}}$$

$$\bar{d} = \bar{n}_1 \times \bar{t}$$

The normal vector $\bar{n}$ is constant for the special case of a smooth surface. Furthermore, for the smooth surface $\bar{t} = \hat{x}$, where $\hat{x}$ is the unit vector along the x-axis.

The general expression for the scattered field at a point P in the direction $\bar{n}_2$ is [23]

$$\bar{E}_s(P) = -j\frac{k \exp(-jkR)}{4\pi R}\, \bar{n}_2 \times \iint \left[(\bar{n} \times \bar{E}) - \eta_0\, \bar{n}_2 \times (\bar{n} \times \bar{H})\right] \cdot \exp(jk\bar{r} \cdot \bar{n}_2)\, dS$$

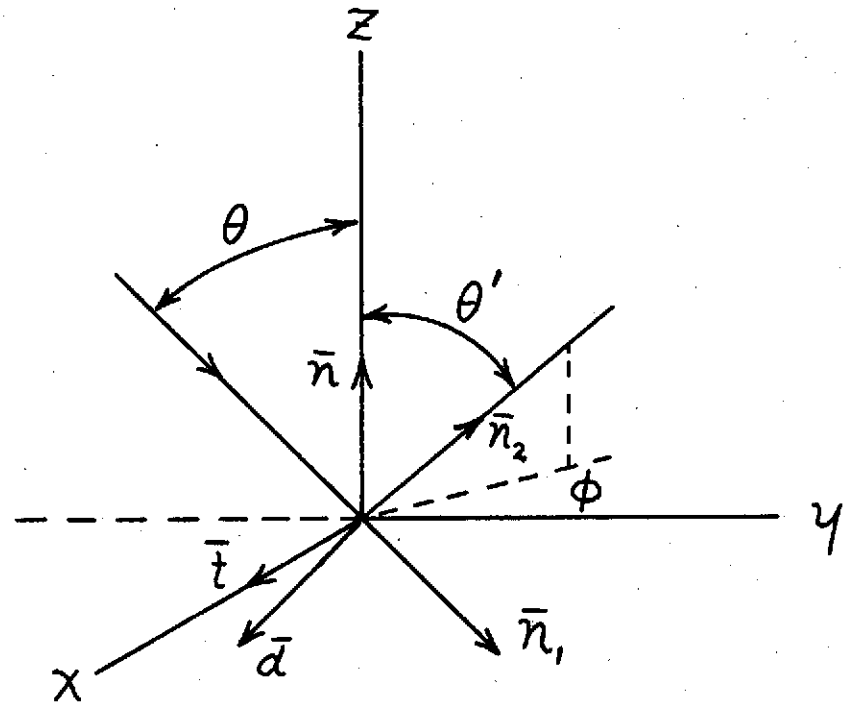

Figure IV-1. Geometry for scattering from a smooth surface.

where k = wave number

R = distance of P from origin

η_o = intrinsic impedance of atmosphere

$\bar{r}$ = position vector of surface element dS

The cross products $(\bar{n} \times \bar{E})$ and $(\bar{n} \times \bar{H})$ denote the local surface currents. Assuming that the incident field is

$$\bar{E}_o = \bar{a} E_o \exp(-jk\bar{n}_1 \cdot \bar{r})$$

with time variation $\exp(j\omega t)$ understood, the surface currents may be expressed as

$$\begin{aligned} \bar{n} \times \bar{E} &= \left[(1+R_H)(\bar{a}\cdot\bar{t})(\bar{n}\times t) - (\bar{n}_1\cdot\bar{n})(1-R_v)(\bar{a}\cdot\bar{a})\,\bar{t} \right] E_o \\ \bar{n} \times H &= \left[(1+R_v)(\bar{a}\cdot\bar{a})(\bar{n}\times\bar{t}) + (\bar{n}_1\cdot\bar{n})(1-R_H)(\bar{a}\cdot\bar{t})\,\bar{t} \right] \left[-\left(\frac{E_o}{\eta_o}\right) \right] \end{aligned} \qquad \text{(IV-3)}$$

where R_H and R_V are the Fresnel reflection coefficients for horizontal and vertical polarizations, respectively. For horizontal polarization

$$\bar{a} = \hat{x}$$

and for vertical polarization

$$\bar{a} = \hat{y}\cos\theta + \hat{z}\sin\theta$$

Therefore, the induced currents on a smooth surface are

$$(\bar{n}\times\bar{E})_H = \hat{y}(1+R_H)E_o$$
$$(\bar{n}\times\bar{H})_H = \hat{x}(1-R_H)\frac{E_o}{\eta_o}\cos\theta \qquad \text{(IV-4a)}$$

for a horizontally polarized incident field, and

$$(\bar{n}\times\bar{E})_V = -\hat{x}(1-R_V)E_o\cos\theta$$
$$(n\times H)_V = \hat{y}(1+R_V)\frac{E_o}{\eta_o} \qquad \text{(IV-4b)}$$

for a vertically polarized incident field. Substituting these expressions into (IV-2) leads to

$$\bar{E}_s(P) = KE_o\iint \bar{A}\exp[jk\bar{r}\cdot(\bar{n}_2-\bar{n}_1)]\,dS \qquad \text{(IV-5)}$$

where

$$K = -j\frac{k\exp(-jkR)}{4\pi R} \qquad \text{(IV-6)}$$

and $\bar{A}$ is a function of incidence and scattering angles and polarization.

$$\bar{A} = \bar{n}_2\left[-(\bar{n}_2\cdot\hat{y})(1+R_V)\right] + \hat{y}(1+R_V) - (\bar{n}_2\times\hat{x})\cos\theta(1-R_V) \qquad \text{(IV-7a)}$$

for vertical polarization, and

$$\bar{A} = \hat{x}\left[(1-R_H)\cos\theta - (\bar{n}_2\cdot\bar{n})(1+R_H)\right] \qquad \text{(IV-7b)}$$

for horizontal polarization.

For the special case of backscatter,

$$\bar{n}_2 = -\bar{n}_1 = -\hat{y}\sin\theta + \hat{z}\cos\theta$$

Thus, (IV-5) becomes

$$\bar{E}_s(P) = KE_0\bar{A}\iint \exp\left[jk\bar{r}\cdot(-2\hat{y}\sin\theta + 2\hat{z}\cos\theta)\right]dx\,dy$$

It is convenient to express the position vector as

$$\bar{r} = -(r\sin\phi)\hat{x} + (r\cos\phi)\hat{y}$$

and to transform the variables of integration to polar coordinates. Thus,

$$\bar{E}_s(P) = KE_o\bar{A}\int_0^{r_1}\int_{-\pi}^{\pi} \exp\left[jk(-2\sin\theta)\cdot r\cos\phi\right] r\, dr\, d\phi \qquad \text{(IV-8)}$$

Noting that Bessel functions of integer order are defined by [24]

$$J_n(x) = \frac{j^{-n}}{2\pi}\int_{-\pi}^{\pi} \exp(jx\cos\theta)\exp(jn\theta)\, d\theta$$

(IV-8) may be written

$$\bar{E}_s(P) = KE_o\bar{A}\int_0^{r_1} 2\pi J_o(-2kr\sin\theta)\, r\, dr \qquad \text{(IV-9)}$$

$$= KE_o\bar{A}\int_0^{r_1} 2\pi J_o(2kr\sin\theta) r\, dr$$

since $J_o(x)$ is an even function.

Applying the theorem [24]

$$\int_0^r x^n J_{n-1}(x)\, dx = r^n J_n(r)$$

leads to

$$\bar{E}_s(P) = \frac{\pi KE_o\bar{A}}{2(k\sin\theta)^2}\, r_1 J_1(r_1) \qquad \text{(IV-10)}$$

The radar cross section of the illuminated surface is determined by inserting (IV-10) into (IV-1).

$$\sigma = 4\pi R^2 \left| \frac{E_s(P)}{E_o} \right|^2$$

$$= 4\pi R^2 \left[\frac{|\bar{A}|}{8k(\sin^2\theta)R} r_1 J_1(r_1) \right]^2 \qquad \text{(IV-11)}$$

$$= \frac{\pi}{16 k^2 (\sin\theta)^4} \left[|\bar{A}| r_1 J_1(r_1) \right]^2$$

The area of illuminated surface is assumed to be πr_1^2. Therefore, the backscatter coefficient for the smooth surface is

$$\sigma = \frac{1}{k^2 (2\sin\theta)^4} \left[|\bar{A}| J_1(r_1) \right]^2 \qquad \text{(IV-12)}$$

For horizontal polarization

$$|\bar{A}| = 2R_H \cos\theta$$

and for vertical polarization

$$|\bar{A}| = \sqrt{(2R_V \cos^2\theta)^2 + (R_V \sin 2\theta)^2}$$

Attenuation by Canopy

That portion of the incident electromagnetic field which eventually reaches the soil experiences attenuation

as it propagates through the canopy. The attenuation constant is defined by (III-17). In terms of the field above the canopy, the electric field incident on the soil is

$$E_i = E_o e^{-\alpha H \sec\theta}$$

where H is the height of the canopy and θ is the angle of incidence.

The effective backscatter coefficient of the soil is determined from the attenuation of power due to propagation through the canopy. Since the incident electric field is reduced by $\exp(-\alpha H \sec\theta)$ before reaching the soil, the incident power is reduced by $\exp(-2\alpha H \sec\theta)$. Furthermore, since the two-way path of the backscattered power is $2H\sec\theta$, the total attenuation of power due to the canopy is $\exp(-4\alpha H \sec\theta)$. Therefore, the effective backscatter coefficient of vegetated soil is

$$(\sigma^\circ)_{eff} = \sigma^\circ e^{-4\alpha H \sec\theta} \qquad \text{(IV-13)}$$

where σ° is the backscatter coefficient of bare soil.

Scattering by Canopy

Two models for the scattering coefficient of a plant canopy have been considered. One is Peake's model for long, thin dielectric cylinders, discussed in Chapter II. The other is the Lommel-Seeliger model [25], which treats

the canopy as an ensemble of randomly oriented flat plates. Obviously, each model is intended to apply only to certain types of vegetation.

The difficulty of applying either of these two models to the present development is that each one assumes the canopy has infinite depth. In other words, the scattering coefficient given by each model is the total average scattering coefficient of vegetated terrain. What is desired is a method of isolating the component of scattered radiation due to the canopy from the component due to the soil.

A modification of Peake's model seems to provide an appropriate solution to the problem. Peake's model is compatible with the model presently being developed because it accounts for exponential attenuation of the field within the canopy. It seems reasonable to assume that if the attenuation of the incident field is less than $\exp(-\alpha H \sec\theta)$, the contribution of scattering from the soil is significant. As the canopy increases in height or density, scattering from the canopy becomes more significant and scattering from the soil becomes less significant. Such effects are accounted for by assuming that the component of scattering due to the canopy is

$$\sigma_c^\circ = \sigma_p^\circ \left(1 - e^{-2\alpha H \sec\theta}\right) \qquad \text{(IV-14)}$$

where σ_p° is the scattering coefficient computed from Peake's model.

Theoretical Predictions

For reference, the backscatter coefficient of a smooth soil surface is illustrated in Figure IV-2. The backscatter coefficients for horizontal and vertical polarizations are plotted as functions of incidence angle for two values of soil moisture content. An increase in moisture causes an increase in σ°. For angles of incidence less than 25°, backscatter is about the same for both polarizations. For larger angles of incidence, backscatter is less for vertical polarization, but is more sensitive to variations of moisture.

Assuming that the power scattered from the soil and from the canopy sum incoherently, the total backscatter coefficient of the vegetated surface is the sum of (IV-13) and (IV-14).

$$\sigma' = (\sigma^\circ)_{eff} + \sigma_c^\circ \qquad \text{(IV-15)}$$

$$= \sigma^\circ e^{-4\alpha H \sec\theta} + \sigma_p^\circ\left(1 - e^{-2\alpha H \sec\theta}\right)$$

The backscatter coefficient of (IV-15) is plotted in Figure IV-3 as a function of incidence angle for two values of soil moisture. The canopy is assumed to be 35 cm deep, and the incident radiation has a frequency of 1.5 GHz. At smaller angles of incidence an increase in moisture of 20%

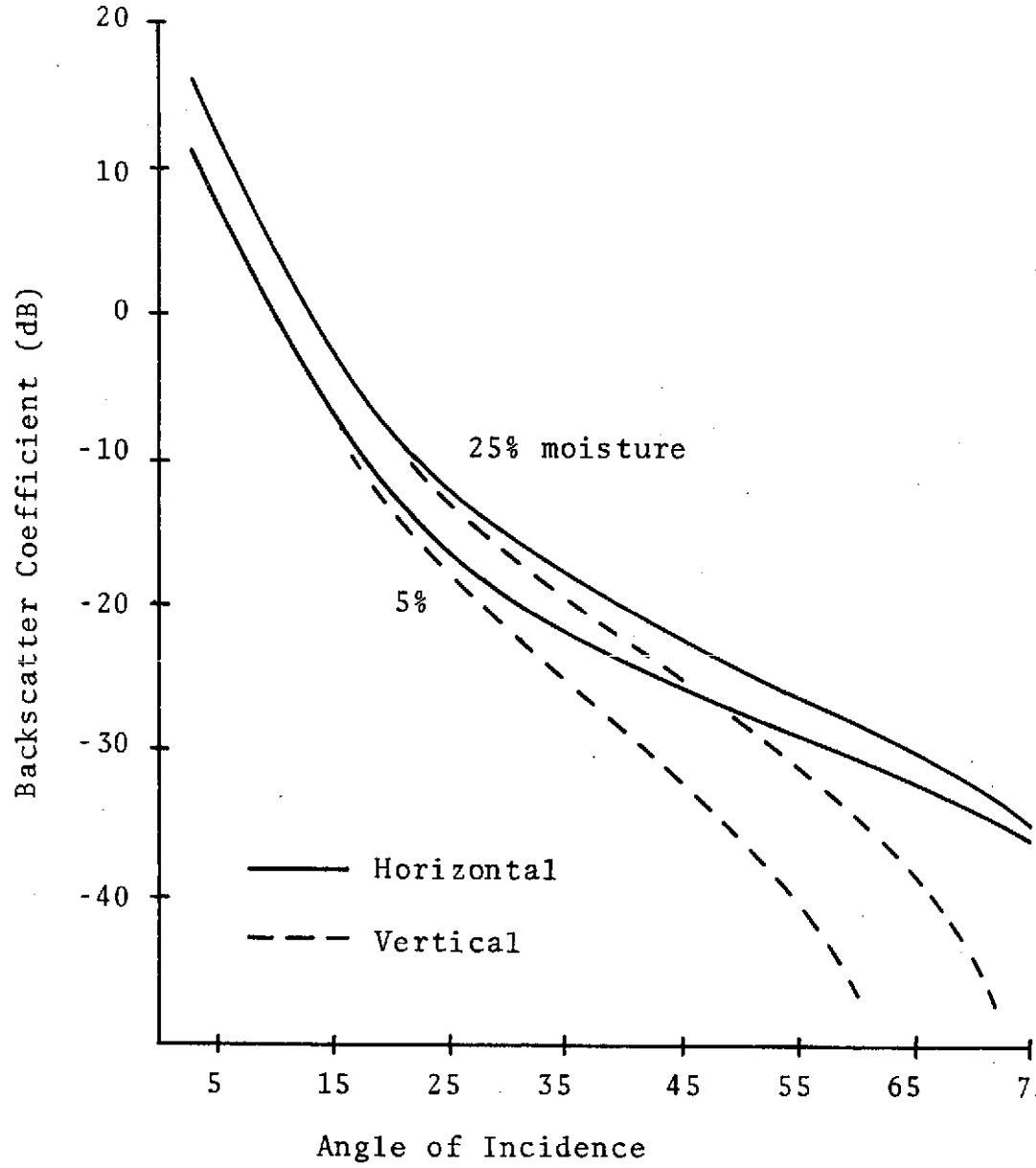

Figure IV-2. Backscatter coefficient of a smooth surface.

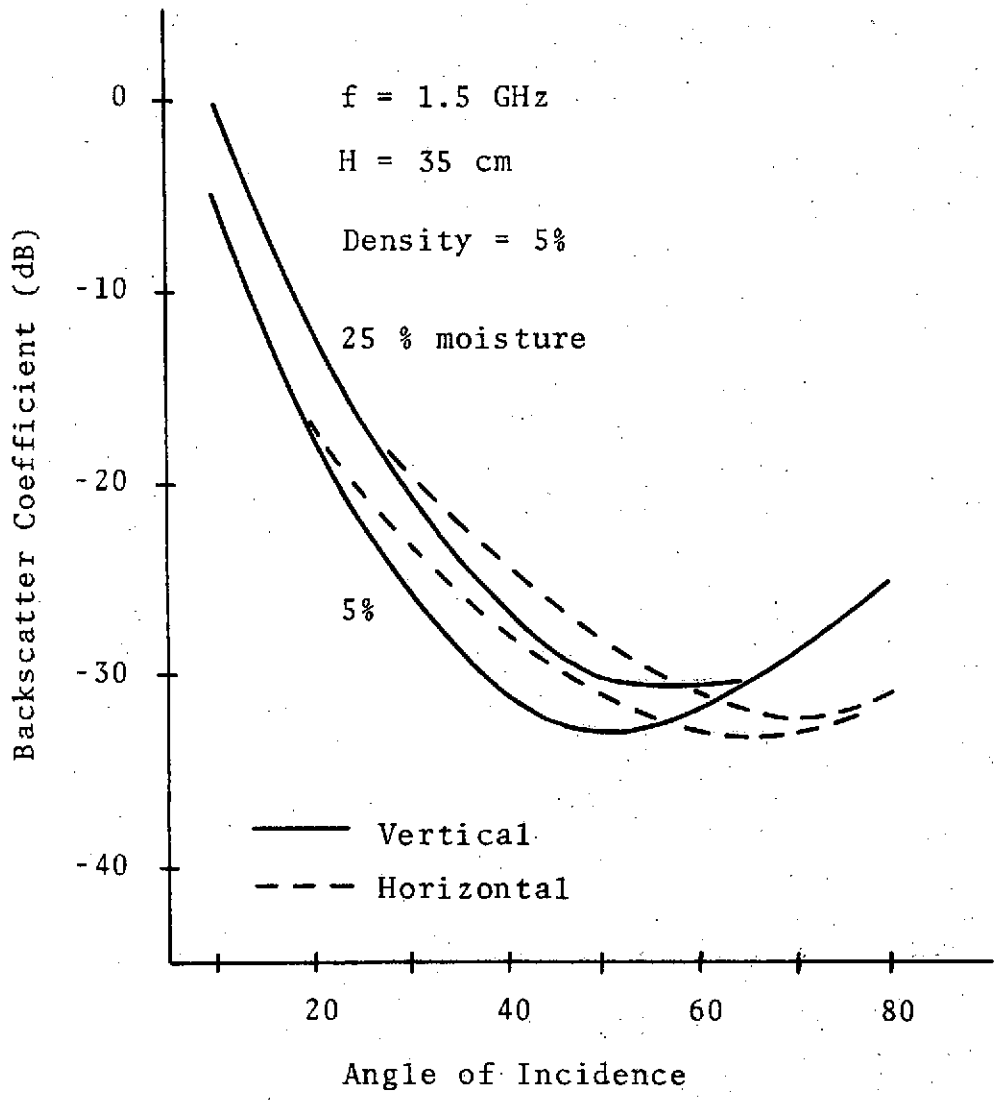

Figure IV-3. Backscatter coefficient of smooth, uniformly vegetated surface as function of incidence angle.

causes an increase in the scattering coefficient of about 5 dB. At incidence angles of about 50° for vertical polarization and 70° for horizontal, scattering from the canopy becomes more significant than that from the soil, causing a general increase in σ'. Furthermore, as scattering from the canopy increases, the variation of σ' due to moisture diminishes.

The effect of changing the frequency of radiation is illustrated in Figure IV-4, in which the backscatter coefficient for frequencies of 3, 5, and 7 GHz is plotted. At higher frequencies (shorter wavelengths) scattering from the canopy becomes predominant at smaller incidence angles. For a single frequency the same effect results from increasing the height of the canopy.

Figure IV-5 illustrates the dependence of the backscatter coefficient on soil moisture content for three frequencies. The angle of incidence is 30°. At 1.5 GHz an increase in moisture of 20% causes an increase in the scattering coefficient of about 5 dB. At 3.0 GHz the change in scattering coefficient is 1.6 dB, and at 5.0 GHz the change is negligible. At 5.0 GHz scattering from the canopy is great enough to cause a general increase in σ'.

Row Crops

Since the contributions to scattering due to the

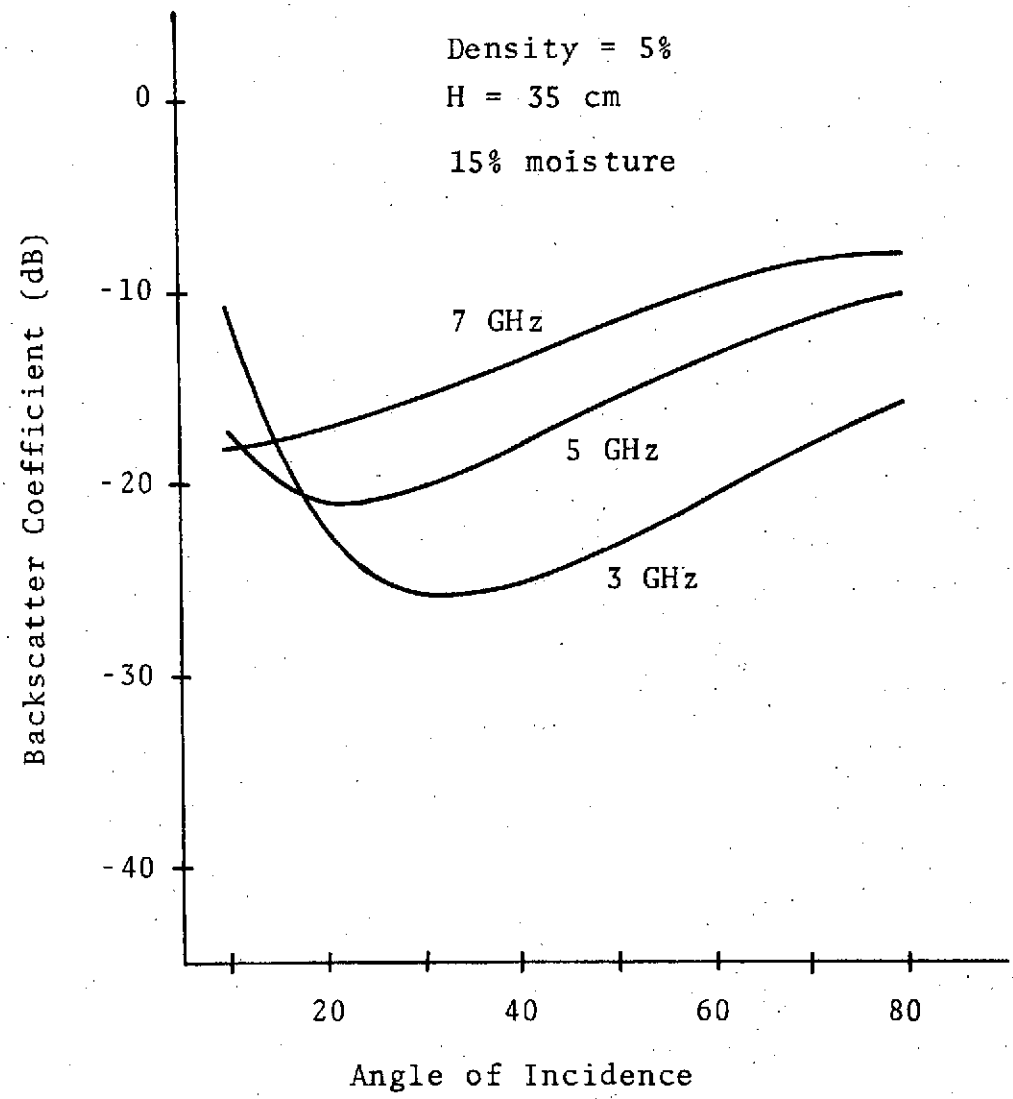

Figure IV-4. Effect of frequency on scattering from the smooth, uniformly vegetated surface.

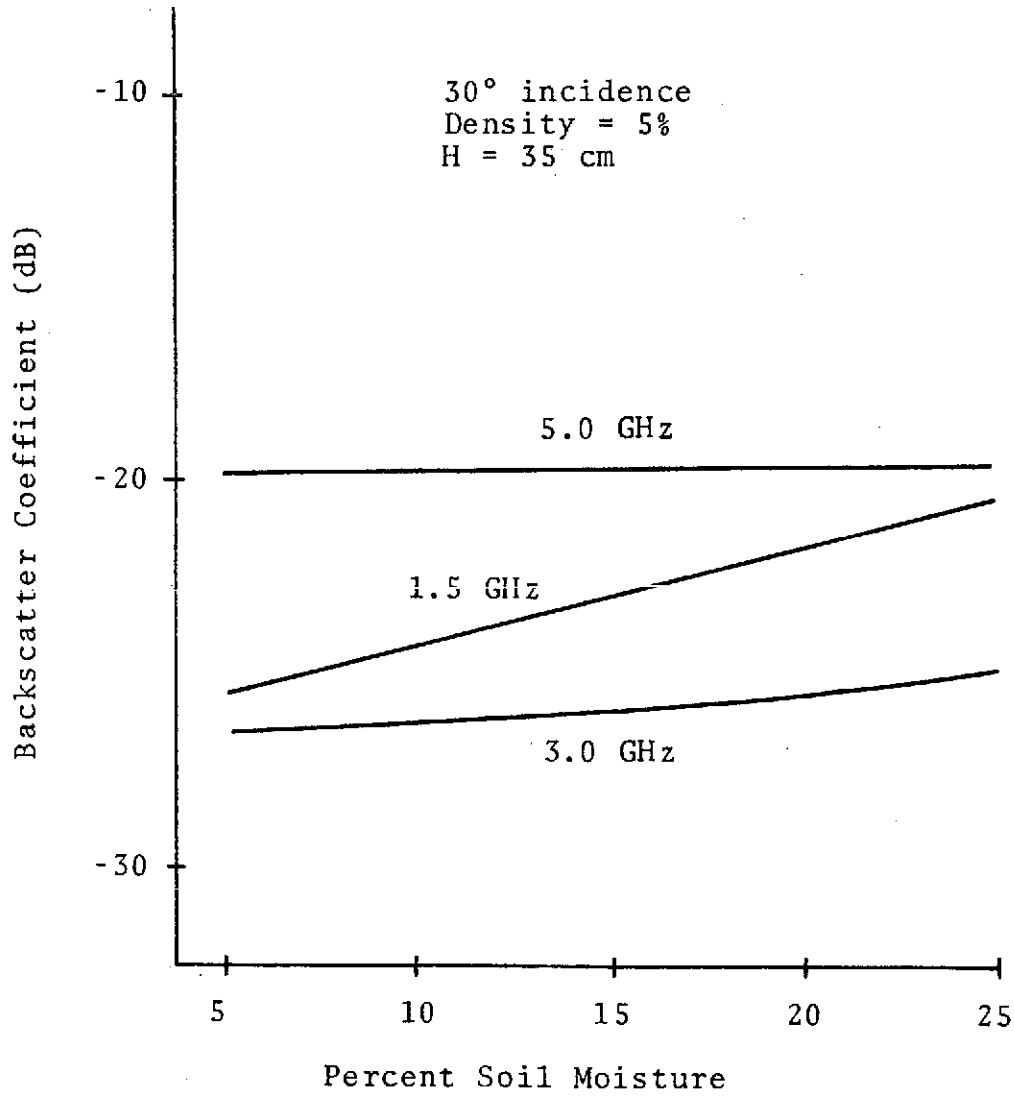

Figure IV-5. Dependence of σ' on soil moisture content for various frequencies.

canopy and to the soil have been determined in general, the determination of the average backscattering coefficient of row crops is primarily a geometrical problem. The results are similar to those obtained for the average apparent temperature of row crops in Chapter III.

Backscatter Perpendicular to Rows

For the special case of incidence and scattering perpendicular to the rows, three scattering regions are defined as in Figure IV-6. In regions I and II both the soil and the canopy contribute to the scattered field, whereas in region III only the soil causes scattering. The angle of incidence in region I is $(\pi/2 - \theta)$ rather than θ as in regions II and III.

The component of the backscatter coefficient due to the canopy is a weighted average of the scattering coefficients in regions I and II. The area upon which the field is incident in region I is projected onto a plane parallel to the surface. Thus, the effective backscatter coefficient of region I is

$$\sigma_I^\circ(\theta) = \sigma_p^\circ(\pi/2 - \theta)\frac{H}{B}$$

The total effective component due to the canopy is

$$\sigma_c^\circ = \frac{\sigma_p^\circ(\pi/2 - \theta)H + W\sigma_p^\circ(\theta)}{B + W}\left(1 - e^{-2\alpha d}\right) \quad \text{(IV-16)}$$

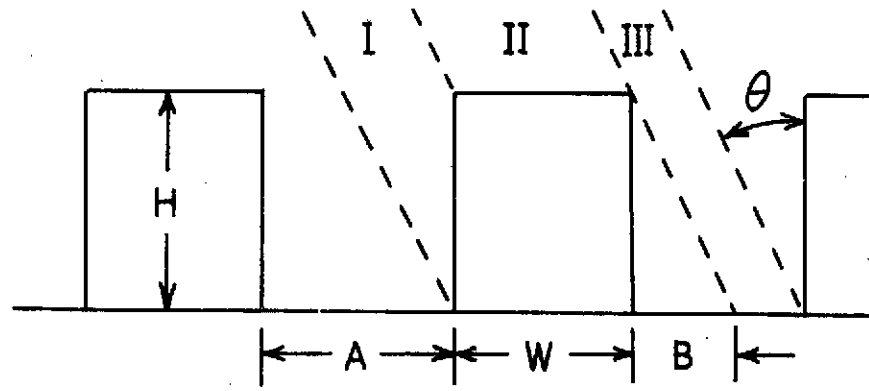

Figure IV-6. Dimensions of rows and basic regions of backscatter.

where d is the average length of propagation through the canopy, as defined by (III-23).

The expression of (IV-16) is not applicable in general, since it was derived for the case in which B < A. However, it can be shown that generality is obtained by substituting the function L(A,B), defined in Chapter III (p. 65), for B and L(A,B)cotθ for H. Thus,

$$\sigma_c^o = \frac{\sigma_p^o(\pi/2 - \theta)L(A,B)\cot\theta + W\sigma_p^o(\theta)}{L(A,B) + W}\left(1 - e^{-2\alpha d}\right) \quad \text{(IV-17)}$$

The total backscattering coefficient is the average of all scattering components in regions I, II, and III.

$$\sigma' = \frac{1}{A+W}\left\{[L(A,B)+W](\sigma_c^o + \sigma^o e^{-4\alpha d}) + [A - L(A,B)]\sigma^o\right\} \quad \text{(IV-18)}$$

where σ_c^o is given by (IV-17) and σ^o is given by (IV-12).

Backscattering at Any Azimuth Angle

Since the expression for scattering perpendicular to the rows is identical in form to the expression for apparent temperature, stated as (III-30), it is reasonable to assume that the generalization for arbitrary azimuth angles, given in (III-28), is also applicable in the present

case. Therefore, it is stated without explanation that the only modification required is to define the distance B as

$$B = H \tan\theta \cos\phi$$

Theoretical Predictions

The relation of the backscatter coefficient to soil moisture content depends on several factors. In general it may be said that as the component of scattering due to vegetation increases, the dependence on soil moisture decreases. However, the effect of vegetation can be increased by changing frequency, canopy dimensions, or angle of incidence.

The effect of frequency on the backscatter coefficient is illustrated in Figure IV-7, in which three curves are plotted as functions of soil moisture. The plant row is assumed to be 50 cm high and 50 cm wide. The angle of incidence is 30°, and the azimuth angle is 45°. The data indicate that at 1.0 GHz an increase in moisture of 20% causes the scattering coefficient to rise 4.0 dB, while at 5.0 GHz the change is negligible.

Figure IV-8 illustrates that the same effect is caused by changing the dimensions of the canopy. The data have been computed for a frequency of 3.0 GHz. For a

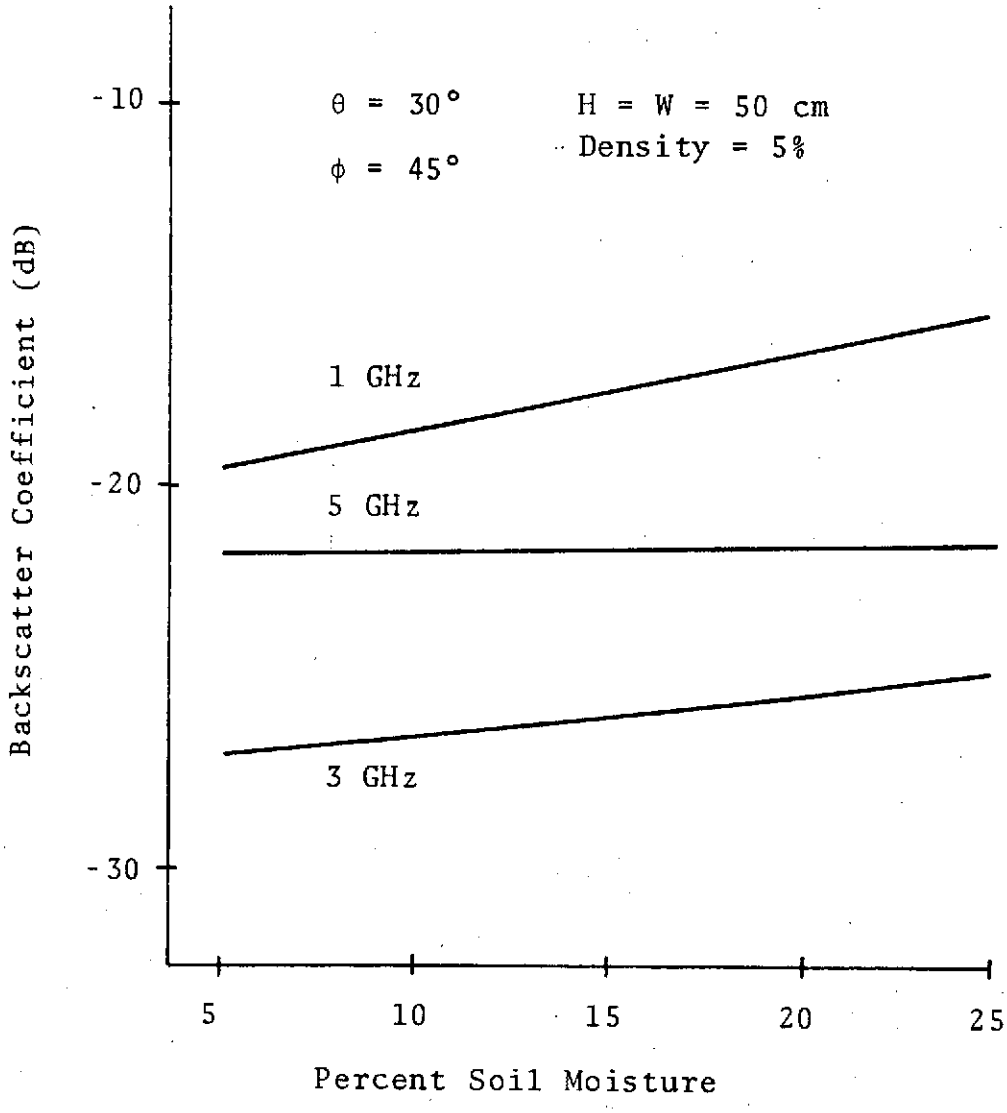

Figure IV-7. Dependence of σ' on moisture content of soil for various frequencies.

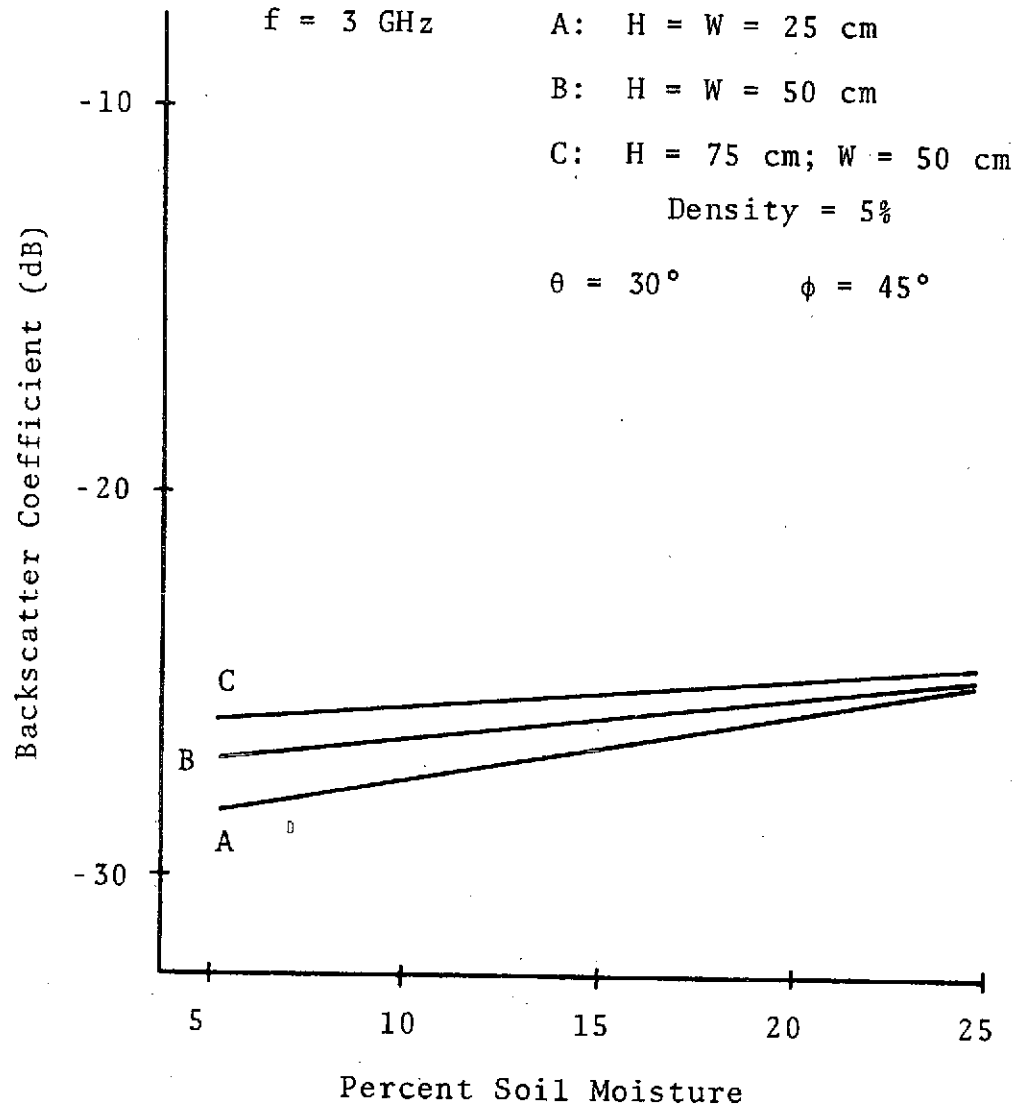

Figure IV-8. Dependence of σ' on soil moisture content for various amounts of plant cover.

canopy height of 25 cm an increase in moisture of 20% causes an increase in the backscattering coefficient of 3.5 dB. For a canopy height of 75 cm the same increase in moisture causes a change in the scattering coefficient of only 1.5 dB.

The angle of incidence partly determines the effect of vegetation on scattering, as illustrated in Figure IV-9. Each curve in this figure represents the backscatter coefficient, as a function of soil moisture, for incidence perpendicular to the rows. At smaller angles of incidence, the dependence of the scattering coefficient on soil moisture is appreciable. However, at larger angles of incidence, in which case more of the soil is shadowed, the scattering coefficient becomes practically independent of soil moisture.

Scattering from a Rough Surface

Surface Model

Johnson's model of a rough surface, defined by a surface roughness factor, δ, and a coefficient of effective area, β, is applicable to the problem of scattering from a vegetated rough surface. The derivation of the model, with application to thermal emission, is discussed in Chapter III. In the present section only those points which pertain especially to the scattering problem are discussed.

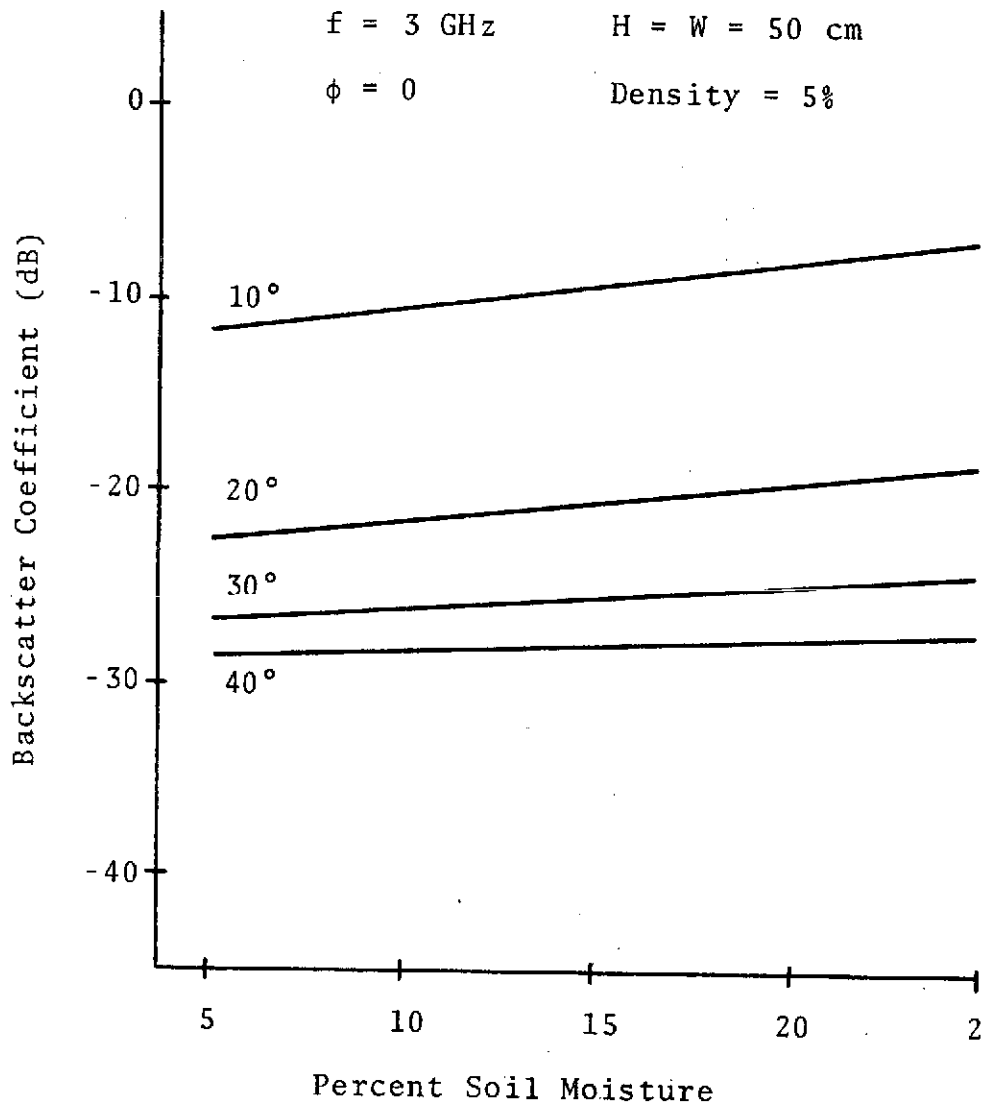

Figure IV-9. Dependence of σ' on soil moisture content for various angles of incidence.

According to Johnson's derivation [7], the incident and scattered radiation are related as follows:

$$N_V = \frac{\beta\delta\cos\theta_{in}}{\cos\theta_i}\left(\gamma_{VV}^2 I_V + \gamma_{HV}^2 I_H\right) \qquad \text{(IV-19)}$$

$$N_H = \frac{\beta\delta\cos\theta_{in}}{\cos\theta_i}\left(\gamma_{HH}^2 I_H + \gamma_{VH}^2 I_V\right)$$

where N_V and N_H are the scattered power densities for vertical and horizontal polarizations, I_V and I_H are the incident power densities, θ_i is the angle of incidence, and θ_{in} is the angle between the incidence direction and the effective normal of the scattering surface element. The scattering coefficients are defined as

$$\gamma_{VV} = \rho_V \cos a_i \cos a_r + \rho_H \sin a_i \sin a_r$$

$$\gamma_{HH} = \rho_H \cos a_i \cos a_r + \rho_V \sin a_i \sin a_r \qquad \text{(IV-20)}$$

$$\gamma_{HV} = \rho_V \sin a_i \cos a_r - \rho_H \cos a_i \sin a_r$$

$$\gamma_{VH} = \rho_V \cos a_i \sin a_r - \rho_H \sin a_i \cos a_r$$

where ρ_V and ρ_H are the Fresnel reflection coefficients and α_i and α_r are the angles of rotation of incident and reflected polarization fields into the local plane of

incidence.

Since only backscattering is being considered, the local angle of incidence must be zero. In other words, the effective normal of the scattering surface element must be parallel to the direction of propagation of the incident radiation. Consequently, $\theta_{in} = 0$ for all incidence angles. Furthermore, since backscatter is assumed to be due only to specular reflection of normally incident fields, there is no depolarization of the incident fields. Therefore, the scattering coefficients given by (IV-20) reduce to

$$\gamma_{VV} = \rho_V$$
$$\gamma_{HH} = \rho_H \qquad \text{(IV-21)}$$
$$\gamma_{VH} = \gamma_{HV} = 0$$

From (IV-19) the backscatter coefficients of the rough soil are

$$\sigma^o_V = \frac{\beta\delta}{\cos\theta}\rho_V^2 \qquad \text{(IV-22a)}$$

for vertical polarization and

$$\sigma^o_H = \frac{\beta\delta}{\cos\theta}\rho_H^2 \qquad \text{(IV-22b)}$$

for horizontal polarization.

Theoretical Predictions

The backscatter coefficient of row crops on a rough surface is given by (IV-18) with σ° defined by (IV-22).

To evaluate the surface roughness factor, δ, and the coefficient of effective area, β, the surface must be described by the distribution of the surface normal. The derivation of Johnson's model assumes that the normal is distributed uniformly with respect to the azimuth angle. Therefore, the specified probability density function is a function only of the angle of incidence. A suitable function for this application is

$$f(\theta) = \frac{4}{\pi} \cos^2\theta$$

which leads to

$$\delta = 1.178$$

and

$$\beta = \frac{2\cos^2\theta}{\pi^2 \sin\theta}$$

The backscatter coefficient is plotted as a function of incidence angle in Figure IV-10 for two values of soil moisture. A 5 GHz signal is assumed to be incident perpendicular to plant rows 60 cm high and 40 cm wide. It is clear that a 20% increase in moisture causes an increase in σ' of about 4 dB for both horizontal and vertical

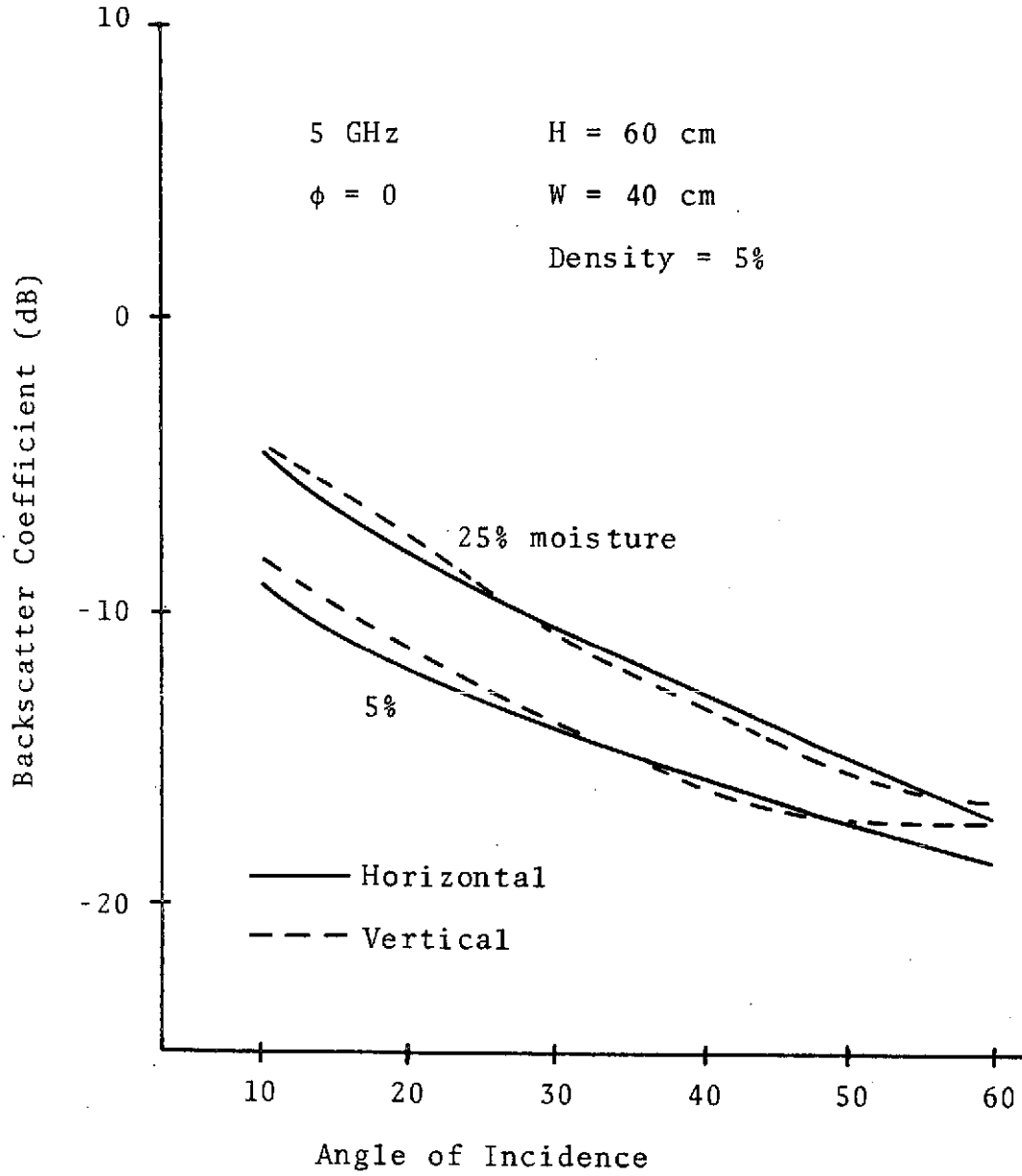

Figure IV-10. Backscatter coefficient of a row crop on a rough surface.

polarizations at small angles of incidence. However, at larger angles of incidence scattering is less sensitive to variations in moisture.

The effect of varying the azimuth angle is illustrated in Figure IV-11. There is no noticeable change in the moisture sensitivity of the scattering coefficient for horizontal polarization. However, for vertical polarization, the sensitivity to moisture is greater at large azimuth angles (approximately parallel to rows).

The sensitivity of the backscatter coefficient to variations of moisture depends upon the operating frequency, as illustrated in Figure IV-12. At 1.0 GHz an increase in soil moisture of 20% causes an increase in the scattering coefficient of 5 dB. At 5.0 GHz the change in the scattering coefficient is 3.5 dB, and at 9.0 GHz it is only 1.4 dB.

The same effect results from changing the dimensions of the plant rows, as illustrated in Figure IV-13. A 5 GHz signal is assumed to be incidence on plant rows of three different sizes. The backscatter coefficient of 38 x 33 cm rows increases 3.83 dB with an increase in soil moisture of 20%. For 100 x 70 cm rows the change in scattering coefficient is 1.12 dB.

As expected, for any particular frequency or vegetation condition, the backscatter coefficient of a rough

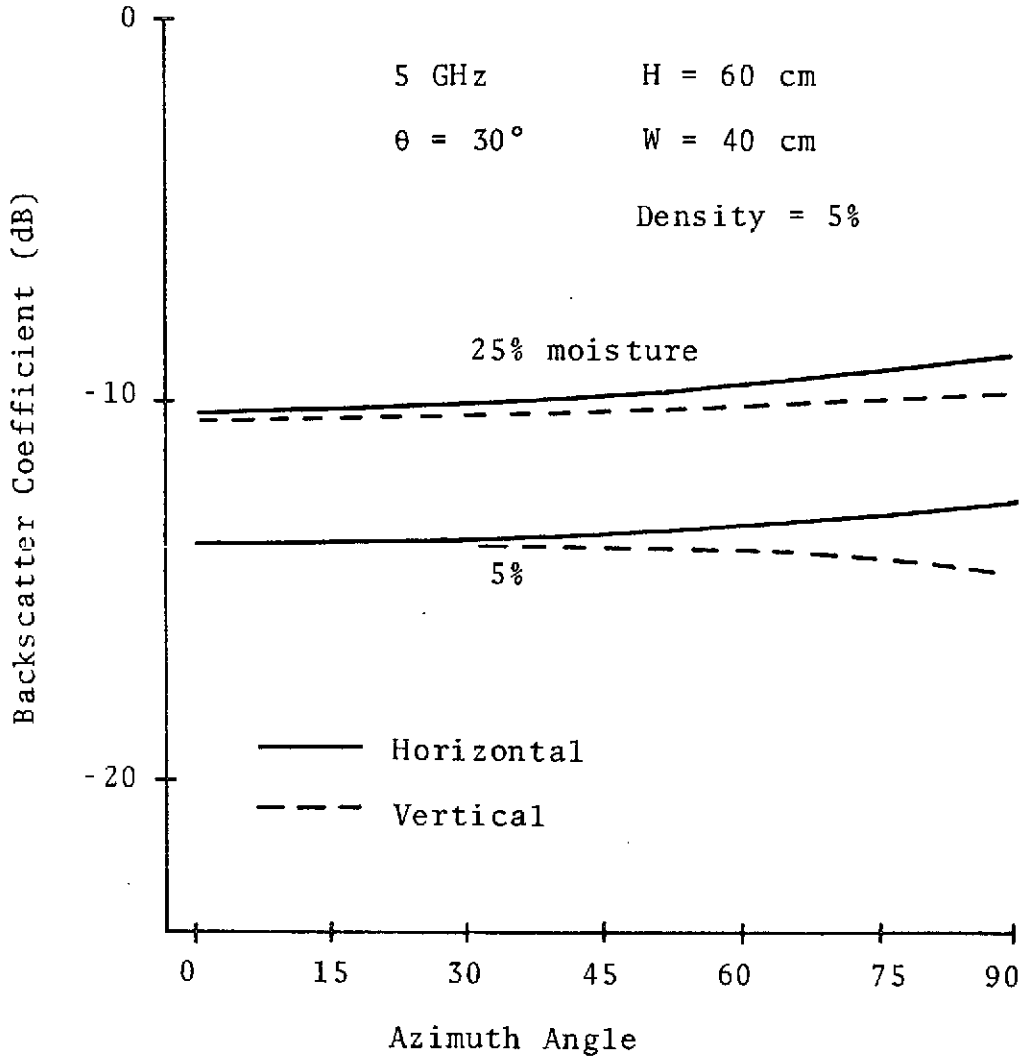

Figure IV-11. Dependence of σ' on azimuth angle.

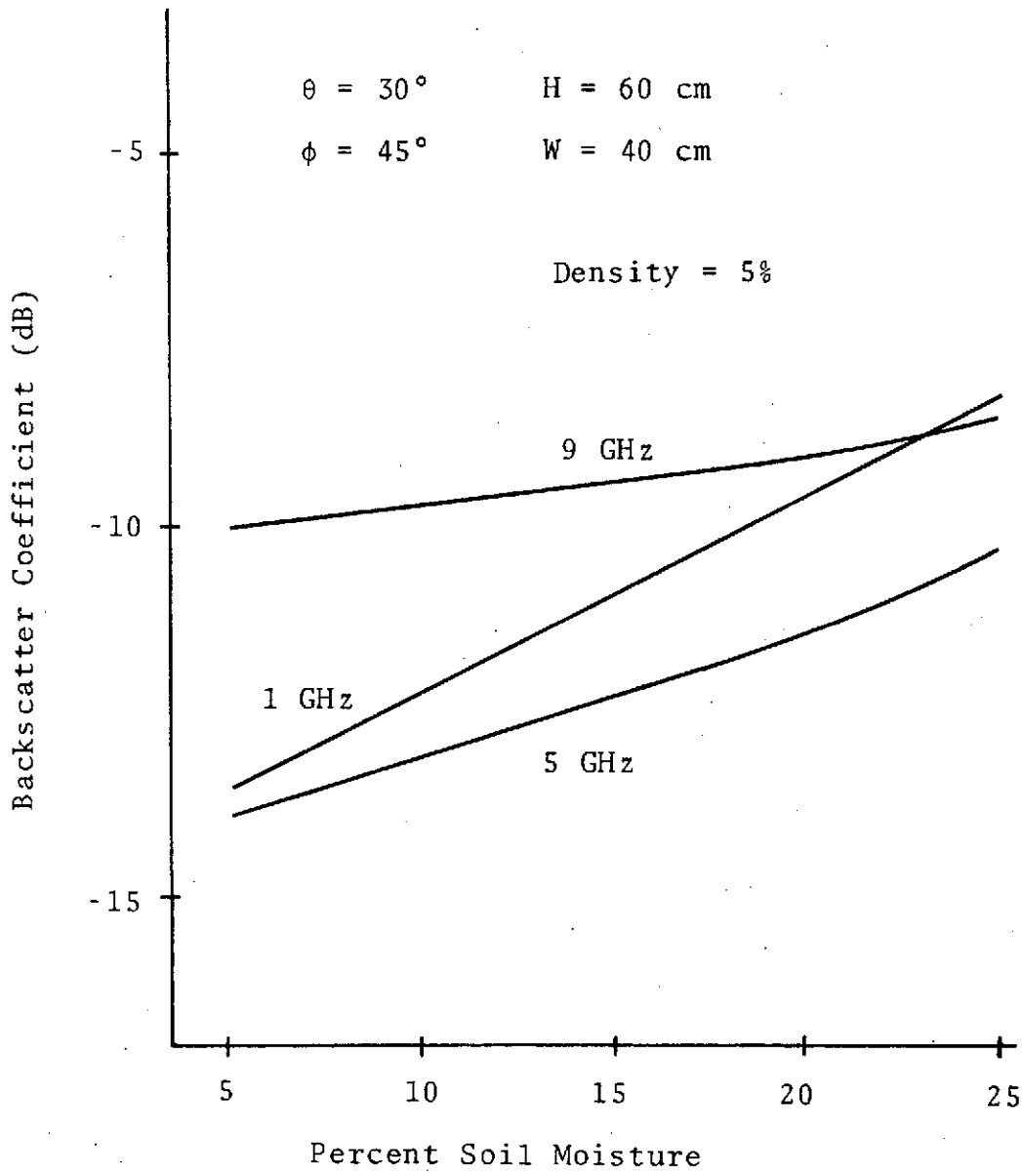

Figure IV-12. Backscatter coefficient of a row crop at various frequencies.

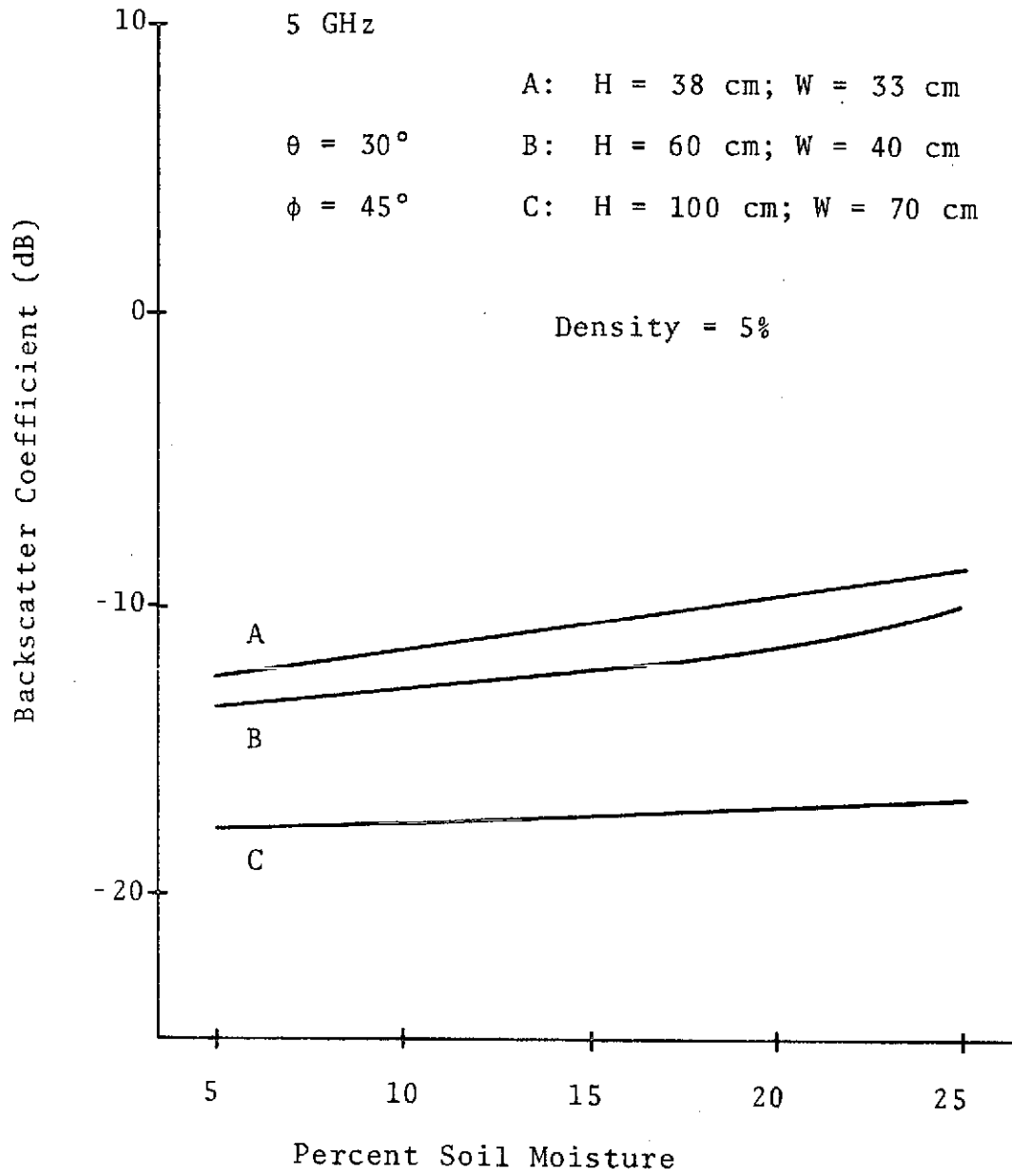

Figure IV-13. Backscatter coefficients of different sizes of plant rows.

surface is more sensitive to soil moisture than that of a smooth surface, since the contribution of backscattering from the soil is greater.

CHAPTER V

COMPARISON OF THEORETICAL PREDICTIONS WITH EXPERIMENTAL DATA

Measured apparent temperatures and backscatter coefficients of vegetated terrain are presented in this chapter to illustrate some of the effects predicted by the models developed in Chapters III and IV. Unfortunately, none of the data, much of which is taken from the literature, is accompanied by documentation of both soil moisture and vegetation. Therefore, apparent temperatures and backscatter coefficients cannot be illustrated as functions of soil moisture. However, the effects of other parameters on scattering and emission can be illustrated.

A program is presently being conducted at Texas A&M University to measure the apparent temperatures of test sites for which soil moisture, surface roughness, and vegetation are well documented. However, no data are yet available.

The increase of apparent temperature due to vegetation is clearly illustrated in Figure V-1. The fields pictured lie along the flight line near Weslaco, Texas. Data from the March 14, 1972, flight over these fields were provided by NASA/Goddard Space Flight Center. The data plotted are from a 1.42 GHz dual-polarization radiometer and a 19.4

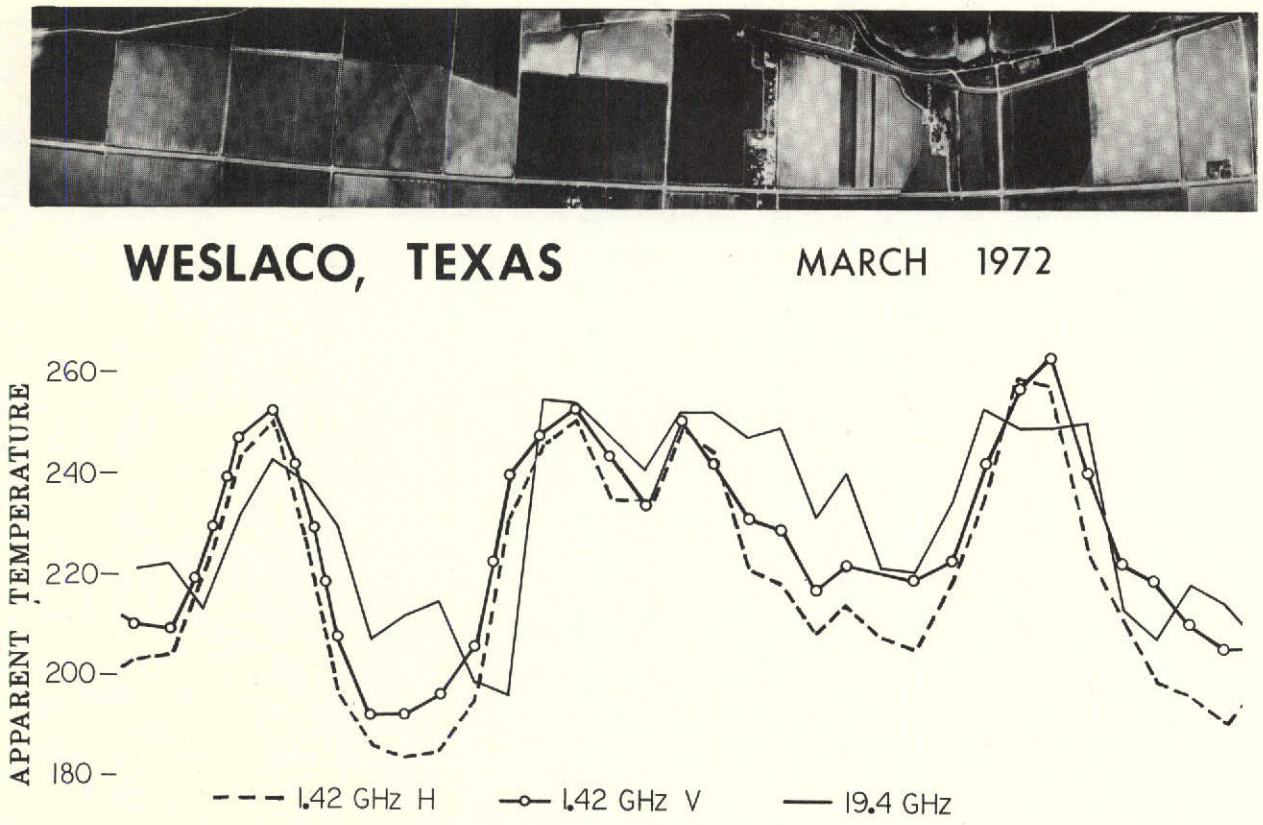

Figure V-1. Apparent temperatures of bare and vegetated fields at Weslaco, Texas.

GHz scanning radiometer. The center line of the digitized scanner image is plotted. The apparent temperature is as much as 65 degrees higher in vegetated fields than in bare fields. This increase is apparently due only to the vegetation, since all fields are believed to have had approximately equal moisture levels.

A change in dependence on polarization, as predicted by Figure III-12 (p. 67), is also apparent in Figure V-1 (p. 117). Although the vertical channel of the 1.42 GHz data is consistently higher than the horizontal channel, the difference between the two channels is considerably less for vegetated fields than for bare fields.

The lack of dependence on polarization is better illustrated by Figure V-2, in which apparent temperatures of alfalfa and oats are plotted as functions of refraction angle. These data and other data presented below were obtained by Peake and Oliver [12]. The apparent temperatures were measured at a frequency of 10 GHz. It is clear that for any angle, a change of polarization causes a change in apparent temperature of no more than about 5°C. The peak at the Brewster angle, characteristic of vertical polarization, is suppressed.

The difference between apparent temperatures of wet and dry fields is illustrated in Figure V-3. The apparent temperatures of two soybean fields, one of which was irri-

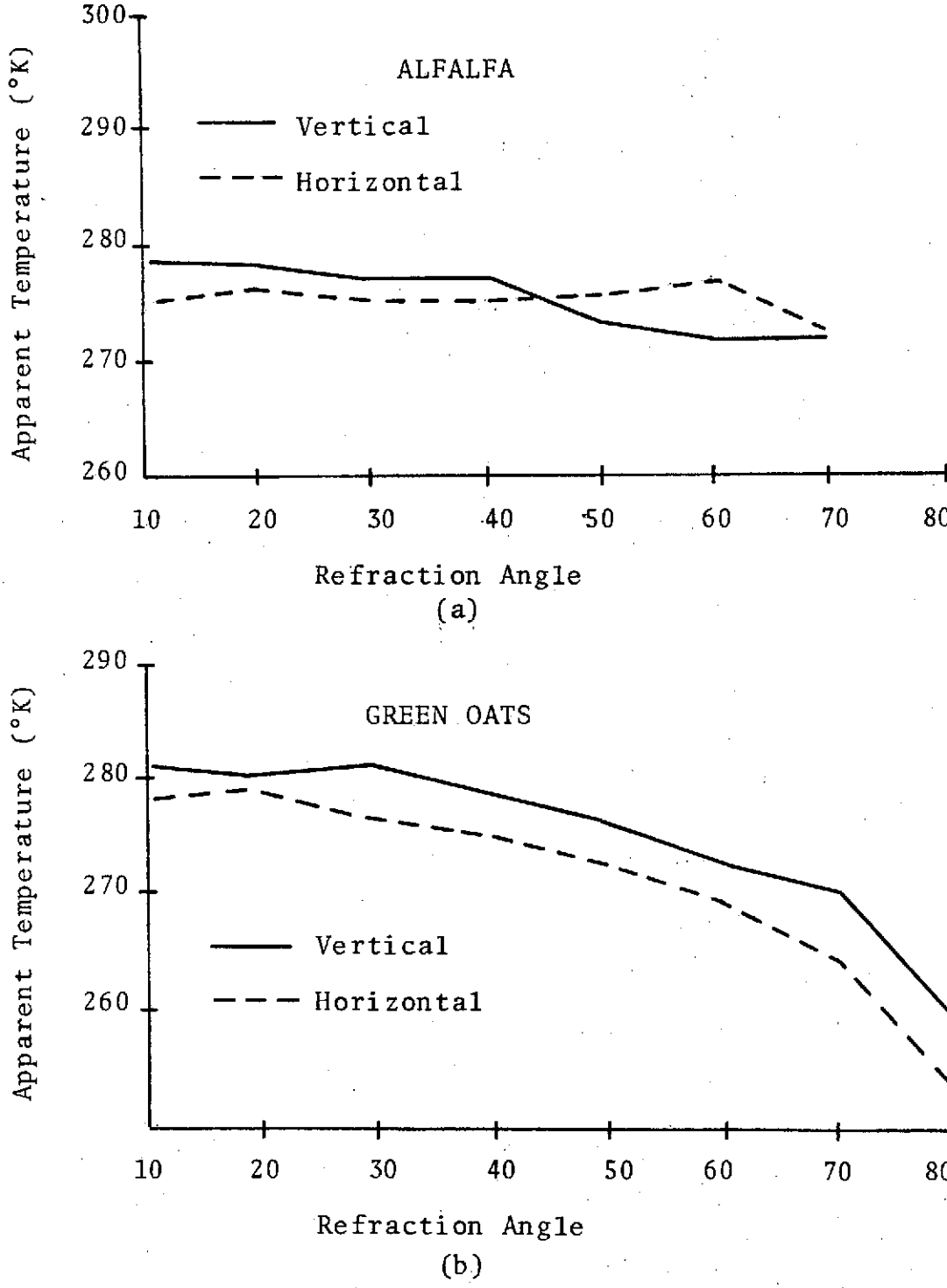

Figure V-2. Apparent temperatures of alfalfa and green oats at 10 GHz [12].

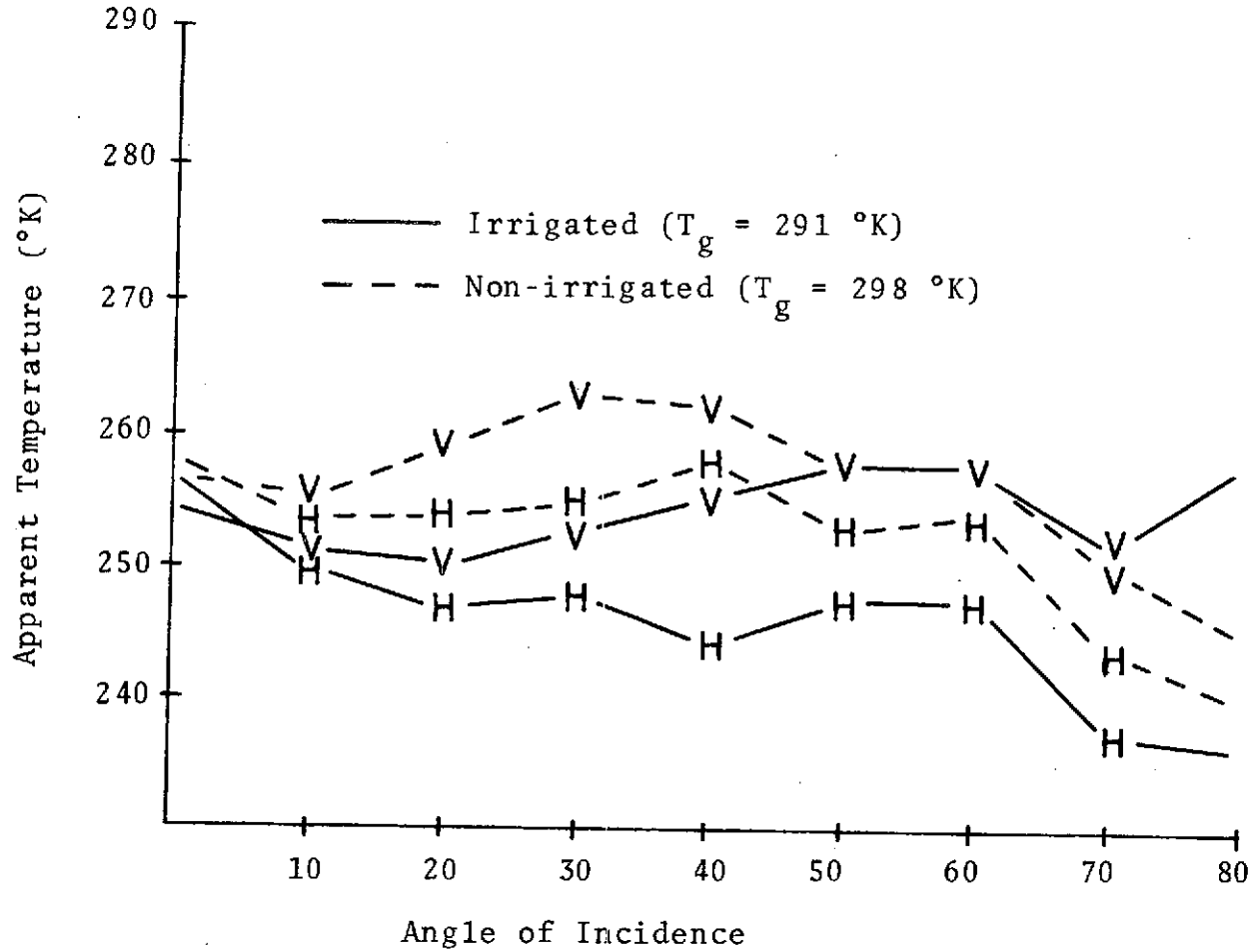

Figure V-3. Apparent temperature of green soybeans at X-band [12].

gated, are plotted as functions of refraction angle. It seems that the apparent temperature of the wet field is significantly lower than that of the dry field for angles greater than 10°. However, it must be noted that the actual surface temperatures differ by 7°C. Raising the solid curves to compensate for this difference, it is seen that the difference in apparent temperatures is actually small at larger refraction angles. There seems to be greater sensitivity to soil moisture at the lower angles, as predicted in Chapter III.

The backscatter coefficient of vegetated terrain is almost independent of polarization (assuming transmitting and receiving polarizations are the same), as illustrated in Figure V-4. In this figure the backscatter coefficient of green oats, measured at X-band is plotted as a function of incidence angle. A change of polarization causes a change in the scattering coefficient of no more than 2.5 dB.

The frequency dependence of the backscatter coefficient is illustrated in Figure V-5. The data plotted are backscatter coefficients of green oats, 25 cm in height, measured at frequencies of 1.8, 10, and 35 GHz. The 1.8 GHz data are from 3 to 6 dB lower than the higher frequency data, whereas the data for 10 and 35 GHz differ by no more than 1 dB. These data imply that at 1.8 GHz a

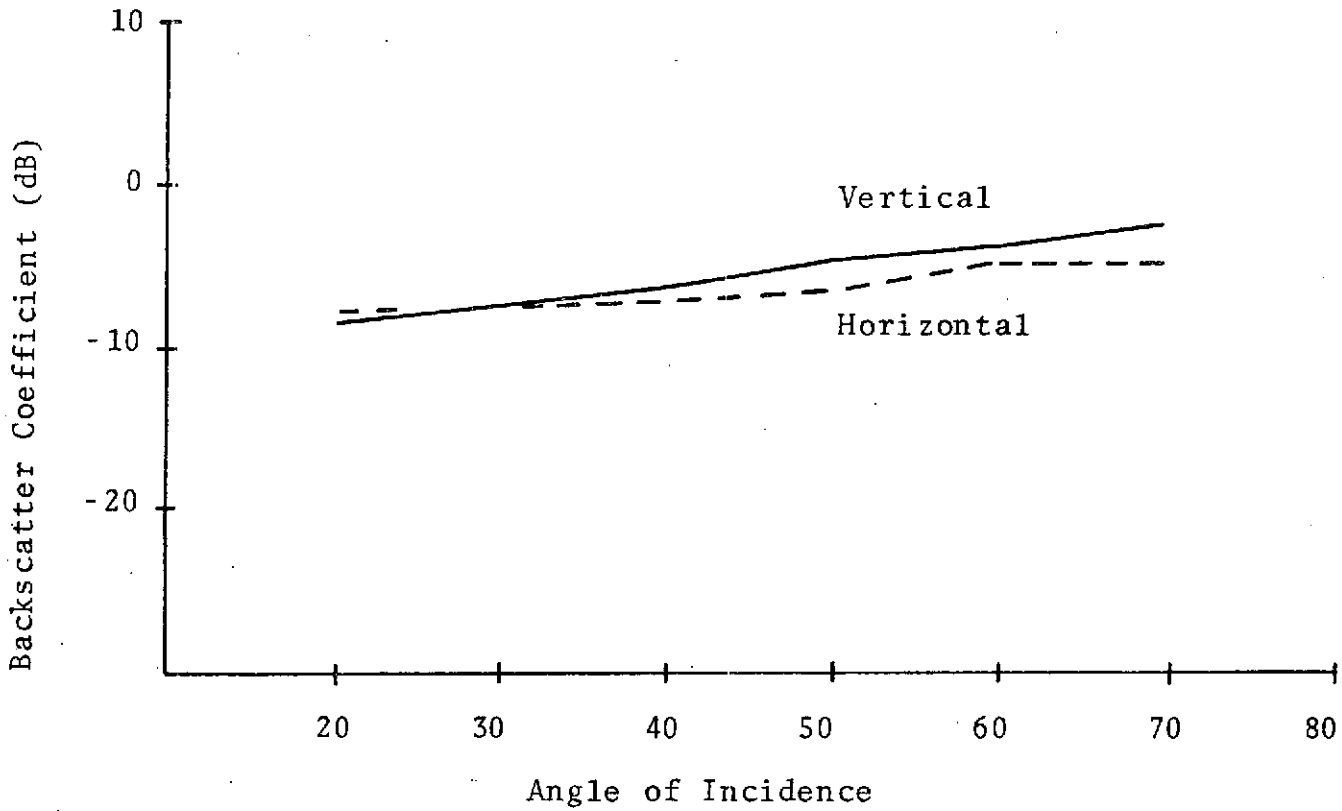

Figure V-4. Backscatter coefficient of green oats at X-band [12].

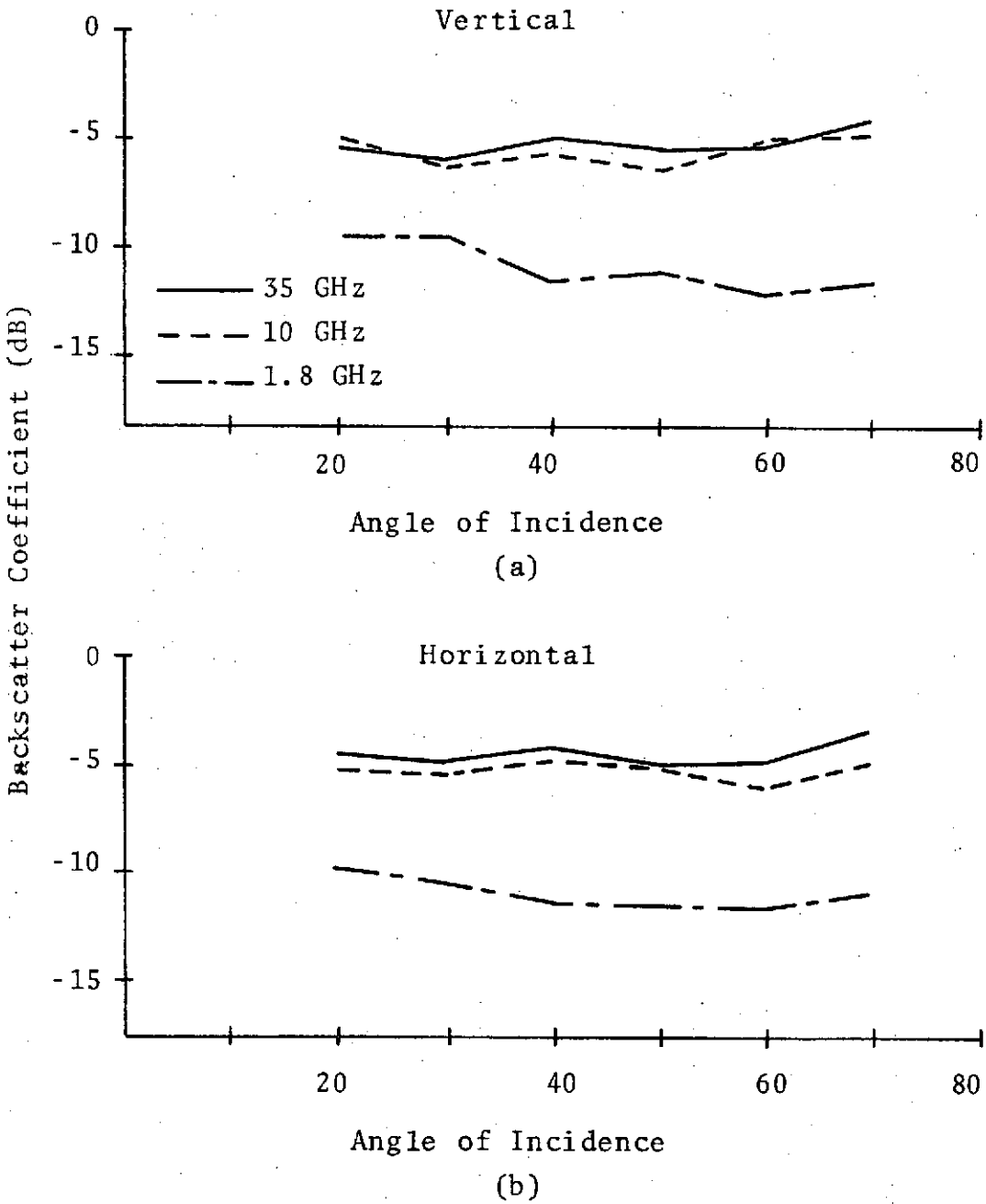

Figure V-5. Backscatter coefficient of green oats 25 cm high at various frequencies.

significant part of the backscatter is due to the soil, whereas at frequencies higher than 10 GHz backscatter is due almost entirely to the vegetation.

The fact that increasing canopy height has the same effect as increasing frequency is illustrated in Figure V-6. Backscattering coefficients of three fields of wheat, 9 cm, 36 cm, and 74 cm in height, are plotted as functions of incidence angle for frequencies of 5.87 GHz and 9.375 GHz. At the lower frequency, data for the 74 cm canopy show little variation with incidence angle. In contrast, the data for the two shorter canopies have steep slopes between 0° and 10°, characteristic of a smooth surface. At the higher frequency, the data for the 9 cm canopy still exhibit a sharp decrease between 0° and 10° incidence. However, the data for the 36 cm canopy tend to look more like the data from the tallest canopy. In effect, the higher frequency makes the canopy appear more heavily vegetated.

From the data presented in this chapter it is not possible to assess the quantitative accuracy of the models developed in Chapters III and IV. However, the results of these models have been shown to be at least qualitatively realistic.

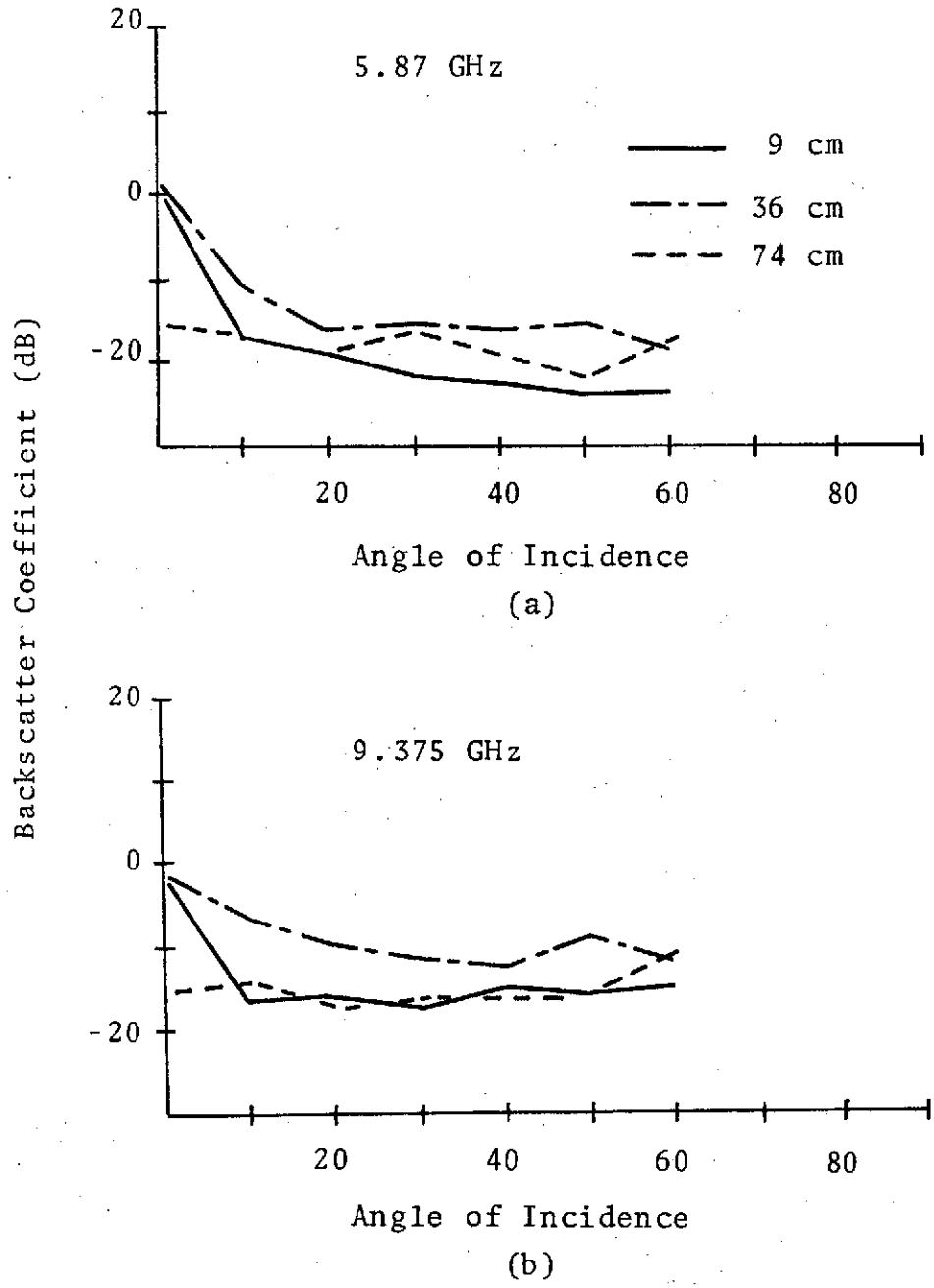

Figure V-6. Effects of frequency and canopy height on backscattering from wheat.

CHAPTER VI

CONCLUSION

In Chapters III and IV, models are developed for the apparent temperature and backscatter coefficient of vegetated terrain. Data computed from these models indicate that the sensitivity of the apparent temperature and backscatter coefficient to variations of soil moisture depends not only on the amount of vegetation, but also on certain system parameters. The various factors which help determine the sensitivity of data to soil moisture are

(1) canopy height
(2) canopy density
(3) row width (for row crops)
(4) row spacing (for row crops)
(5) signal frequency
(6) angle of incidence
(7) azimuth angle (for row crops)

Since several parameters have similar effects on the data, it should be expected that numerous equivalent states exist. Equivalent states are defined as different combinations of the above parameters which cause equivalent apparent temperatures or backscatter coefficients. By holding the system parameters constant, the number of variables is reduced to two (for 100% coverage) or four (for rows). It

is desirable to find a single parameter by which equivalent vegetation states may be identified.

Several equivalent states, determined by inspection of calculated apparent temperatures, are listed in Tables VI-1 through VI-3. The data represented by the tables are for frequencies of 1, 3, and 5 GHz. In each table the vegetation states are defined by canopy height and vegetation density. A uniform canopy (100% coverage) is assumed. Vegetation density is defined as the volume of plant matter per unit volume of space containing the canopy. Comparison of the tables indicates that equivalence of states is dependent on frequency. However, for a uniform canopy, equivalence is independent of the angle from which the terrain is observed.

Also listed in Tables VI-1 through VI-3 are the products of height and density of each state. In Table VI-1 it is seen that the equivalent states having densities of 0.04 and 0.05 have approximately equal height-density products. It is seen in Tables VI-2 and VI-3 that all equivalent states have approximately equal height-density products. Therefore, the height-density product may be used to identify any of the equivalent states.

The model developed in Chapter III predicts that the presence of vegetation decreases the sensitivity of the apparent temperature to variations of soil moisture by

TABLE VI-1

EQUIVALENT VEGETATION STATES AT 1 GHZ

Vegetation Density					
0.03		0.04		0.05	
Canopy Height (cm)	Height-Density Product	Canopy Height (cm)	Height-Density Product	Canopy Height (cm)	Height-Density Product
50	1.50	29	1.16	23	1.15
60	1.80	35	1.40	28	1.40
70	2.10	41	1.64	33	1.65
80	2.40	46	1.84	38	1.90
90	2.70	51	2.04	42	2.10
100	3.00	56	2.24	47	2.35
		70	2.80	60	3.00
		80	3.20	68	3.40
		90	3.60	77	3.85

TABLE VI-2

EQUIVALENT VEGETATION STATES AT 3 GHZ

Vegetation Density					
0.03		0.04		0.05	
Canopy Height (cm)	Height-Density Product	Canopy Height (cm)	Height-Density Product	Canopy Height (cm)	Height-Density Product
40	1.20	30	1.20	24	1.20
50	1.50	38	1.52	31	1.55
60	1.80	45	1.80	37	1.85
70	2.10	53	2.12	43	2.15
80	2.40	61	2.44	49	2.45
90	2.70	68	2.72	55	2.75
100	3.00	76	3.04	62	3.10
		90	3.60	73	3.65
		100	4.00	82	4.10

TABLE VI-3

EQUIVALENT VEGETATION STATES AT 5 GHZ

Vegetation Density					
0.03		0.04		0.05	
Canopy Height (cm)	Height-Density Product	Canopy Height (cm)	Height-Density Product	Canopy Height (cm)	Height-Density Product
50	1.50	40	1.60	32	1.60
60	1.80	46	1.84	38	1.90
70	2.10	54	2.16	44	2.20
80	2.40	62	2.48	49	2.45
90	2.70	69	2.76	56	2.80
100	3.00	76	3.04	63	3.15
		90	3.60	73	3.65
		100	4.00	83	4.15

increasing the apparent temperature with respect to that of bare soil. Figure VI-1 illustrates the difference between the apparent temperatures of bare and vegetated soil for various frequencies and vegetation states. All data are computed for $\theta = 0$. A soil moisture content of 20% is assumed. As expected, the difference in apparent temperatures is relatively small at 1 GHz, whereas it is quite significant at higher frequencies. For a height-density product of 4, the temperature difference is 5°K at 1 GHz, 39°K at 3 GHz and 70°K at 5 GHz.

The effect of differences in apparent temperatures of bare and vegetated soil on the ability to determine moisture content is illustrated in Figure VI-2. The moisture content plotted is that which would cause bare soil to have the same apparent temperature as vegetated soil with a moisture content of 20%. It is clear from this figure that vegetation causes the soil to appear to have a lower moisture content. For a vegetation height-density product of 2, the soil appears to have a moisture content of 19% at 1 GHz, 14% at 3 GHz, and 4% at 5 GHz.

Inspection of backscatter coefficients computed from the model developed in Chapter IV reveals that the height-density product of vegetation is a good indicator of equivalent states for backscatter. However, for a smooth surface, equivalence depends on angle of incidence. It is

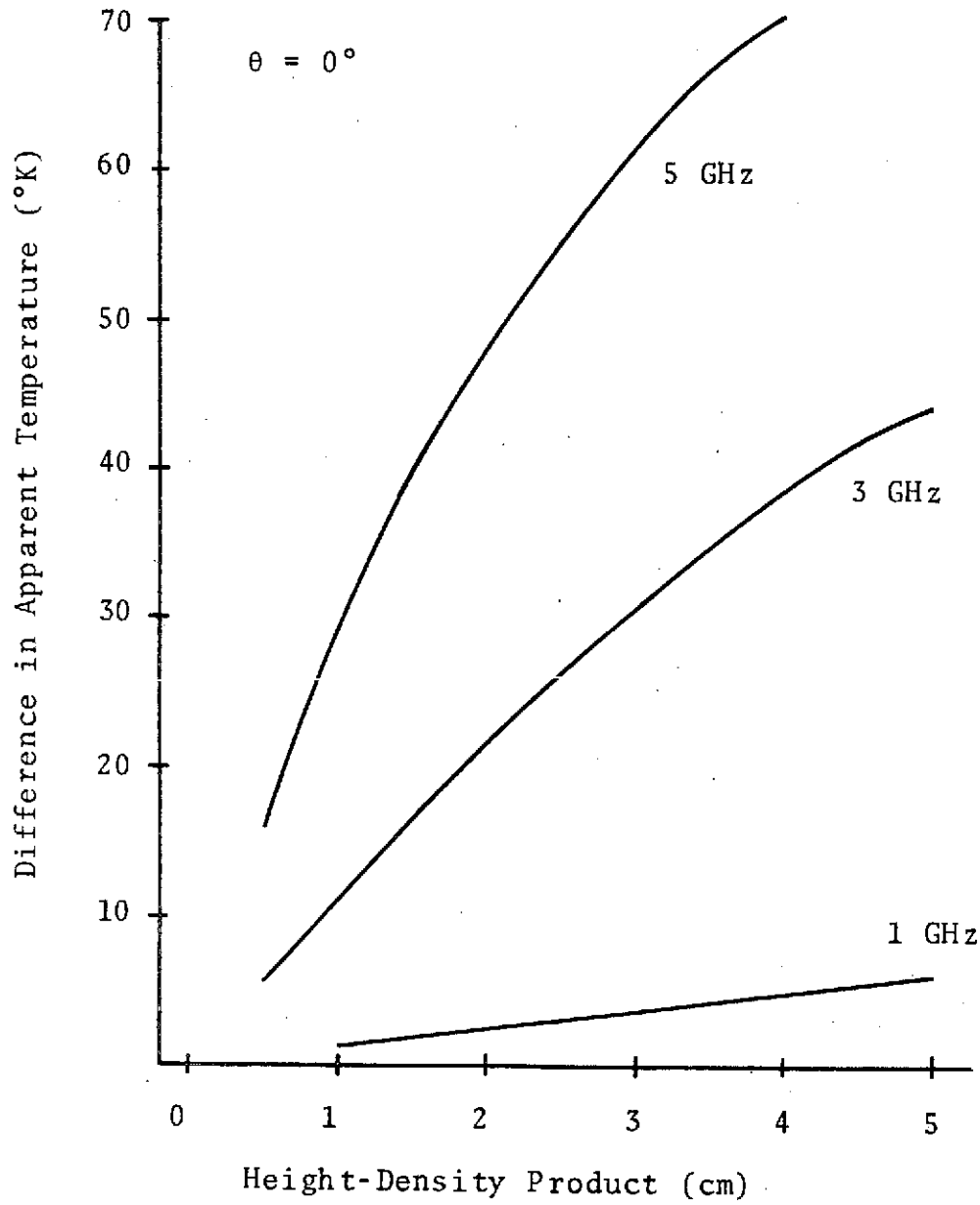

Figure VI-1. Difference in apparent temperatures of bare and vegetated soil.

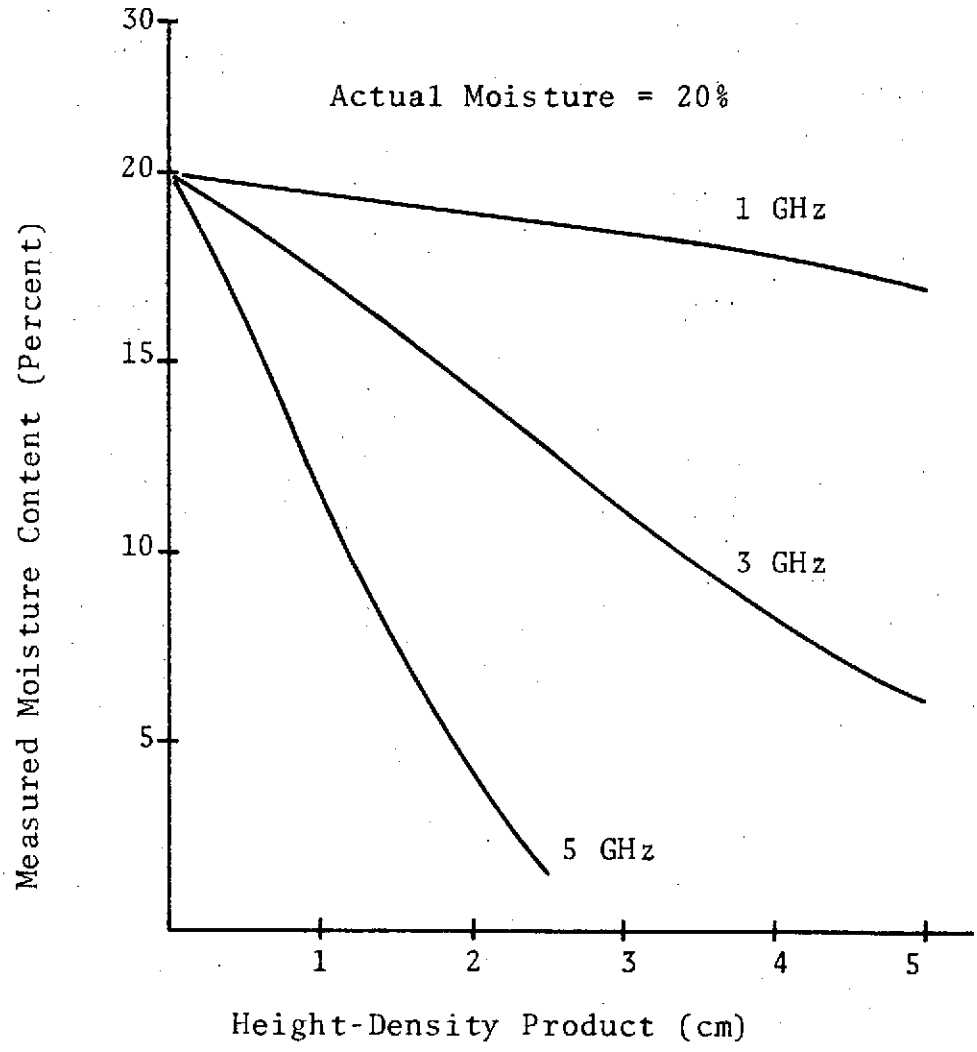

Figure VI-2. Moisture content determined from apparent temperature of vegetated soil.

found that vegetation states having the same height-density product have backscatter coefficients differing by no more than 10% for incidence angles less than 30°. For such angles, equivalence may be assumed when height-density products are equal. However, for angles of incidence greater than 30°, equal height-density products do not necessarily imply equivalence of states.

Plant rows are more difficult to describe than a uniform canopy. In addition to the parameters already considered, row width, row spacing, and azimuth angle must be considered. The height-density product is not adequate to identify a vegetation state, even if azimuth angle and row spacing are held constant. Nevertheless, it is expected that a suitable factor can be found to identify equivalent states of row vegetation. Having determined such an indicator, curves such as those plotted in Figures VI-1 (p. 132) and VI-2 (p. 133) can be plotted for a number of other vegetation states.

Plots of measured moisture content vs. vegetation state make it possible to improve the accuracy of remote soil moisture measurements of vegetated terrain. However, such curves are difficult to produce in practice, since many parameters must be known. Obviously the vegetation state must be identified by a suitable indicator (such as the height-density product). Furthermore, the actual

surface temperature must be known. For all calculations in this report the surface temperature is assumed to be 298°K. In addition, surface roughness and atmospheric effects must be accounted for.

There is clearly a need for more experimental data from terrain for which soil moisture and vegetation are known, little of which is available at present. The results of this investigation indicate that the effect of vegetation on microwave data from terrain is greater than has been anticipated in some previous work. From the theoretical and experimental data presented here, it is clear that the ability to measure soil moisture by remote sensing techniques is highly dependent on the amount of vegetation over the soil. However, the sensitivity of data to variations of soil moisture can be improved by adjusting certain system parameters. For example, airborne radiometer data have already verified that low frequency sensors are more sensitive to variations of soil moisture [11]. Ground-based experiments are needed to determine critical amounts of vegetation, above which soil moisture cannot be determined, for various frequencies. If data from future airborne experiments are to be of any value for soil moisture measurement, efforts must be made to compensate for vegetation. It is hoped that the result of such efforts will be to improve the techniques by which soil moisture content

is measured by microwave remote sensors.

REFERENCES

[1] Remote Sensing with Special Reference to Agriculture and Forestry, Washington, D.C.: National Academy of Sciences, 1970.

[2] W. H. Peake, "Interaction of Electromagnetic Waves with Some Natural Surfaces," IRE Transactions on Antennas and Propagation, AP-7, pp. S324-S329, December 1959.

[3] R. Kumar, "Radiation from Plants--Reflection and Emission: A Review," Report AA&ES 72-2-2, Purdue University, Lafayette, Indiana, February 1972.

[4] G. T. Ruck, et al., Radar Cross Section Handbook (2 vol.), New York: Plenum Press, 1970.

[5] J. R. Lundien, "Terrain Analysis by Electromagnetic Means," Technical Report 3-693, Report 5, U. S. Army Engineer Waterways Experiment Station, Vicksburg, Mississippi, February 1971.

[6] B. R. Davis, et al., "Feasibility Study of the Use of Radar to Detect Surface and Ground Water," Technical Report 3-727, U. S. Army Engineer Waterways Experiment Station, Vicksburg, Mississippi, April 1966.

[7] M. L. Wiebe, "Laboratory Measurement of the Complex Dielectric Constant of Soils," Technical Report RSC-23, Remote Sensing Center, Texas A&M University, College Station, Texas, October 1971.

[8] J. A. Richerson, "An Experimental Evaluation of a Theoretical Model of the Microwave Emission of a Natural Surface," Technical Report RSC-27, Remote Sensing Center, Texas A&M University, College Station, Texas, August 1971.

[9] W. H. Stiles, W. P. Waite, C. H. Turner, and J. A. Rich, "Broad Spectrum Reflectivity of Surfaces with Varying Permittivity and Roughness," 1973 SWIEEECO Record, pp. 73-75, April 4, 1973.

[10] B. R. Jean, "Selected Applications of Microwave Radiometric Techniques," Technical Report RSC-30, Remote Sensing Center, Texas A&M University, College Station, Texas, August 1971.

[11] C. L. Kroll, "Remote Monitoring of Soil Moisture using Airborne Microwave Radiometers," Technical Report RSC-43, Remote Sensing Center, Texas A&M University, College Station, Texas, June 1973.

[12] W. H. Peake and T. L. Oliver, "The Response of Terrestrial Surfaces at Microwave Frequencies," Technical Report AFAL-TR-70-301, Electroscience Laboratory, Ohio State University, Columbus, Ohio, May 1971.

[13] J. B. Hasted, "The Dielectric Properties of Water," Progress in Dielectrics, vol. 3, pp. 101-149, New York: John Wiley & Sons, Inc., 1961.

[14] R. H. Cole, "Theories of Dielectric Polarization and Relaxation," Progress in Dielectrics, vol. 3, pp. 47-99, New York: John Wiley & Sons, Inc., 1961.

[15] S. Evans, "Dielectric Properties of Ice and Snow," Journal of Glaciology, vol. 5, no. 42, pp. 773-792, October 1965.

[16] S. Ramo and J. R. Whinnery, Fields and Waves in Modern Radio, 2nd ed., p. 299, New York: John Wiley & Sons, Inc., 1953.

[17] E. C. Jordan and K. G. Balmain, Electromagnetic Waves and Radiating Systems, 2nd ed., Englewood Cliffs, New Jersey: Prentice-Hall, Inc., 1968.

[18] A. K. Fung and F. T. Ulaby, "The Apparent Surface Temperature at Microwave Frequencies," Fall URSI Meeting, Austin, Texas, December 8-10, 1969.

[19] L. F. Johnson, "On the Performance of Infrared Sensors in Earth Observations," Technical Report RSC-37, Remote Sensing Center, Texas A&M University, College Station, Texas, August 1972.

[20] M. I. Skolnik, Introduction to Radar Systems, New York: McGraw-Hill Book Co., 1962.

[21] S. Silver, Microwave Antenna Theory and Design, MIT Radiation Lab Series 12, New York: McGraw-Hill Book Co., 1947.

[22] A. K. Fung, "Theory of Cross-Polarized Power Returned from a Random Surface," Applied Scientific Research, vol. 18, no. 1, pp. 50-60, August 1967.

[23] J. C. Leader, "Bidirectional Scattering of Electromagnetic Waves from Rough Surfaces," presented at Spring Meeting of USNC/URSI, Washington, D. C., April 16, 1970.

[24] R. V. Churchill, Fourier Series and Boundary Value Problems, 2nd ed., New York: McGraw-Hill Book Co., 1969.

[25] C. Don, "Lommel-Seeliger Scattering from Leaf Vegetation," Final Report 2832-2, Electroscience Laboratory, Ohio State University, Columbus, Ohio, May 1970.

[26] M. I. Skolnik, ed., The Radar Handbook, New York: McGraw-Hill Book Co., 1970.

[27] J. A. Richerson, "Discussion of a Model of the Apparent Temperature of Natural Surfaces in the Microwave Range," Technical Report RSC-10, Remote Sensing Center, Texas A&M University, College Station, Texas, May 1970.

APPENDIX A

PENETRATION OF MICROWAVES INTO SOIL

The depth of penetration, or skin depth, of a medium is defined as the distance over which an electric field is attenuated to 1/e (37%) of its initial strength as it propagates through the medium [17]. Since the intensity of a field propagating in the x-direction is

$$E(x) = E_0 e^{-\alpha x}$$

it is easy to see that the skin depth is equal to the reciprocal of the attenuation constant. In terms of the electrical properties of the medium, the skin depth is

$$\delta = \left[\omega \sqrt{\frac{\mu\epsilon}{2}\left(\sqrt{1 + \left(\frac{\sigma}{\omega\epsilon}\right)^2} - 1\right)} \right]^{-1} \qquad \text{(A-1)}$$

where ω = radian frequency of signal

μ = magnetic permeability of medium

ϵ = dielectric constant of medium

σ = conductivity of medium

The skin depth of soil is a function of the soil moisture content, as illustrated in Figure A-1. In this figure the skin depth of three types of soil, the permittivity of which was measured by Wiebe [7], is plotted as a function of soil moisture for a frequency of 9 GHz. For these three

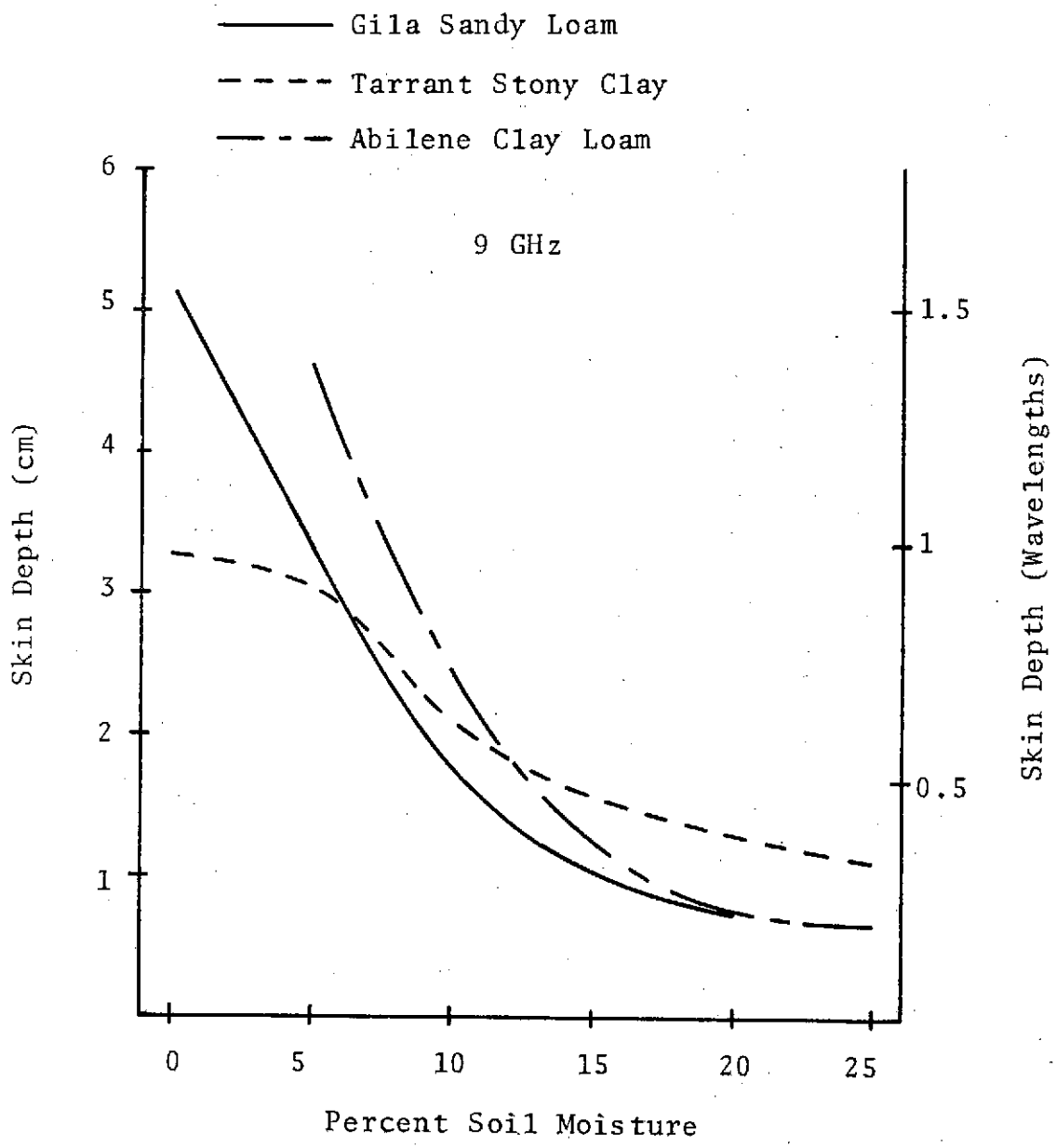

Figure A-1. Skin depth of various soils as a function of moisture content.

soils the skin depth is greater than half of a wavelength at moisture contents less than 10%, and less than half of a wavelength at moisture contents greater than 15%.

From (A-1) it is clear that the skin depth is also a function of frequency. The skin depth of Gila Sandy Loam is plotted in Figure A-2 for frequencies of 1.5 GHz and 9.0 GHz. The permittivity of the soil is assumed to be the same at both frequencies. At the lower frequency the skin depth is greater than 4 cm for all values of moisture content up to 20%. At the higher frequency the skin depth is less than 2 cm for any moisture content greater than 10%.

A knowledge of the skin depth of soil at various frequencies is helpful in assessing the value of passive microwave sensors for remote measurement of soil moisture. The skin depth is an indication of the depth from which radiation contributes significantly to the apparent temperature. Since the surface of the ground is usually dry, regardless of subsurface moisture content, it is desirable that the apparent temperature include a significant contribution from several centimeters beneath the surface. Therefore, longer wavelength sensors are advisable for this application.

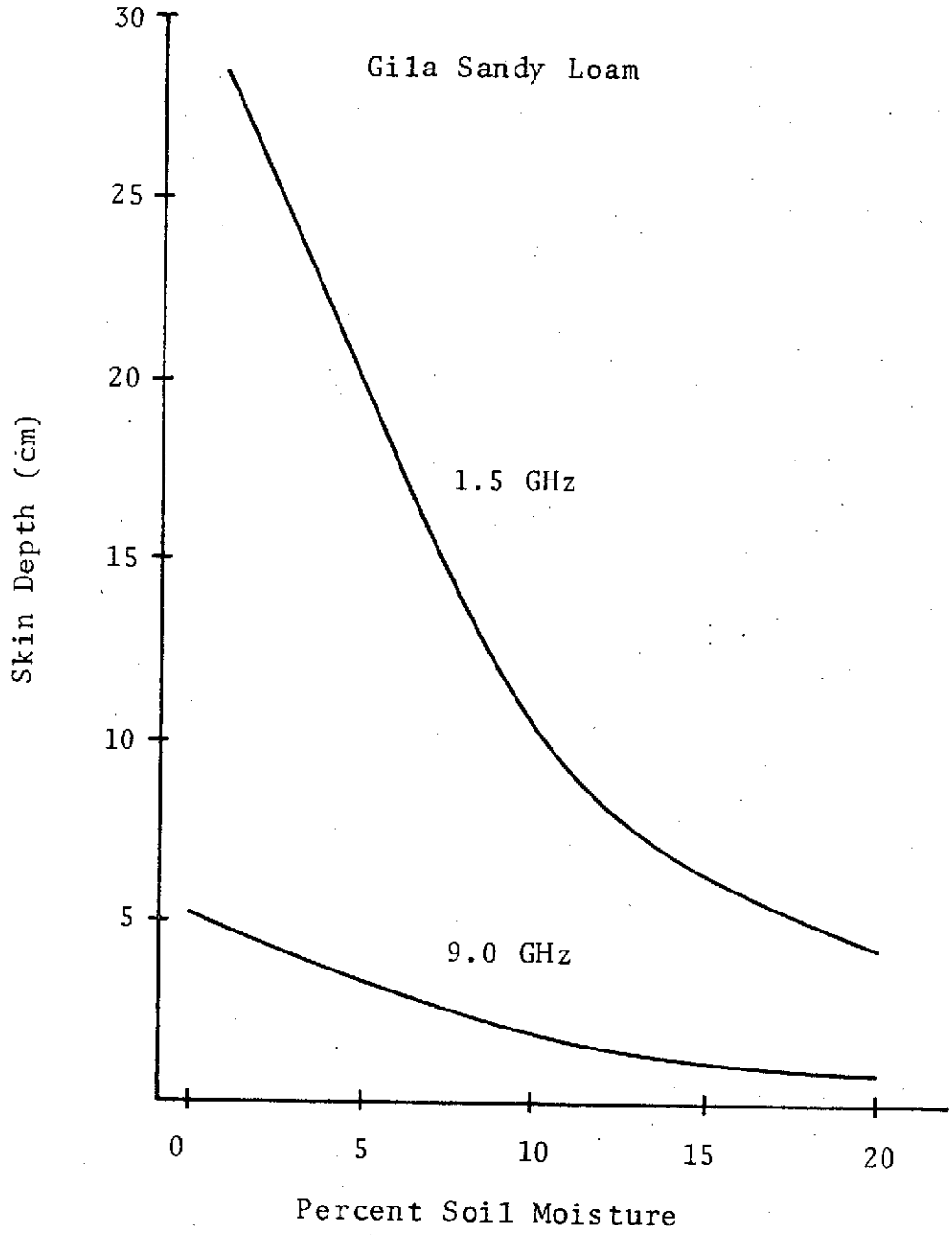

Figure A-2. Effect of frequency on the skin depth of soil.

APPENDIX B

ATMOSPHERIC EFFECTS ON APPARENT SURFACE TEMPERATURE

The atmosphere acts in several ways to alter the electromagnetic signal which radiates from the ground. Some of the diffuse radiation from the atmosphere is scattered by the target into the antenna beam, augmenting the signal due to thermal radiation from soil and vegetation. As the combined radiated and scattered energy propagates toward the antenna, it is attenuated by the intervening atmosphere. At the same time, however, the atmosphere between the target and the sensor is radiating energy directly into the antenna, adding another component to the total apparent temperature.

At microwave frequencies the primary causes of atmospheric attenuation are water vapor and oxygen. The attenuation due to each of these gases is illustrated in Figure B-1. These curves are computed using a modified form of Van Vleck's model [26]. The attenuation curve for water vapor has maxima at 22.3 GHz and about 180 GHz. (The higher frequency is not included in the figure.) The curve of oxygen absorption has maxima at 60 GHz and 120 GHz.

Summing the attenuation due to water vapor and oxygen

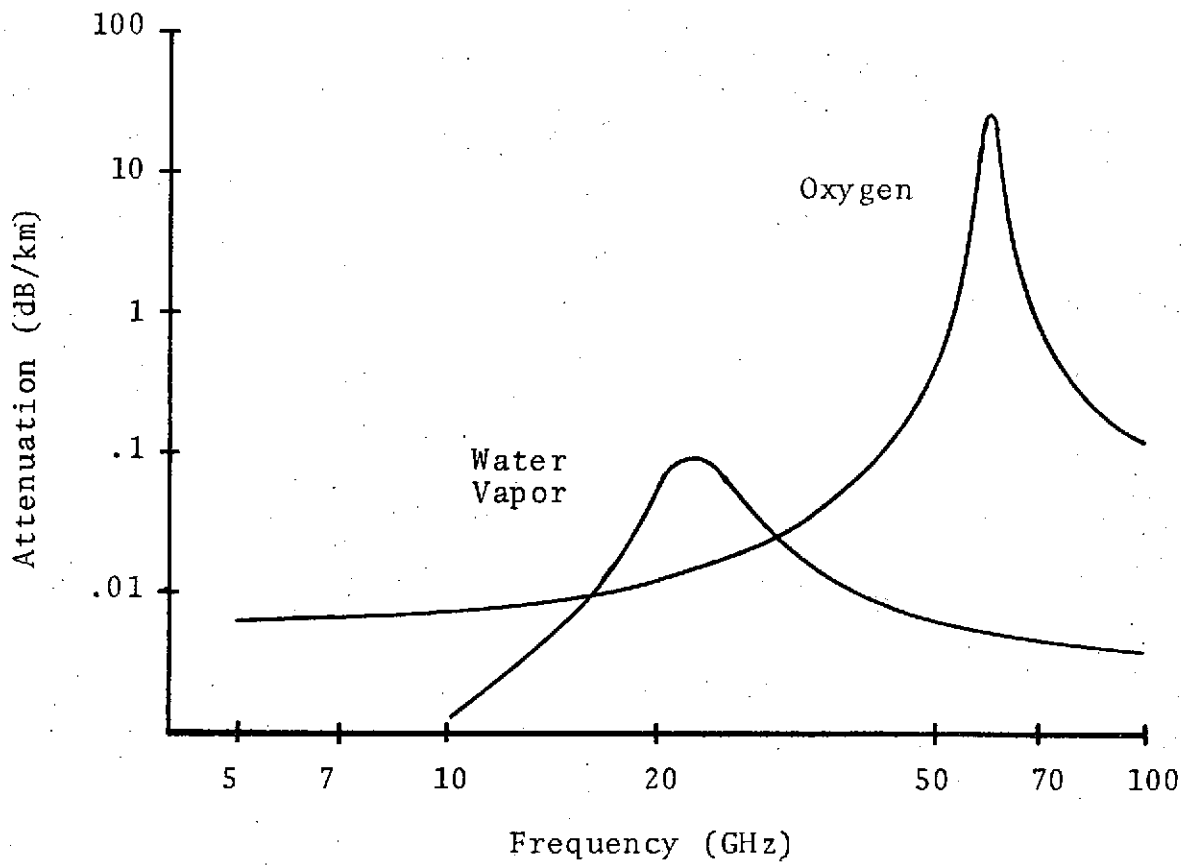

Figure B-1. Atmospheric attenuation due to water vapor and oxygen.

along with a third term to account for absorption by other gases, gives the total atmospheric attenuation, as illustrated in Figure B-2. The peaks at 20 and 60 GHz are still apparent. It is clear that atmospheric attenuation decreases constantly below 20 GHz, becoming negligible below about 1 GHz.

The actual effect of atmospheric attenuation and radiation is better understood by evaluating the apparent temperature of a theoretical rough surface at different frequencies. Figure B-3 illustrates apparent temperatures computed from Peake's model as modified by Richerson [27]. The sensor is assumed to be at an altitude of 609.6 m (2000 ft) above the surface. Data were computed for various values of humidity at frequencies of 1.42, 10.69, 19.35, and 31.4 GHz. It is clear that the effect of changing humidity is negligible at 1.42 GHz, but becomes more pronounced at higher frequencies. The number at the right-hand end of each curve is the apparent temperature which would be measured if the atmosphere only attenuated the signal, radiating no energy itself. At the lower frequencies the atmosphere adds about 2 degrees to the measured apparent temperature, whereas at higher frequencies the contribution of the atmosphere may be 9 or 10 degrees.

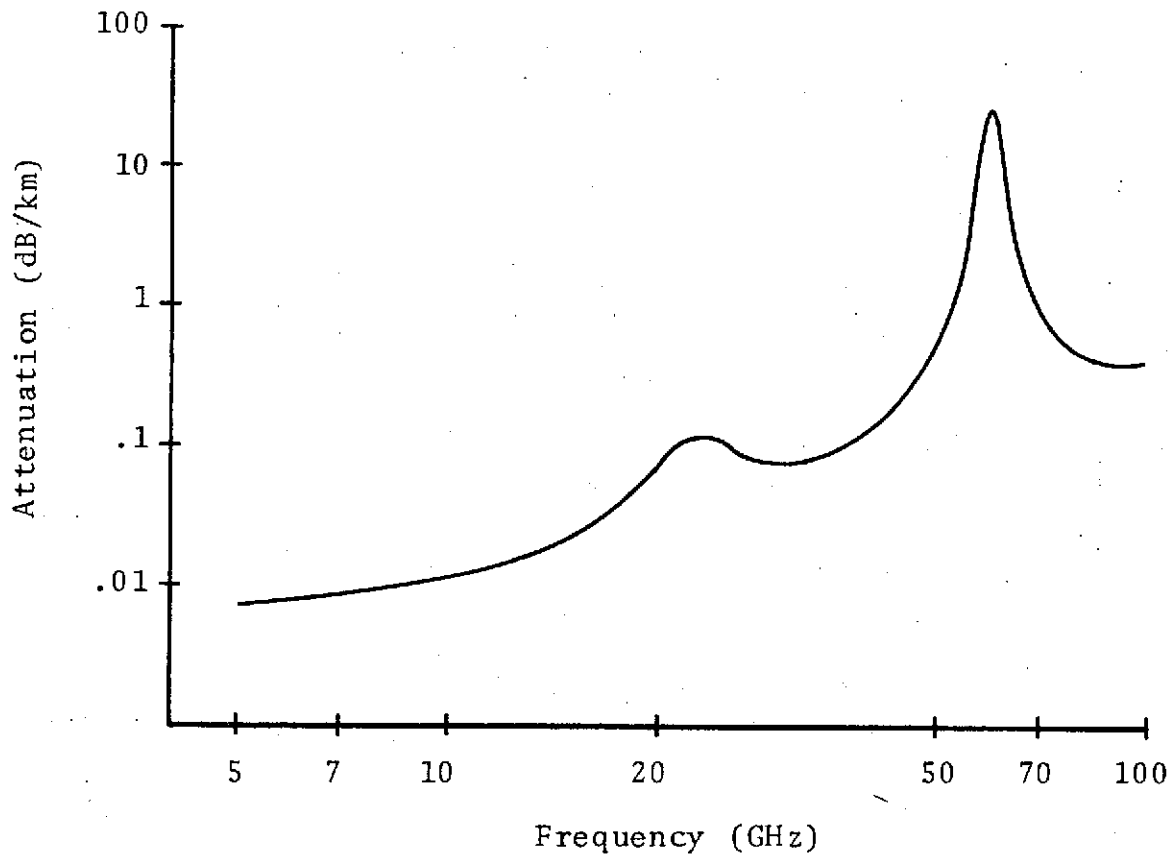

Figure B-2. Total atmospheric attenuation at microwave frequencies.

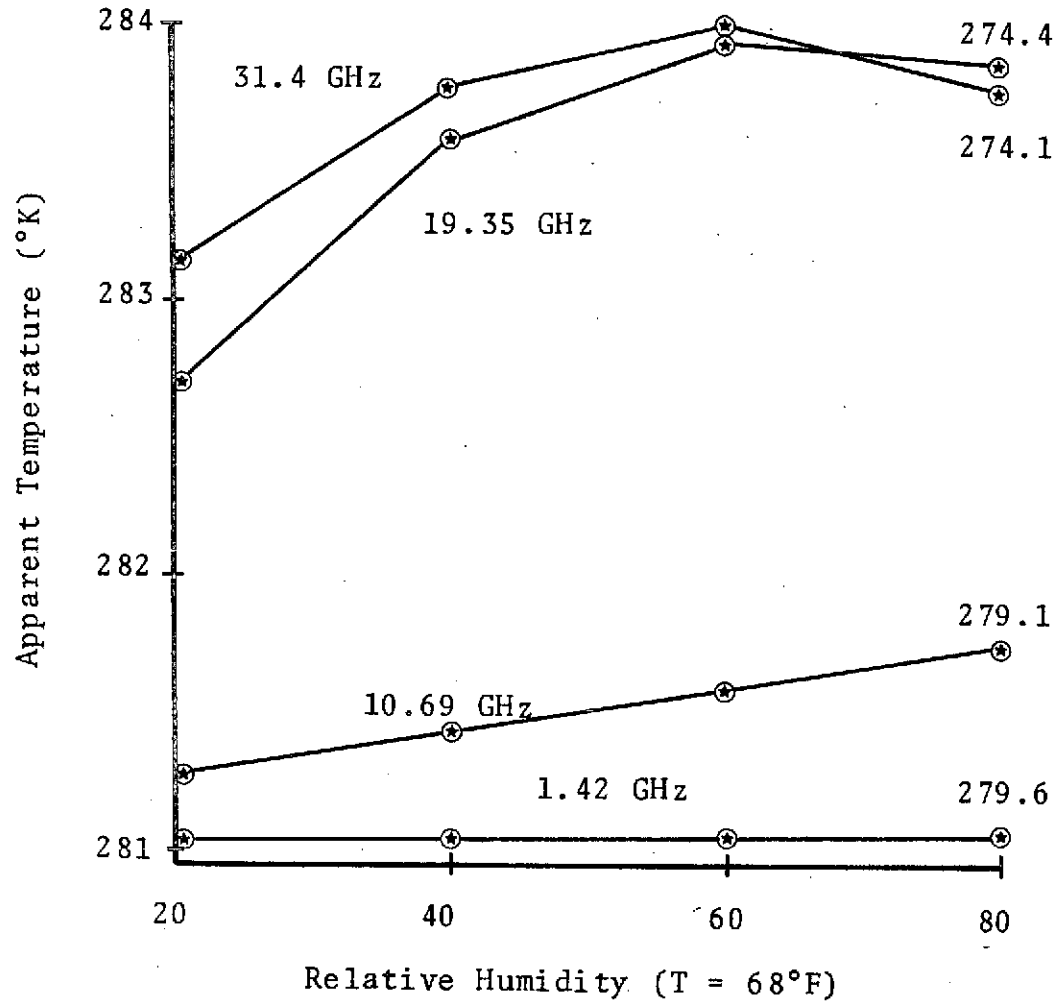

Figure B-3. Atmospheric effects on measured apparent temperature at various frequencies.